BIOMIMETIC ACOUSTIC METAMATERIAL DESIGN FOR ARCHITECTURAL APPLICATIONS

A THESIS SUBMITTED TO

THE GRADUATE SCHOOL OF ENGINEERING AND SCIENCE

OF BILKENT UNIVERSITY

IN PARTIAL FULFILLMENT OF THE REQUIREMENTS FOR

THE DEGREE OF

MASTER OF SCIENCE

IN

ARCHITECTURE

By

Beyza Yazıcı

August 2020

BIOMIMETIC ACOUSTIC METAMATERIAL DESIGN FOR ARCHITECTURAL APPLICATIONS

By Beyza Yazıcı

August 2020

We certify that we have read this thesis and that in our opinion it is fully adequate, in scope and in quality, as a thesis for the degree of Master of Science.

Zühre Sü Gül(Advisor)

Aysu Berk Haznedaroğlu

Ayşe Tavukçuoğlu

Approved for the Graduate School of Engineering and Science:

Ezhan Karaşan
Director of the Graduate School

ABSTRACT

BIOMIMETIC ACOUSTIC METAMATERIAL DESIGN FOR ARCHITECTURAL APPLICATIONS

Beyza Yazıcı
M.S. in ARCHITECTURE
Advisor: Zühre Sü Gül
August 2020

This study investigates the potentials of acoustic metamaterial (AMM) applications in room and building acoustics by means of impedance tube experiments. With their extreme properties in either sound absorption or transmission loss, AMMs can perform better than many traditional acoustic materials in buildings. Importantly, they are also more sustainable and hygienic than fibrous and porous materials. Depending on the matrix material used, AMMs can vary in transparency and color. Considering both their acoustic and aesthetic values, this study develops different types of metamaterial for possible uses as a partition wall, a surface layer, or a design element. The proposed metamaterials are primarily based on the exploration of ratios and forms from nature – the golden ratio, web-labyrinthine structures, genetic and neural systems such as DNA molecules and the synapse structures in the brain – reproduced on a sub-wavelength scale. These abstractions are then combined with the 3D space coiling and 3D labyrinth approaches of AMM design. Modules of the proposed AMMs are manufactured in a 3D printer and tested in an impedance tube to estimate their normal incidence sound absorption coefficients and transmission loss characteristics. Based on the results obtained, the modules with the higher performances are used in the design of partition walls of varying heights. Two real-case architecture studios are simulated with and without the proposed AMM interventions over field test-tuned acoustical models of the studios to assess the effectiveness of such an approach in a possible acoustical design problem.

Keywords: Acoustic Metamaterial, Space-Coiling, Sound Absorption, Transmission Loss, Bio-mimicking, Impedance Tube Measurements, Room and Building Acoustics.

ÖZET

MİMARİ UYGULAMALAR İÇİN BİOMİMETİK AKUSTİK META-MALZEME TASARIMLARI

Beyza Yazıcı
Mimarlık, Yüksek Lisans
Tez Danışmanı: Zühre Sü Gül
Ağustos 2020

Bu çalışma, durağan dalga tüpü deneyler yöntemini kullanarak, oda ve bina akustiğinde akustik metamalzeme(AMM) uygulamalarının potansiyellerini araştırmaktadır. AMM'ler ses emilimi veya iletim kaybındaki üst düzey performans özellikleri ile binalardaki birçok geleneksel akustik malzemelerden daha iyi performans gösterebilirler. Daha da önemlisi, lifli ve gözenekli malzemelere kıyasla daha sürdürülebilir ve hijyeniktirler. Kullanılan matris malzemesine bağlı olarak, AMM'ler saydamlık derecesi ve renk bakımından değişebilir. Hem akustik hem de estetik değerler göz önüne alındığında, bu çalışma; bölme duvarı, yüzey katmanı veya tasarım ögesi olarak olası kullanımlar için farklı tipte metamalzeme geliştirmektedir. Önerilen metamalzemeler, öncelikle doğadan oranların ve formların - altın oran, web-labirent yapıları, DNA molekülleri gibi genetik ve nöral sistemler ve beyindeki sinaps yapıları - bir alt dalga boyu ölçeğinde araştırılmasına dayanmaktadır. Bu soyutlamalar, daha sonra 3D uzay sarmalı ve AMM tasarımının 3D labirent yaklaşımlarıyla birleştirilir. Önerilen AMM'lerin modülleri bir 3D yazıcıda üretilir. Yüzeye dik gelen ses dalgalarının, ses yutma katsayılarını ve ses iletim kaybı özelliklerini tahmin etmek için bir durağan dalga tüpünde test edilir. Elde edilen sonuçlara dayanarak, daha yüksek performansa sahip modüller, farklı yükseklikteki bölme duvarlarının tasarımında kullanılır. Bilkent Üniversitesi'ndeki iki tasarım stüdyolarında mevcut olan akustik probleme böyle bir yaklaşımın etkinliğini değerlendirmek için öncelikle sahada akustik testleri yapılır, sonrasında akustik model saha ölçümlerine göre akord edilir veya ayarlanır, stüdyo modellerinin akustik modelleri üzerinde önerilen AMM önerisi ile ve öneriler bulunmadan benztime sokulur. Sonucunda, AMM önerilerinin potansiyele sahip olduğu gözlemlenir.

Anahtar sözcükler: Akustik Metamalzeme, Mekan Sarmalı, Ses Yutma Katsayısı,

Ses İletim Kaybı, Biomimesis, Durağan Dalga Tüp Ölçümleri, Oda/Hacim ve Bina Akustiği.

Acknowledgement

First and foremost, I would like to express my deepest thanks and appreciation to my supervisor, Asst. Prof. Pract. Dr. Zühre Sü Gül for her endless support, deep knowledge, enthusiasm and being an inspirational role model for me. I am grateful for her guidance and support throughout this challenging process. I sincerely thank her for providing me such unique opportunities during my research. Her positive attitude, patience and invaluable suggestions have become key elements in helping me to stay motivated during my studies.

I would also like to thank to all examining committee members, Assist. Prof. Dr. Aysu Berk Haznedaroğlu and Assoc. Prof. Dr. Ayşe Tavukçuoğlu, for their valuable critics and comments.

My special thanks are extended to Renan Gökyay, partner of Nurus, for making the 3D CNC printer available, for the funding of the base material and for his special role in initiating this study on AMMs. I also appreciate all members in the departments of AR-GE and Design in Nurus company for their countless help.

I also acknowledge my sincerely gratitude to Prof. Mehmet Çalışkan for his valuable consultations and to Mezzo Stüdyo for providing the laboratory facilities for the impedance tube measurements. I would also like to thanks to the members of Mezzo Stüdyo for their special support.

I would like to thank to my classmates and my friends for making my time in master's degree valuable and joyful with their friendly attitudes.

Last but not least, I would like to dedicate my thesis to my parents, Bilgen Yazıcı and Mehmet Rıza Yazıcı, and to my siblings, Belgin Yazıcı Alp and Berkay Yazıcı. I always feel very fortunate to have them as my family and to feel their unconditional love, support and endless trust in me.

Contents

List of Figures

List of Tables

Chapter 1

Introduction

1.1 Problem Statement

Research on materials is a fundamental topic in room and building acoustics. A range of materials are either applied in construction systems for noise control or used as a surface finish layer or decorative object for reverberation control. Even though electronic devices are capable of manipulating and magnifying sound waves only once they are regenerated to electronic form, it is highly more desirable to control the acoustic waves with the structure of the new artificial material. Thus, advances in technology have made it possible to control sound within the structure of novel materials [17]. Meanwhile, green technology considerations have brought in new requirements for buildings such as hygiene standards, limitations on toxic gas emissions and recyclability or re-usability. One of the objectives of this research is to combine the form, acoustics, and technology of materials to develop sustainable, eco-friendly acoustical design solutions for use in room and building acoustics. Since some traditional acoustics materials do not have these qualities in general, a new type of material has started to be investigated as an alternative to address these issues. Also, even though it is easier to handle with high-frequency sound waves, low-frequency range always creates a problematic situation in building acoustics, traditionally necessitates

thick wall/panel sections or heavy materials. However, acoustics metamaterials provide extreme efficiency even in low frequencies with a broadband frequency range in specific form and configurations.

1.2 Aim and Scope of the Thesis

The main aim of this research is to develop alternative 3D labyrinthine type acoustic metamaterials for sound control in room and building acoustics applications. For that purpose, the first objective is to evaluate an alternative application technic for building systems as an interior partition, an interior surface layer, or a design element. Second aim is to dispose and optimize architectural and physical variables of metamaterial systems for improving their acoustical performances specifically in the low-frequency range. Lastly, a multi-use approach is investigated in a single matematerial unit for providing both sound absorption and transmission depending on its composition and layout. This research also searches after proposing sustainable, eco-friendly acoustical material solutions. In a broader scope, this study aims to contribute to the ongoing scientific field and research of acoustic metamaterials by a focus on its architectural applications.

1.3 Structure of the Thesis

This thesis is divided into six chapters and is structured as follows:

The first chapter includes the problem statement, aim, scope and structure of the thesis and gives a brief information about this thesis. In chapter 2, the detailed literature review including previous on metamaterials (MMs), acoustic metamaterials (AMMs), bio-mimicking and thesis contributions have been presented. Chapter 3 sets out the phases of design and production of the three different AMM prototypes proposed in this thesis. Chapter 4 specifies the measurement procedure of the sound transmission loss and absorption performance of AMMs

and theoretical calculations on estimating different parameter outputs, which is held for testing the efficiency and application potential of proposed AMMs. In Chapter 5, the results are discussed. Chapter 6 concludes the thesis by emphasizing the major findings and suggests novel alternatives for future work.

Chapter 2

State of the Art

2.1 Basic Terminology

Acoustic Band Gap: A frequency range in which acoustic waves cannot circulate within a periodic structure is represented by a band gap [18].

Bulk Modulus: Bulk modulus is defined as the measurement of a reduction in volume with enhancement in pressure [19]. It is related to reaction of a substance against compression (Fig. 2.1).

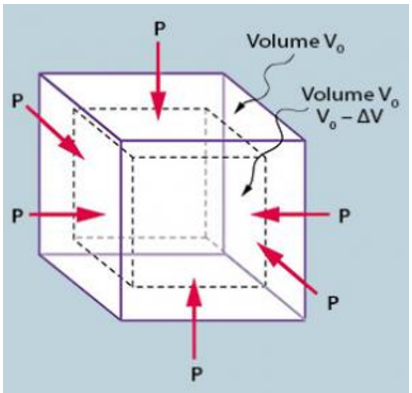

Figure 2.1: Diagram explanation of bulk modulus [1].

Negative Refractive Index: The studies on metamaterials are mainly on either electromagnetic or acoustics. Discussions about the new properties and phenomena of materials made on metamaterials emphasize the possibility that effective ambient parameters (such as electrical permeability and magnetic permeability) can be negative. At a given radiation frequency, if a medium whose magnetic permeability and dielectric permeability is negative is called a negative refractive index medium, or a left-handed medium. [20]. As shown in Fig. 2.2, positive refraction is a usual way that can be found in nature while negative refraction is artificial and can not naturally exist.

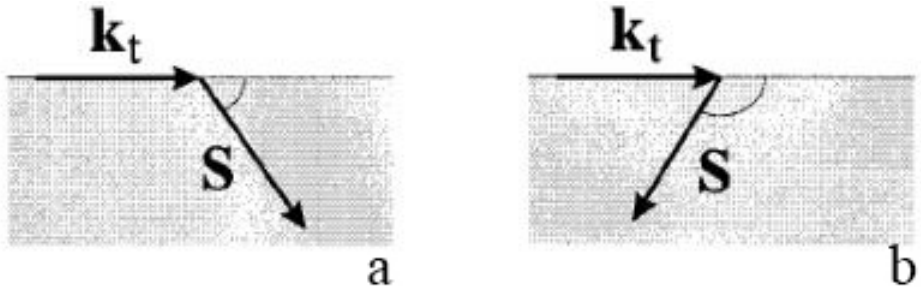

Figure 2.2: a) Positive refraction S $\cdot k_t \geq 0$, b) negative refraction S $\cdot k_t \leq 0$ [2].

Reverberation Time: The most important indicator of the room auditory environment and the characteristics of acoustic have been accepted as reverberation time [22]. T symbolizes reverberation time which is the conventional objective measurement of sound quality in a space. In 1900, W.C. Sabine studied this phenomenon [21]. Reverberation time is a time necessitates for sound to decay 60 dB from its initial sound level [23]. The decay slope is measured lower than the start value in practice, which is a range between -5 dB to -35 dB (or -5 dB to -25 dB) (Fig. 2.3).

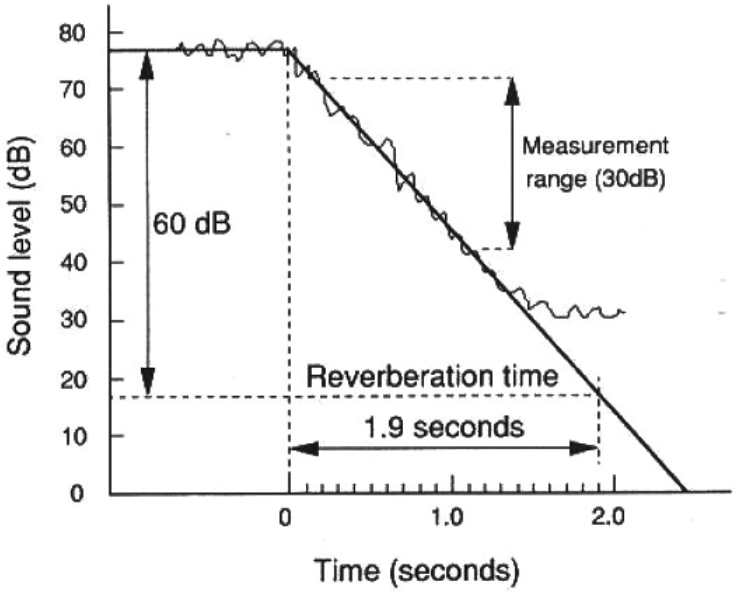

Figure 2.3: Reverberation time definition [3].

For calculating reverberation time in a room, three main formulas are applicable. Sabine's formula, which is the first one, is appropriate for live rooms. The second and third ones are appropriate for dead rooms. These are Eyring's formula and Millington&Sette formula. All of three formulas is appropriate for reverberation time calculation and it is required for a sound field to be a diffuse field [22].

These three formulas are as follows:

1) Sabine's Formula:

T = (0,163 V) / A in seconds, Where, A = the equivalent sound absorption area in m^2 ($= \sum S\alpha_{av}$)

$\sum S\alpha_{av} = S_1\alpha_1 + S_2\alpha_2 + \ldots + S_n\alpha_n$

V = the volume in m^3 S = the surface area in m^2 α = sound absorption coefficient [24].

2) Eyring Formula:

$\alpha_1 \approx \alpha_2 \approx \alpha_3 \approx ... \approx \alpha_n$,

T = (0,163 V) / [-S$\log_e$ (1 -α)] in seconds. Where, $\alpha = \sum S\alpha_{av}$ / S

3)Millington & Sette Formula:

$\alpha_1 \neq \alpha_2 \neq \alpha_3 \neq ... \neq \alpha_n$,

T = (0,163 V) / [$\sum$ -$S_n \log_e$ (1 - α_n)] in seconds [22].

Sound Absorption Coefficient (α)**:** The sound absorption coefficient defines the ratio of incident sound energy absorbed by a material. It depends on the frequency. This coefficient value theoretically differ from "0" (no absorption of sound energy) to "1" (perfectly absorption including all incident sound energy) [23].

Sound Transmission Loss (dB): TL is a measure of how much of a reduction in the transmission of sound energy through the material. It is measured in decibels (dB) [23].

Speech Transmission Index (STI): An objective measurement method for estimating speech intelligibility [25]. The range of rating is between "0" and "1". "0" refers to bad intelligibility and "1" indicates excellent intelligibility.

2.2 Sound Absorption Coefficient Measurements

There are different techniques for measuring sound absorption coefficient values. Two of them are commonly used, which are reverberation room method and impedance tube transfer function method. Reverberation chamber testing standards are based on ISO 354:2003 and impedance tube measurement follows ISO

10534-2:1998.

2.2.1 Reverberation Room (or Random Incidence) Method

It is one of the most commonly used techniques for testing sound absorption coefficient values of a material. The shape of the room can be cubic or rectangular room[26]. The diffusivity existing in the chamber is crucial for the reliability of tests. A room requires two main features to be considered as diffuse. These are: manufacturing uniform local energy density and having uniform incident energy from all directions onto the surface [4]. Fig. 2.4 exemplifies transparent diffusers hanging from the ceiling and shows the atmosphere of a reverberation room.

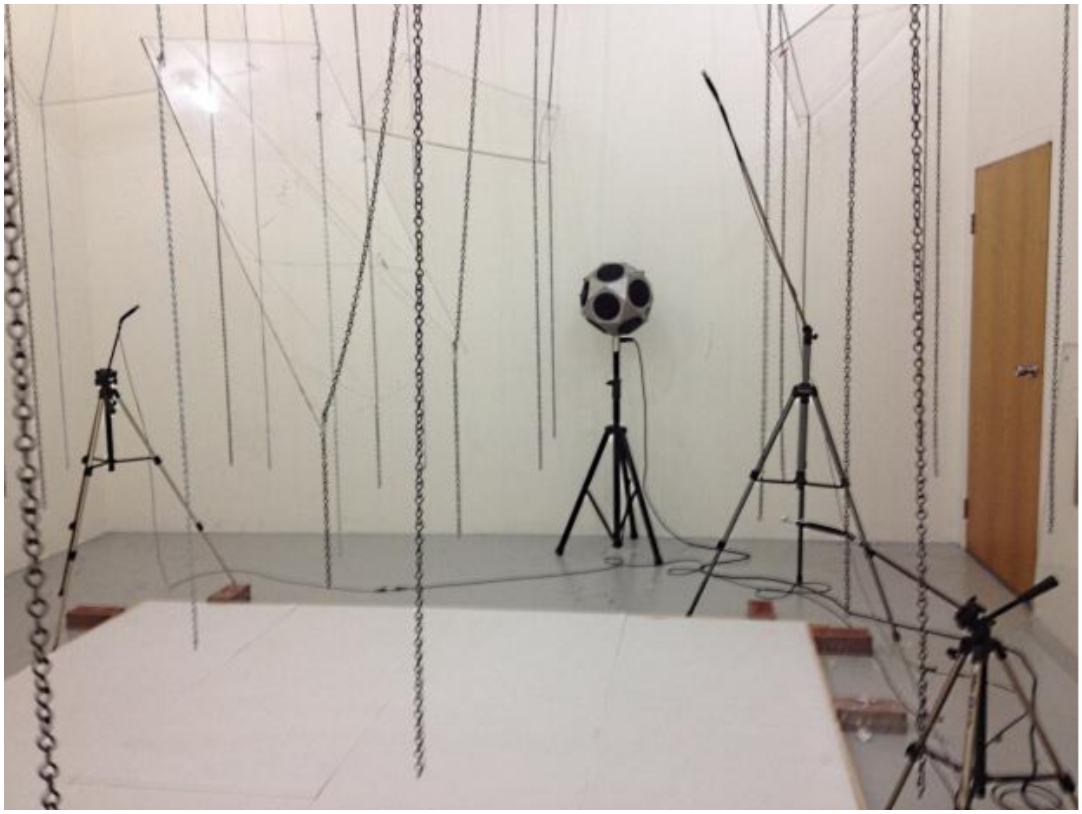

Figure 2.4: A photography showing reverberation room measurement set-up [4].

There are some differences between the standards of specimens depending on

their types. For example plane absorbers should have an area between $10m^2$ and $12m^2$ within the room. If it is a discrete sound absorber, such as chair, it should be placed in the room as in practice. There sould be at least 1 m between the sample and any boundary, microphone and room diffuser [26].

For testing the reverberation time of the room, there should be a minimum of 1,5 m distance between each microphone position and all of them should be 2 m away from any sound source. Microphones are also all be 1 m apart from any room surface, and test sample. Each sound source position should be at least 3 m apart from each other and the directivity of the sources necessitates to be omnidirectional. The avarage reverberation time in the reverberant chamber is tested with and without absorber material within the room. For measurements, temperature and relative humidity are effective factors too [26].

2.2.2 Impedance Tube Transfer Function Method

Impedance tube measurement method includes two microphone locations and an analysis system of digital frequency for estimating normal incidence sound absorption coefficient of sound absorbing materials. This transfer function method theory is based on 10534-2:1998 standards. It is additionally used for estimating surface admittance of sound absorbers or impedance of acoustic surface. This testing method is useful to develop a product and have advantages for basic research because physical properties, such as porosity, density, airflow resistance and elasticity of a sound absorbing material have impacts on the impedance ratios of the materials [27].

For testing an absorptive material in impedance tube, the test sample placed in the tube at one end and a sound source attached to one end are required. In this measurement technique, a noise source generates the plane waves in the tube. The interference area decomposition is obtained by the testing of acoustic pressures which are fixed at two locations by using an in-tube traversing microphone or microphones that are mounted to the wall [27]. In following chapters, this method is explained and detailed more since it is used in the scope of this study. When

considering the outcomes of the impedance tube method, this technique provides cost efficiency and also leads to a reduction of time expected through the product development of a new variety of material by producers [4].

2.3 Metamaterials (MMs)

Trends in materials applied in different fields change with advancing technology. Metamaterials are rationally man-made structures with sub-wavelength components organized periodically or non-periodically [28, 29, 30, 31] and they show supernatural behaviour [32]. In other words, metamaterials are engineered materials consisting of small meta-structures with non-traditional effective properties [33]. Studies on artificial structures commenced with phononic [34] crystals analogous to the photonic [35] crystals used in optics. Metamaterials, acoustic or electromagnetic, have recently been handled by many researchers as a new technique to realize wave propagation models that are impossible to reach by using regular composite materials [36, 37, 38].

Electromagnetism is a research field in physics including the electromagnetic force and shows the electrical interaction that physically happens between charged particles [39]. It has been fundamentally investigated in metamaterial. This area of research has mainly begun in Veselago's research on electromagnetism in 1968. Veselago introduced a different perspective to material research by asking what happens when both a material's electrical and magnetic permeability is negative. He claimed that this would cause both backward wave and negative refractive index. According to Veselago, if both material constants are negative, the refractive index shows negative behavior and therefore the refraction is observed as negative. [40]. Until his suggestion, a material was believed to exhibit only a positive index of refraction, as can be found in nature. Shamonina and Solymar described this study more detailed in their research [37]. Three decades later, Smith et al. [41] proposed a fabricated material that can generate negative permittivity and negative permeability in the same frequency band. They demonstrated experimentally that electromagnetic waves cannot travel in an environment where one

of the material constants is negative, and propagation is rebuilt only if both are negative. In an experiment by Smith et al. [41], they emitted an electromagnetic wave at a frequency of 10.5 GHz on a negative index prism, and the direction of the refraction occurred extremely unusual, which is negative/opposite side of the boundary (Fig. 2.2), although the refraction was as naturally expected. If the refractive index was taken negatively, the angle of refraction is in line with Snell's law.

As a result of the studies [30, 41, 42] , although the possibility of a negative refractive index is emphasized, the applications are not sufficient in practice. Pendry's "perfect lens" study stated in 2000 resolved this deficiency [43]. This is related to the probability of perfect imaging manufactured. Different from the conventional materials, he introduced a metamaterial having thin slab with the negative refractive index for "perfect lens" including all details perfectly. Because of the limit of lens' diffraction, a traditional lens is not able to focus light to a field less than a square wavelength. The reason for this limitation is that, as the scale gets smaller, the disappearing waves decrease exponentially, and these waves carry the object's sub-wavelength details. Therefore, these fine characters are not visible in the image and loss occurs. Nevertheless, with the help of a metamaterial with a negative refractive index, "perfect lens" is able to focus propagation waves. In addition, it can generate sub-wavelength imaging by amplifying disappearing waves.

These research are fundamental ones conducted on metamaterials and after these former research, studies on metamaterials have accelerated and the interest on metamaterial research have increased. Then, electromagnetic (EM) metamaterials have reached a significant progress since the beginning of metamaterials [44, 45, 46]. Due to the similarity between light and sound waves, electromagnetic and acoustic metamaterials have the same design freedom, but there has been less progress on the experimental data of the study on acoustic waves.

Associated with unusual properties of electromagnetic metamaterial, the desired negative refractive index can be obtained by negative values of permittivity and permeability and these values provide double negative materials as discussed

above [40]. Different from electromagnetic metamaterial, in acoustics, negative refractive sound waves can be achieved by negative bulk modulus and negative mass density, which creates double negativity in acoustic metamaterial (AMM). Thus, the studies on AMM mainly focus on negative material properties, bulk modulus and mass density as presented in the following section.

2.4 Acoustic Metamaterials (AMMs)

The attention on acoustic metamaterials (AMM) has initially raised due to their extreme properties in either sound absorption or transmission loss in specific forms and configurations. AMMs have great performance than many traditional 'acoustic materials.' Moreover, depending upon the selected base material, produced AMMs can be relatively more hygienic, lighter or thinner, can vary in color as well as transparency to range in between opaque to translucent.

Some conventional acoustic materials have limited performance on manipulation of low-frequency sound waves [47] since they require thick wall/panel sections or heavy materials. Recently, research in acoustical materials has acquired new perspectives as a result of the introduction of metamaterial applications in various fields including acoustic cloaking [48, 49, 50, 51], imaging [52], one-way transmittance [53, 54], focusing and lensing [55] via negative refraction [56, 57, 7] and surface wave manipulation [8].

These new features are often associated with acoustic band gap that can prevent the propagation of acoustic waves. Their actual applications in architectural systems have not been widely employed, yet. The field is still under progress and necessitates more scientific input in that respect. For that reason, this study is motivated by the possible contribution to the current development of acoustic metamaterial (AMM) research with a specific focus on sound improvement and noise control within architectural spaces.

The use of the term 'meta' stems from the unusual properties of designed

acoustic metamaterials. Physical properties like negative mass density, negative bulk modulus and/or negative effective refractive index values result in extreme acoustic performance [58]. In recent research, single negative bulk modulus and negative mass density have been deeply investigated for obtaining different AMMs with double negativity [59, 60, 61]. Many AMMs have been proposed to adjust the effective quantity to these extreme values, including material properties like negative [62] and near-zero values [63], or to obtain high anisotropic density [64]. Locally resonant acoustic metamaterials are of special interest due to their sub-wavelength scale compared to their unit cell sizes. In one of the early studies on artificial AMMs, Liu et al. [5] used silicone rubber-coated spheres for sub-wavelength performance, utilizing a locally resonant construction in a periodic structure to manipulate acoustic waves, although Liu's early work is highly limited by the functioning frequency range. In this study, they produced sonic crystals, the idea of which was localized resonant structures, and the spectral spaces were exhibited by means of two fixed size lattice constants smaller than the corresponding wavelength. Also, the structure of the metamaterial and the materials used are as follows in detail: A basic cubic crystal involves a heavy solid core material which is lead. This lead is covered with silicone-rubber elastomer that is a soft material elastically. Then, it is inserted into a rigid matrix material consist of epoxy (Fig. 2.5). Irregular composites with such localized resonant structures act as a material with a total wave response within certain adjustable sonic frequency ranges and effective negative elastic constants.

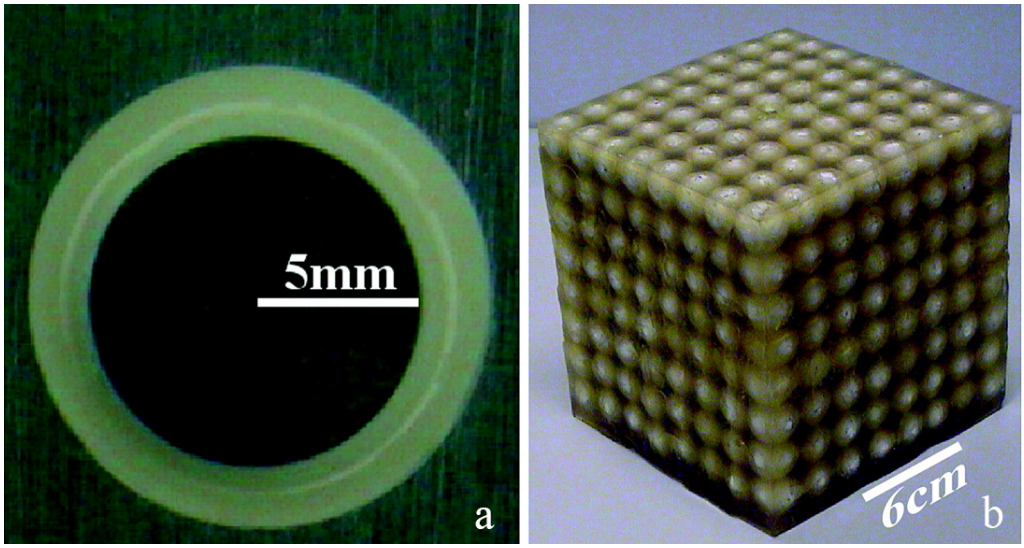

Figure 2.5: a) Cross section of a coated lead sphere that forms the basic structure unit, b) for an $8 \times 8 \times 8$ sonic crystal [5].

Negative density can be stimulated by the local resonance of the structure. Inspired by results obtained in electromagnetics, Fang et al. [65] introduced a novel ultrasonic metamaterial class, generating a series of sub-wavelengths of Helmholtz resonators with designed acoustic capacitance and inductance. These materials, which have an effective dynamic module, also have negative values and these values are close to the resonance frequency. To conclude, these experimentally observed ultrasonic metamaterials can ultimately carry acoustic waves with a group velocity anti-parallel to the phase velocity. Other new AMMs which have emerged include perforated plate-type AMMs [48, 66], space-coiling-type AMMs [55, 56, 7, 8, 67, 68, 69] (explained in the following paragraphs in detail), and membrane-and-plate-type AMMs [62].

One of the first studies on membrane-type AMMs is by Yang et al. [70], who proposed manipulating the sound waves in the low-frequency range between 50 Hz and 1000 Hz by ensuring negative mass density in the band gap. They provided clear experimental evidence that the transmission at minimum level was achieved when the area average of membrane pulse was zero. A broadband sound shield was investigated to incorporate simple stacking of membrane-type metamaterials

operating at different frequency regimes. Some advantages of membrane-and plate-type AMMs are that they are generally lightweight structures and thus desirable materials for the aerospace and automotive sectors, where performance and weight are both important. Their geometrical forms are less complex than those of other types of AMM (Fig. 2.6), and their effective density can be optimized easily [6].

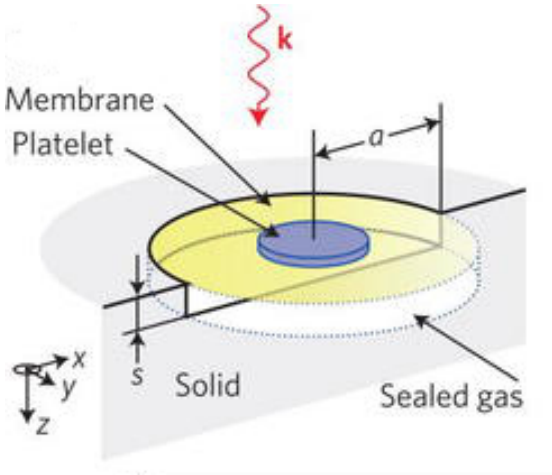

Figure 2.6: The schematic structure of the ultrathin membrane-type AMM (meta-surface) [6].

Another group of AMMs embodies the labyrinthine or space-coiling approach, which helped to stimulate this study. With coiled-up spaces, it is possible to create efficient geometrical configurations. Research has shown that AMMs of this type offer several benefits such as including a remarkable degree of sound absorption due to the isotropic response related to their highly symmetrical nature [69]. One of the very first studies on space-coiled acoustic metamaterials is by Liang and Li [7]. By applying curled perforations, they extended the transmission pathway that sound waves follow inside the material to make it much longer than the external dimensions. Such a structure has folding of band in an effective environment regime, without the need to utilize a local resonance structure with sub-wavelength. This principle also applies to three dimensions. As a result, double negative prism and tunnelling with a density of material close to zero value, providing negative refraction were shown numerically (Fig. 2.7).

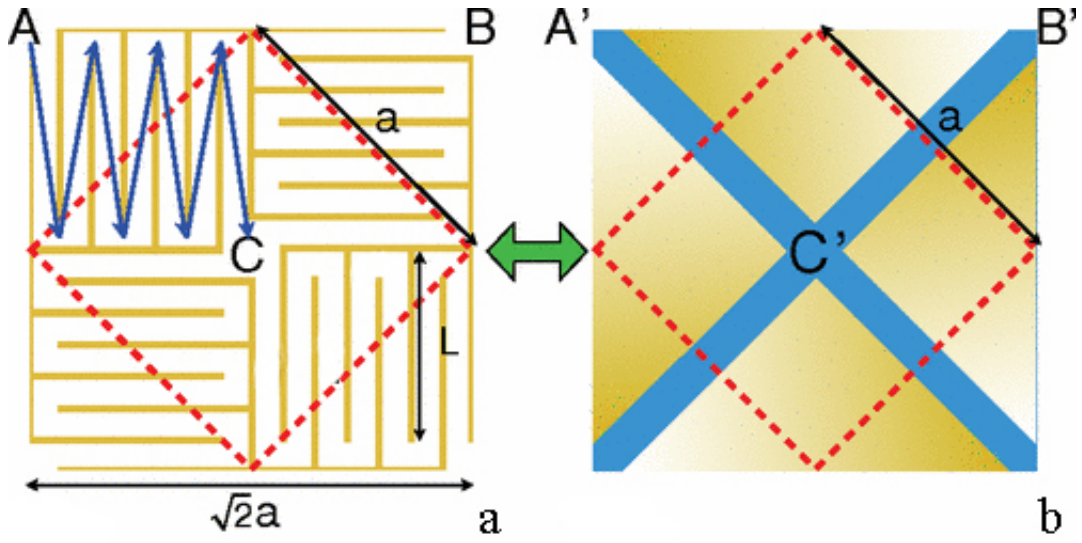

Figure 2.7: a) Schematic diagram of metamaterial-repeating units in coiling up space. The connected arrows show the zigzag path of the propagation of acoustic waves, b)the simplified view with straightened channels [7].

Xie et al. [8] demonstrated by experiment that the acoustic metamaterial of a suitably designed labyrinth could achieve a wide frequency range of the negative refractive index (Fig. 2.8). They used two different ways to demonstrate the negative index nature of the metamaterial. These are as follows: the first one is 1D extractions of effective parameters resulting from transmission and reflection measurements. The second way is 2D prism-based measurements which present the angle of transmission related to negative refraction. The angles that arise as a result of these situations also match well with the refractive index observed in numerical simulations and 1D measurements. Also, one of the expectations of authors by doing this study is that this maze structured metamaterial is to make unit cell preferable for practical acoustic metamaterial devices which necessitate negative refractive indices and broadband.

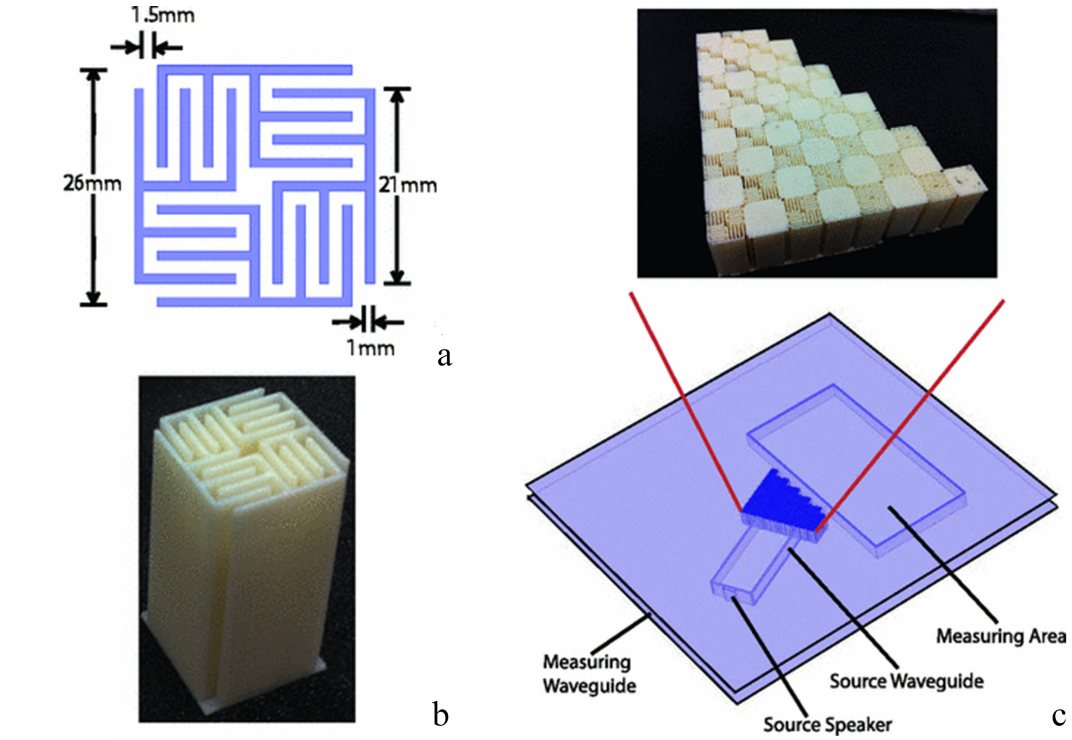

Figure 2.8: a) Section of AMM structure, b) 3D fabricated unit cell of AMM module, c) photography of 55 identical labyrinthine unit cells placed as lattice structure for the experiment (on the top), and 2D experimental setup for measurements [8].

Frenzel et al. [9] made possible the transition from two-dimensional labyrinth-type metamaterials to three-dimensional ones with the objective of devising a broadband all-angle acoustic absorber. In this study, an acoustic metamaterial that is almost isotropic and 3D airborne labyrinth type was designed and produced. The research is based on recent experimental and theoretical studies in two-dimensional form of acoustic metamaterials. The metamaterial module proposed in this study includes 6 layers which have openings on either at corners or at the center as shown in Fig. 2.9. Apertures define the sound pathway because the sound inside of the module travels through the air-gap. As a result of the experiments, structures consisting of aluminum, exhibit group velocities and phase approximately 8 times factor over a wide frequency range of 1 to 4 kHz, which is smaller than air. This performance is compatible with calculations of

3D band-structure, involving first and higher bands.

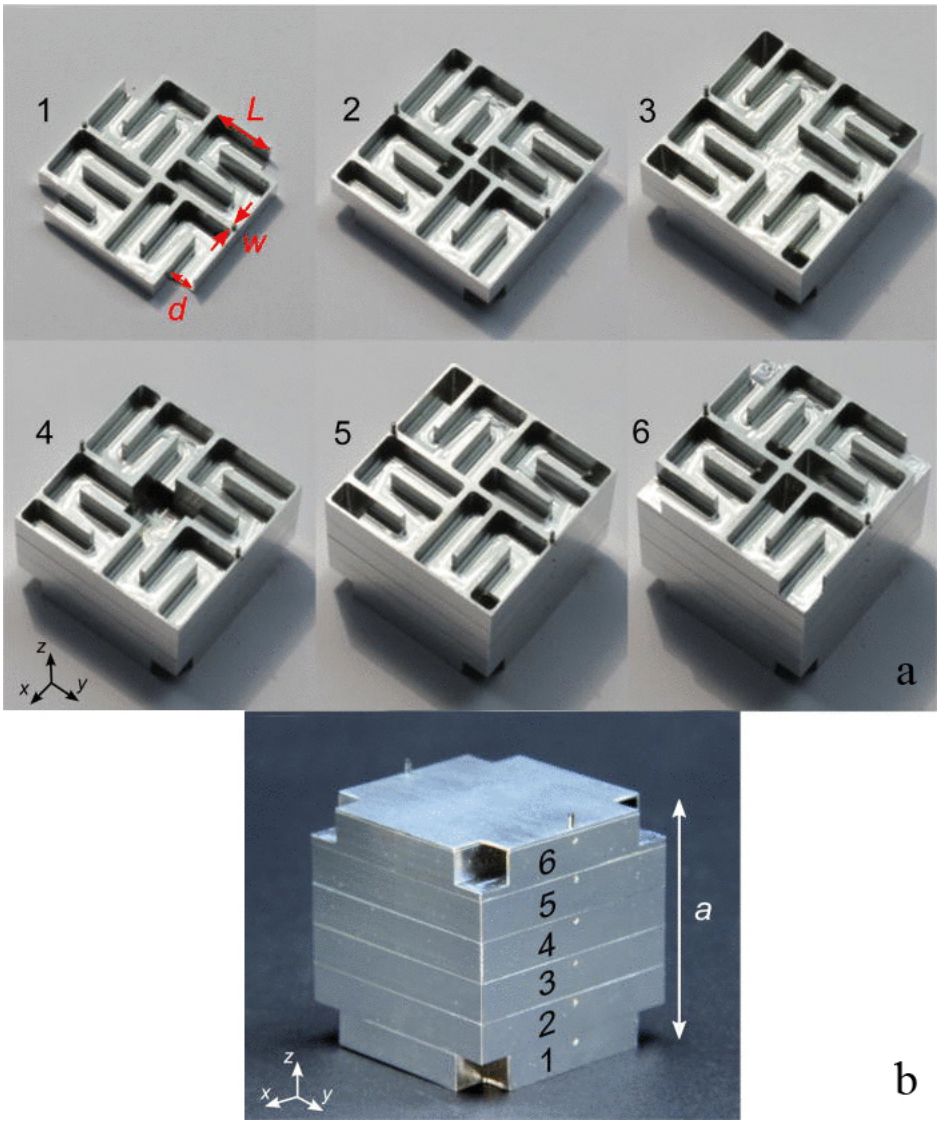

Figure 2.9: a) Photographs of six different layers of one 3D labyrinthine type metamaterial extended unit cell. The dimensions of the unit cell: a=2,4 cm, channel width d=0,32 cm, wall width w=0,08 cm, and wall length L=0,8 cm. b) photograph of one unit cell made of aluminium [9].

Krushynska et al. [71] proposed spider web structure and they argued that particularly, labyrinthine type AMMs perform extremely high wave reflectivity.

They also showed multiple fabricated resonant modes stemming from the special-designed topological structures and conical dispersion. For supporting their idea, a new type of LAMM (Labyrinthine type Acoustic Metamaterial) was developed in this study, inspired by the structure of natural spider webs and to have hybrid sound wave manipulation features. They observed that Mie resonances were adjusted to lower frequencies and extended the band gap size by almost four times, while maintaining architectural dimensions with the help of the asymmetry of the typical structure of natural spider webs. They showed that in order to extend the practicality of the metamaterial, the predicted insignificant structural modification of square frame placement was possible by changing the dynamics inside and outside the band gaps. In another study by Krushynska et al. [10] aimed to analyse two alternatives that depend on the use of coupled and interactive resonators in absorbent panels by reducing panel thickness. They numerically showed that a peak absorption can be changed to a broadband absorption, while it is possible to provide broadband at the various frequencies with the use of coupled resonators. The idea of proposed compositions is based on old Slavic culture pattern. Particularly, these ornaments (Fig. 2.10a) have hidden meanings and this anonymity of them has been taken as inspiration. It is an a significant vision in AMM design to include aesthetic concerns for using an artistic figure as a design notation (Fig. 2.10).

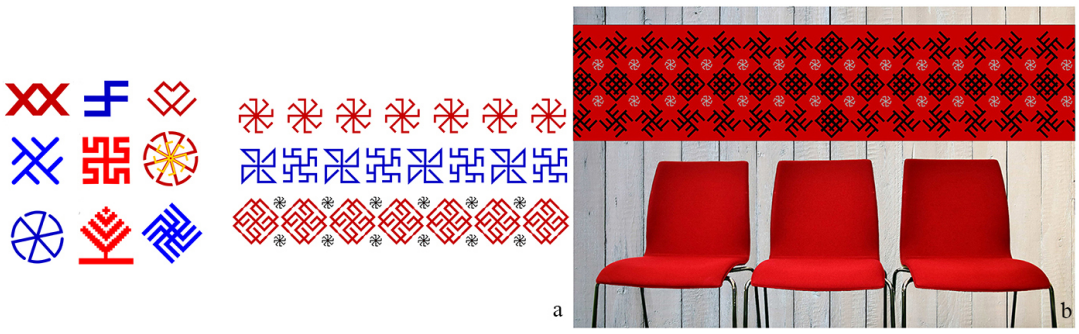

Figure 2.10: a) Symbolic examples of Slavic ornaments, b) metamaterial example applied in a room [10].

In general, space-coiling acoustic metamaterials can achieve adjustable operating frequency by varying the number of curls for higher reflection [69]. The metamaterials incorporating space coiling in their 3D labyrinthine type structures utilize a zig-zag movement to increase the efficient sound path, as zig-zag movement leads to wave-front manipulation [68] and extreme acoustic transmission [7, 9]. In addition to the zig-zag path, the clockwise-anti-clockwise direction has been shown to be effective in reducing the energy of sound waves. Liu et al. [11] proposed a Spiral and Labyrinthine Acoustic Metamaterial (SLAM), with transmission path in this form, which is considerably different from the zigzag path. They were able to cut off the sound waves in the waveguide effectively by forcing them to propagate alternatively through the path in a clockwise direction and an anticlockwise direction (Fig. 2.11).

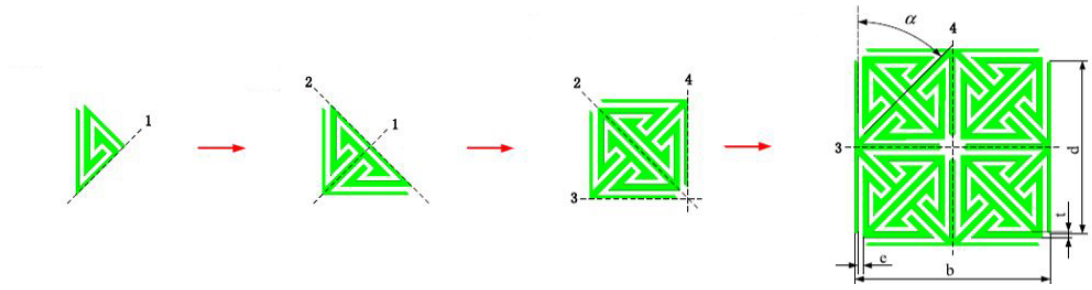

Figure 2.11: Design Steps of SLAM proposed by Liu et al. [11]

A study done by Godbold et al. proposed a novel sound absorber based on the principle of Passive Destructive Interference (PDI) (see Section 4.2.2), addressing its technical performance, its manufacture and its design for room acoustics applications. Their findings showed that the original absorber they proposed might constitute a desirable alternative to the conventional Helmholtz resonator since the Helmholtz device requires a bulky cavity to operate, while the novel absorber needs less space [72]. In another study making use of PDI, Setaki et al. compared experimental and analytical estimates of a material containing cylindrical structures of different lengths. They investigated the sound absorption by systematically changing the inner geometry of the tubes with a view to developing an effective acoustic element for use in architectural spaces [73].

2.5 Bio-mimicking

Although AMMs are named after their 'beyond nature' characteristics or proportions, the limits of nature are not fully known and there is considerable potential for abstracting forms and ratios from nature and making use of them. Another major source of inspiration for this research, therefore, is biomimicry. Many researches have been studied on biomimicry in other fields like Superhydrophobic surfaces [74, 75, 76, 77]. One of them is done by Liu et al. about improvements of utmost wettability existing in nature and bio-mimetic examples, and concentrating on surface wetting performance beyond nature, which means surface wetting properties are artificially made [78]. In parallel this research, the main idea of presented study is to create features that cannot be found in nature by inspiring from the existing ones.

There are also many studies on biomimicry in material science and architecture. For example, spider web geometry [58] provides a strong fiber net, even stronger than steel, and has a lightweight structure. For this reason, it is frequently preferred in applications where both strength and light weight are critical, such as bulletproof vests or aerospace structures [13]. As shown in Fig. 2.12, the golden ratio is found in nature in flowers, various fruits, vegetables, plants and ferns, spiral leaves, shells, fish, body parts of ants and human beings, the physical universe, architecture [12]. This caught the attention of many scientists, architects and industrial designers in recent decades, especially in the form of the golden rectangle. Lastly, honeycomb structures, which are frequently used in metamaterials [79], are also a product of biomimicry. They are both strong and light in weight and have an optimal packing shape with their hexagonal cellular units. For these reasons, honeycomb structures are widely used in aircraft control surface [13].

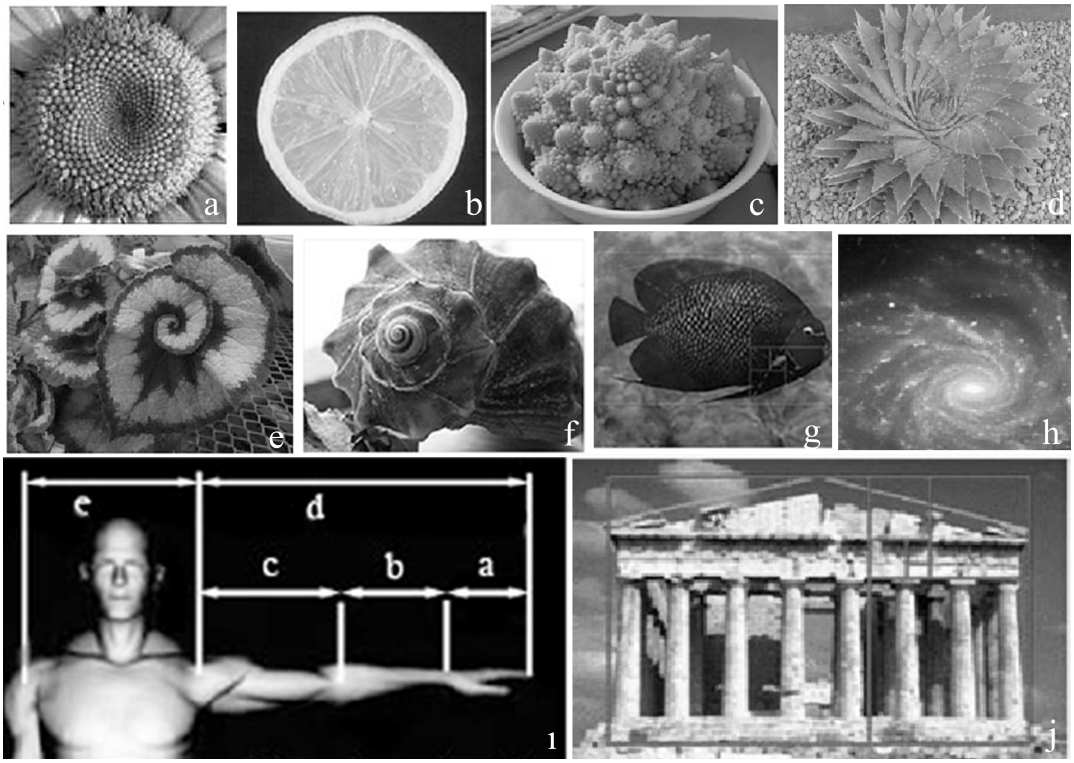

Figure 2.12: Golden Ratio examples existing in nature: a) A sunflower, b) orange with ten sections grouped into five, c) Romanesco Brocolli d) a cactus e) spiral leaves of orchid f) a garden snail g) blue angle fish h) galaxy ı) human hand and shoulder j) Parthenon [12].

Origami [80] -paper folding- structure is also another inspirational idea for AMMs. The structure is not only aesthetically pleasant, but also provides transformable mechanical materials, which is desirable for AMMs. Many researches on AMMs inspired by origami are in 2D folding patterns [81, 82]. In addition to this, re-configurable 3D metamaterials involving several extruded polyhedra are also efficient for redirecting and controlling sound waves [83].

The main use of biomimicry in this study is to design features that may not be found in nature exactly but are still inspired by and abstracted from existing structures. Ratios and forms from nature are utilized on a sub-wavelength scale, similar to locally resonant metamaterials, within the 3D space coiling and 3D labyrinth approaches to AMM design. The design proposals have their origins

in the golden ratio (GR), web-labyrinthine (WL) forms, genetic and neural systems such as DNA molecules, and the synapse structures in the brain, as will be discussed in detail in the following sections.

2.6 Thesis Statement and Contributions

AMMs have attracted the attention of researchers in various fields, and new designs and classes of material are being introduced continuously. In the field of architectural acoustics, however, AMM research is still very new and much more experimental and theoretical investigation is needed for possible real-case applications. This study is motivated by the idea of employing novel design tools for the development of AMMs with a specific focus on sound improvement and noise control in architectural spaces. Architectural applications pose challenges since parameters such as aesthetic appeal, design flexibility, fire-resistance and hygiene need to be satisfied in addition to acoustic performance requirements. The study seeks to optimize the performances of space-coiling type AMMs in terms of sound absorption and transmission loss at low-frequencies, which is a problematic range in room acoustics, mainly by adjusting the geometry of the inner structure of the proposed AMMs. A semi-transparent base material resin is selected for manufacturing, exposing the inner design and offering potential for light and color integration.

According to studies in the literature, AMMs have the potential to control the sound in a broadband low frequency spectrum. It is concluded that they provide efficiency in both sound absorption and transmission loss in many types of AMMs and in this study, the space-coiling type is investigated. It is aimed to optimize performances at low-frequency range in terms of sound absorption and sound transmission loss mainly with the geometry of the structure. In this research, both aesthetic and acoustic concerns have been taken into account in developing AMM proposals for architectural applications. These proposals are named as golden ratio (GR), web-labyrinthine (WL) and DNA. Modules of the sample materials designed are then manufactured in a 3D printer. These manufactured

AMM units are subsequently tested in an impedance tube to obtain their normal incidence sound absorption coefficients and transmission loss characteristics in the frequency range below 1 kHz. Finally, in order to evaluate the effectiveness of the proposed AMM modules in a real-life acoustical design problem, two architecture studios are tested in their existing states and simulated with and without the AMM applications.

Chapter 3

Design and Production

3.1 Design

In the light of the potentials of biomimicry, the design ideas used in this study have been taken from the golden ratio (GR), web-labyrinthine (WL) forms, genetic and neural systems such as DNA molecules & the synapse structures in the brain as detailed in the following sections. The abstraction of the original forms and their transformations into final outputs are presented in Fig. 3.1, 3.2, 3.3, Fig. 3.4, 3.6, 3.5 and Fig. 3.7, 3.8, 3.9 for three different AMM design proposals. The sample units manufactured are limited in size to a diameter of 10 cm due to the impedance tube measurement set-up.

3.1.1 Golden Ratio (GR) Module Design

The potential of the golden ratio as an acoustic cavity in a Helmholtz resonator arrangement is integrated here with the space-coiling principle used in AMMs. Thus, the first module is inspired by the Fibonacci sequence (Fig. 3.1a) and the proportions are applied to a spiral cavity at its central aperture. The form of the golden ratio is created using appropriate codes on a plug-in named Grasshopper

3D that runs within the Rhino 5 architectural software.

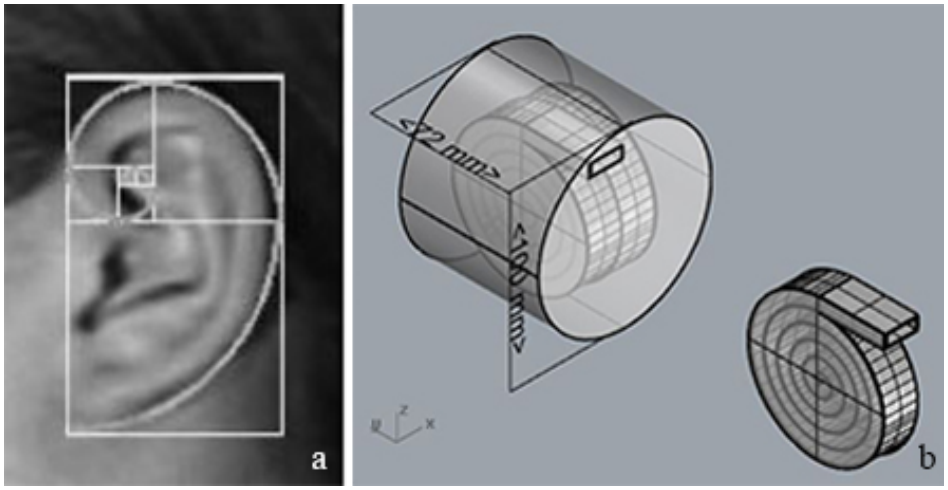

Figure 3.1: a) Golden rectangle and golden spiral on-ear [12], b) 3D model of GR-AMM prototype placed in a solid cylindrical module.

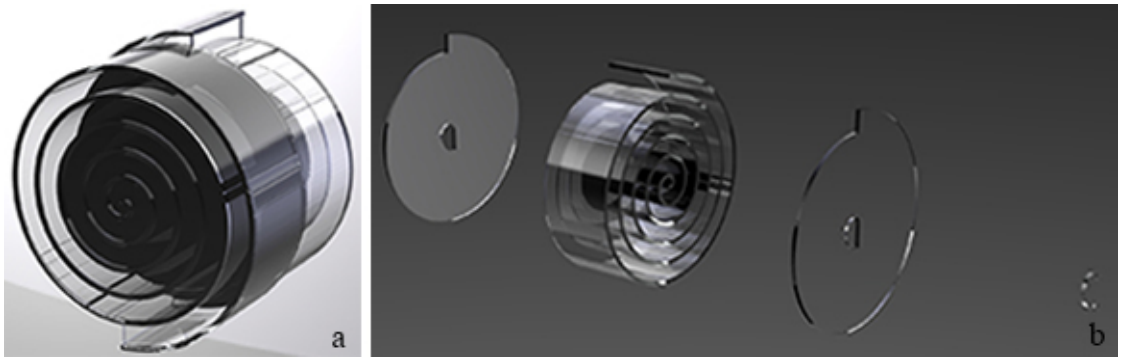

Figure 3.2: a) 3D models of two units attached at their centers, b) 3D rendering of the exploded axonometric unit.

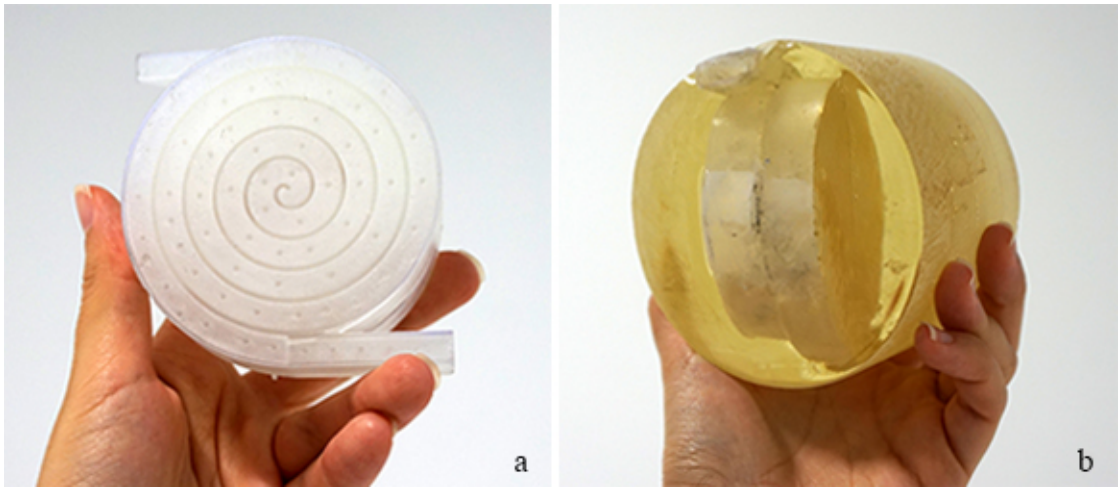

Figure 3.3: a) Inner structure of sample GR unit manufactured in the 3D printer, b) molded GR unit ready for measurement.

The GR system fundamentally consists of two identical units located side by side and attached to one another, with one opening on the opposite surfaces of each unit. Thus, a module contains two units of a single type, and these are placed in such a way that one unit is rotated 180 degrees along the y-axis to the other (Fig. 3.2a). The spiral systems of the two units are connected at the center by an internal opening on their intersecting surfaces. The central aperture has the geometry of the golden ratio. The voids switch to a spiral form in the direction of the outer shell of the structure after three cycles of the Fibonacci Sequence have been completed at the aperture. The path of the inner void starts on one side of the first module, connects to the second module at the inner center, and ends on the other side of the second module (Fig.3.2b and 3.3a). The GR sample is 10 cm in diameter and 7.2 cm in depth (Fig. 3.1b). The length of inner void is 1.527 m.

3.1.2 Web Labyrinth (WL) Module Design

The second proposed AMM is named the web labyrinth (WL) system. The design idea has its origin in the spider's web in nature (Fig. 3.4a). The silk net woven by spiders in a two-dimensional form is inherently very strong due to the tensile properties of its geometry. When the spider's web, which is created in 2D, is extrapolated to 3D, the web itself becomes a mass, and the voids form the paths along which sound waves travel (Fig. 3.4c).

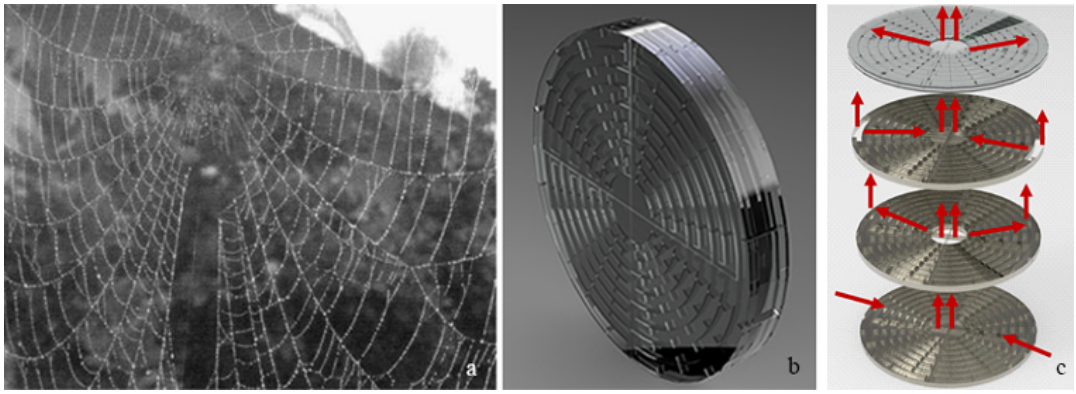

Figure 3.4: a) A spider's web as it exists in nature [13], b) WL 3D models, c) exploded unit indicating apertures on the sides and at the center and showing sound pathway.

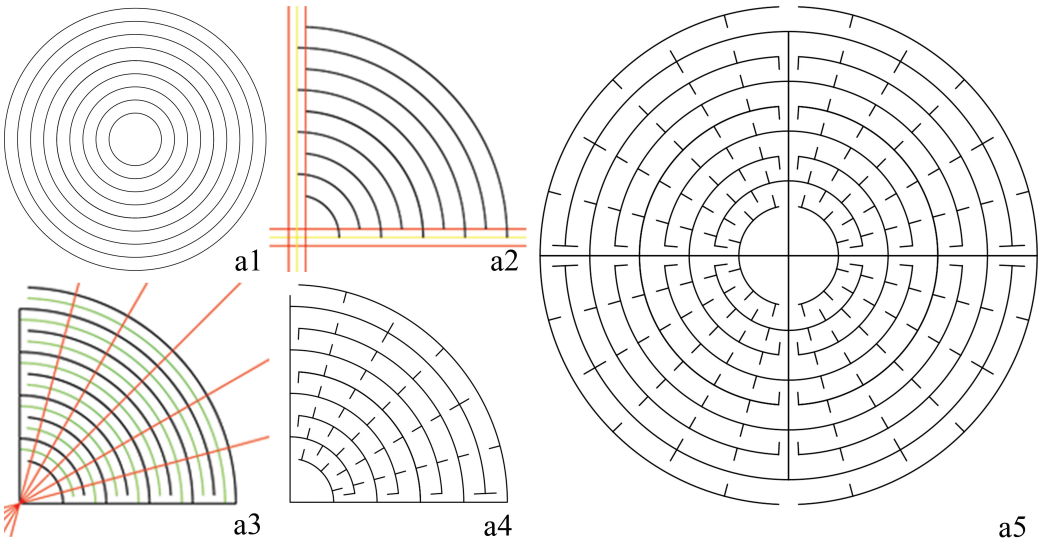

Figure 3.5: Plan drawings showing the phases of the WL design.

The abstraction of the WL proposal and the development of its design consist of the following steps. Firstly, a circle 8 cm in diameter is taken and offset 4 mm inward several times to create concentric circles. Secondly, one-quarter of the circle is cut out. Rays are then introduced 15 degrees apart, and small masses are repeatedly placed along these rays in such a way that the distance between each mass in the same cavity with the corresponding mass in the same axis is 1.5 mm. Then this quarter-circle segment is mirrored to make a semi-circular segment, and the semi-circular piece is in turn mirrored to form the full circle back again. This constitutes the first layer of the WL module (Fig. 3.5).

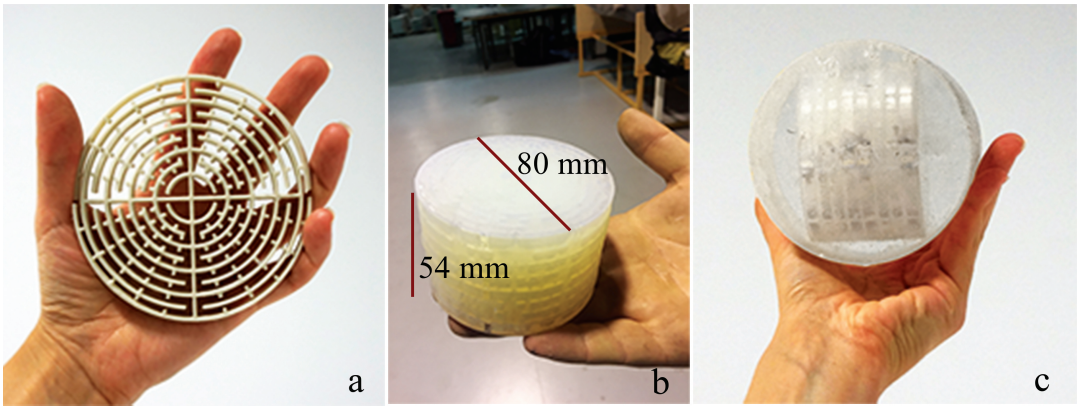

Figure 3.6: a) One typical layer of the printed inner structure, b) one manufactured unit combining eight layers in actual size, c) epoxy molded sample ready for measurement.

Unlike the GR proposal, the WL unit has a multi-layered structure. In total there are four types of layers. Two of them have openings on the sides and the other two have openings at the center. The openings enable each layer to connect with the two adjacent layers above and below it (Fig. 3.4c). Two layers of the same type are not permitted to overlap: each layer must be different from the one below it and the one above it. The junctions in the central parts of the units are for extending the path and for coiling up the sound waves. There is no limitation on the number of times the layers can be repeated, so the depth of the module is adjustable. The 3D-printed unit has a depth of 8 cm and there are eight layers with a total width of 5.4 cm (Fig. 3.6b). The final output, with outer parts of the web filled with resin and ready to test in an impedance tube, has a diameter of 10 cm and a depth of 8 cm (Fig. 3.6c). The length of inner void is 10.068 m.

3.1.3 DNA Module Design

The third proposed AMM module is the DNA module. The idea is taken from natural transmission systems, such as the spiral structure of DNA that provides for the transfer of genes (Fig. 3.7a). The spiral form serves to extend the path

that the sound waves travel, as intended. The multi-directional/branched structure of synapses, which allow for the transmission of senses in the neural system (Fig.3.7b), is used in the sample AMM to divide the sound pathway into two tubes, thus further reducing its energy. This is why the DNA specimen has more than one tube. Finally, the semi-spherical parts of the DNA unit, with their apertures, have their origins in the spherical structure of the nodes that connect the particles in a molecule structure including atomic particles (Fig. 3.7c). The specimen prepared for measuring in the impedance tube is 10 cm in diameter and 9.5 cm in depth (Fig.3.9a). The length of inner void is 65.8 cm.

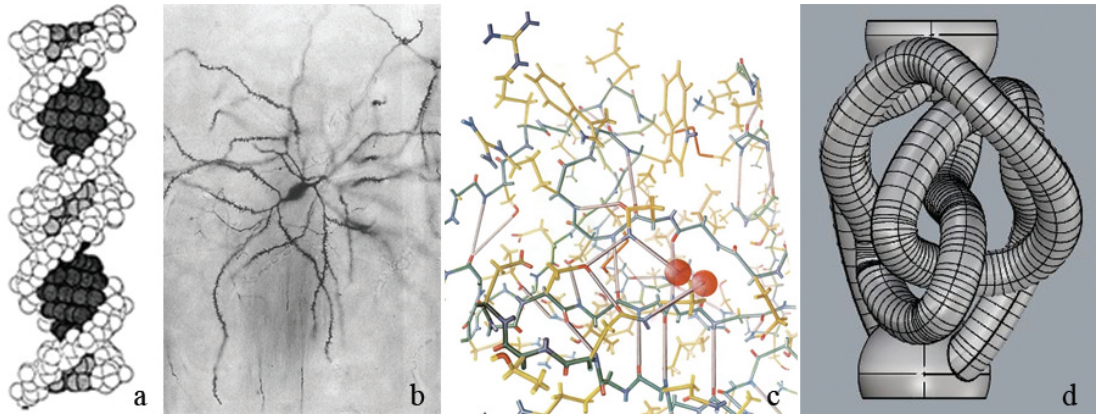

Figure 3.7: Examples of a) DNA [14], b) Synapse [15] c) Molecule [16] structures reflecting the idea of bio-mimicry, d) DNA module top view.

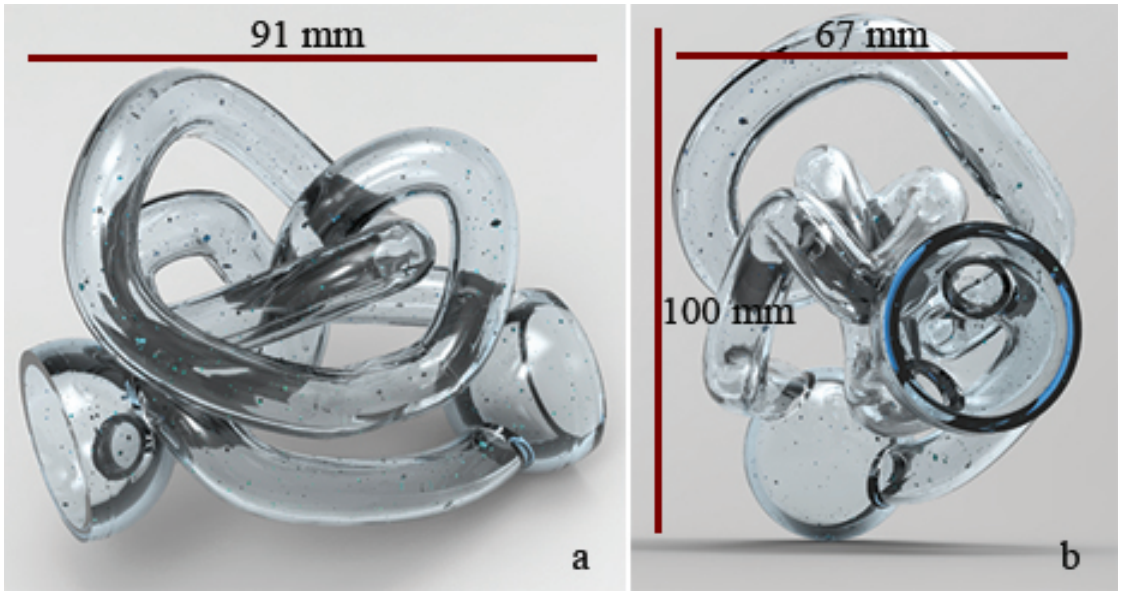

Figure 3.8: Dimensions of, a,b) 3D Models of DNA module.

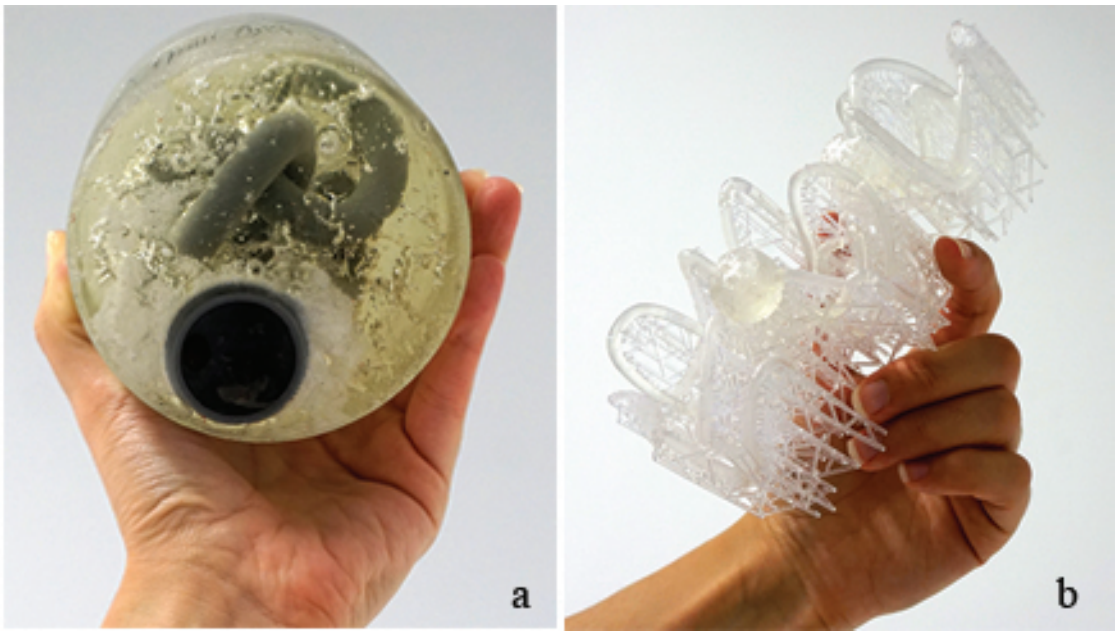

Figure 3.9: Examples of, a) molded sample ready for measurement, b) a faulty 3D print result.

In the designed structure of the DNA module, as shown in Fig. 3.8, the openings on the opposite sides are approximately hemispherical. The tubes have a diameter of 10-13 mm, as the manufacturing tool available for this piece of research is not sensitive in dimensions of less than 5 mm. Due to the limited sensitivity of the equipment used, several unsatisfactory results were printed initially (Fig. 3.9b). The design and manufacturing process continued until the diameter of the pipes could be optimized and a reasonable end-product obtained.

3.2 Production Process

3D labyrinthine type metamaterials, which are new materials in the field of acoustics, apply some principles as of manipulating the sound waves and creating complex structures. Also, they will be used in an architectural application and they provide many solutions for aesthetic problems with their designed architecture. For the novel proposed products, tube measurements show the potential for estimating the performance of the materials in practice. Therefore, the improved alternatives should be printed again and enveloped again. In traditional manufacturing techniques, for example, manual manufacturing, there is no direct connection with the designed product in architectural software and the actual product. While a 3D CNC printer prints out the same model exactly, the manual method is only able to imitate the design product existing in software. Since the scale of metamaterials has a very small complex structure, the exact similarity between the model in 3D software and the model that is actually produced is very important. Besides, there is no need to do any extra work like creating a mold for the real product, so it also saves time.

The actual production of the designed modules depends on the available manufacturing technology. Manufacturing coiled-space materials which use forms like labyrinths and spirals presents difficulties. Many challenges and limitations have been encountered in the fabrication of metamaterials, even when using modern technology that is capable of producing complicated forms. One problem is that a material designed to achieve a certain acoustic performance may not have the

necessary practical or mechanical strength. The costs of the base materials and of access to manufacturing tools may also constitute a challenge. Mass production is also taken into consideration, and modular units are proposed that will make a partition wall or panel system. Classrooms or open space offices are common spaces, where interior design is also a concern.

Epoxy resin, which is the material used, has the desired properties required by the acoustical metamaterial in terms of material properties. It is one of the materials that is close to the optimum values for AMMs naturally in terms of mass density (around 1000 kg/m^3 [84]) and is available to use in 3D printing.

The voids or cavities inside the AMM modules shape the path of the sound, while the solid parts provide the necessary impedance. The cleanness or smoothness of the tubes in spiral and labyrinth patterns are critical for the coiling-up of the voids and hence for the intended manipulation of the sound paths. It is therefore of great importance that the manufactured product should be an exact rendering of the design. Design optimization and production efforts continued until satisfactory end-products were obtained for all three of the AMM modules developed in this study.

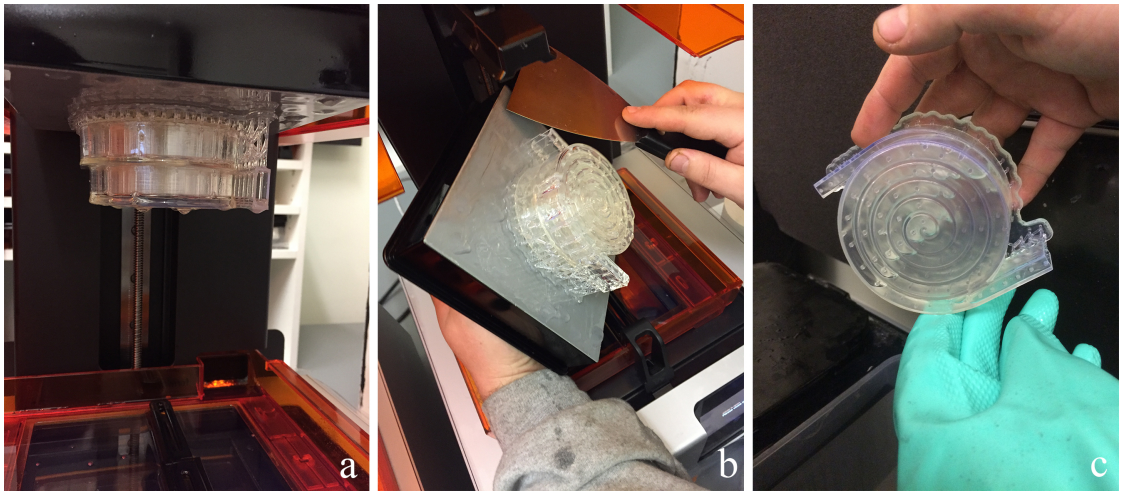

Figure 3.10: Printing phases: a) the output of 3D CNC printing, b,c) cleaning of extra resin outside and inside of the material for preventing any undesired filling.

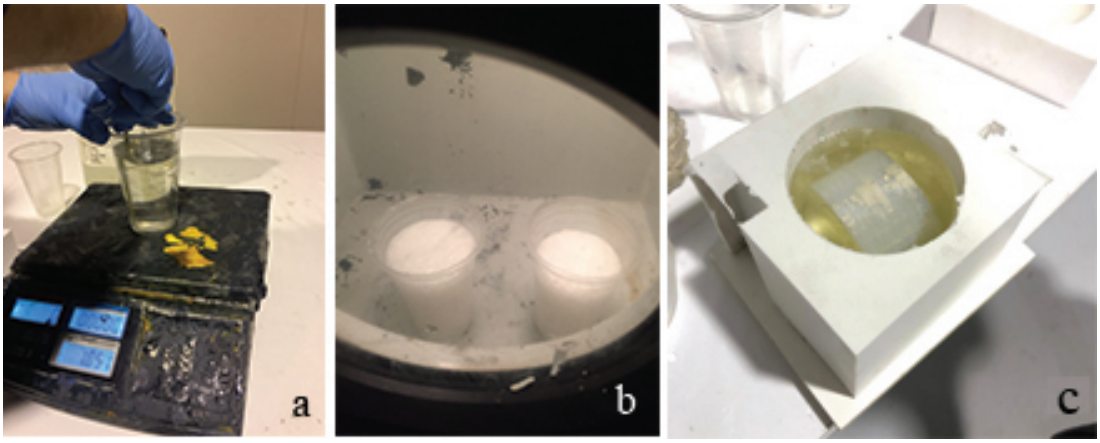

Figure 3.11: Molding phases: a) mixing epoxy with the required amount of dryer, b) vacuuming air to ensure a smooth inner surface, c)epoxy being poured around the 3D printed inner structure and left to dry.

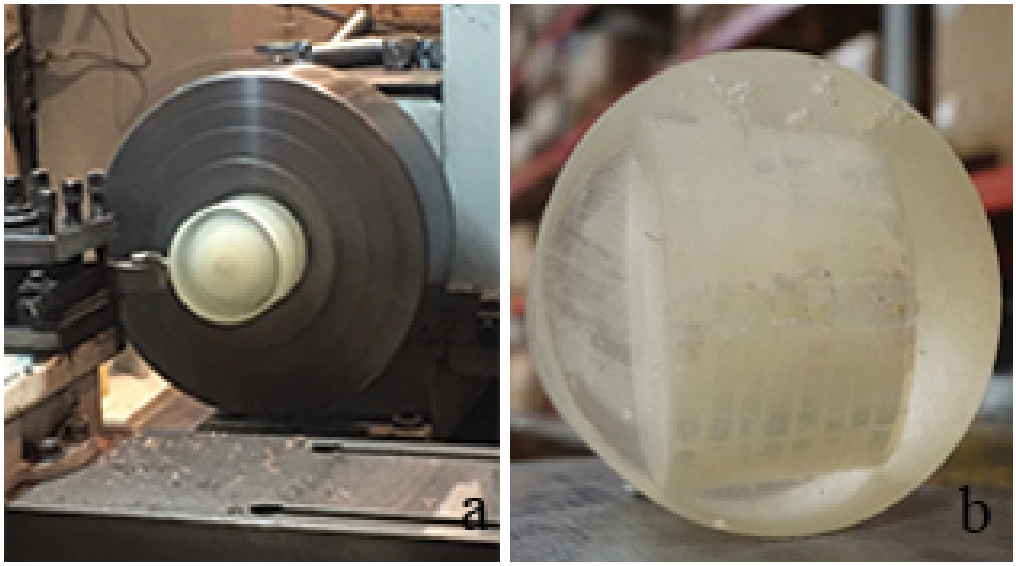

Figure 3.12: Molding phases: a)smoothing the surface to fit the impedance tube exactly, b) AMM prototype ready for measurement.

This study makes use of 3D printing and additive manufacturing techniques to produce units of the proposed AMMs accurately. There are studies in room acoustics [85] and many other fields which apply this method for in-depth scientific

research with prototypes [86, 87]. During the manufacturing process, the inner structures (tubes or void walls) are initially produced by the 3D CNC printer (Fig. 3.10). The AMM modules are finalized through the molding and filling of the outer cylinder, to be fitted in the impedance tube. The apertures on the opposite surfaces are protected while molding. In an actual application, the inner structures would remain the same while the rest of the filled form would be variable, depending on design decisions. Fig. 3.11 and 3.12 present the molding phases of the AMM production process. The main reason for molding the outer envelope of the cylindrical module is to be able to use a less expensive type of resin compared to that used in the 3D printing.

As the following step of printing the inner structures by the 3D CNC printer, the AMM modules are finalized with the molding of the outer cylinder. In production, the sample unit sizes are limited to a 10 cm diameter in width due to the impedance tube measurement set-up. After the first two molding phases, the module is left to dry at room temperature. The time required for drying at room temperature is approximately 24 hours (Fig. 3.11c). If the whole process were completed by printer, the time take by the process would be shorter. The 3D CNC printer would take approximately 12 hours to produce the full form ready for measurement in an impedance tube. However, the project budget would be too higher with this method, so only the inner structure is printed out using the 3D CNC. This production technique could accelerate the process depending on the key factors of resolution, layer thickness, and printing strategy [88].

The shapes formed inside, which is the middle part of the structures, have gaps and fillings in sensitive dimensions by coiling the space for manipulating sound waves. Therefore, it is of great importance that the designed product and the actual model are exactly the same. Among the existing production techniques, as a reliable production technique, where the model and the real product match exactly, is chosen as 3D CNC for these three specimens.

Chapter 4

Acoustical Test and Assessment Methods

In empirical part of this research, impedance tube transfer function method is held for testing the sound absorption and transmission performance of AMM proposals. All tests are done at least 10 times for the reliability of tests. In theoretical part, transmission loss estimations including drywall systems are examined. Also, analytical assessment of sound absorption coefficients of proposed materials are investigated. These assessments are Neckless Helmholtz Resonator and Passive Destructive Interference (PDI) Calculations. Final part of this chapter represents a case study set-up involving field measurements and room acoustics simulations.

4.1 Impedance Tube Measurements and Transmission Loss Estimations

Once the proposed AMM modules have been produced, they are tested in an impedance tube (S.C.S. Kundt Impedance Tubes) to obtain sound absorption

and sound transmission loss values for 1/3 octave bands below 1200 Hz. The absorption coefficient and acoustic impedance measurements are made using a two-microphone transfer function method in line with the ISO 10534-2:1998 standard [27], while the transmission loss measurements are done using a four-microphone transfer function method (Fig. 4.1). The AMM tests in this study are conducted using a Ø100mm tube for measurements in the frequency range from 50 Hz to 1200 Hz. It should also be noted that impedance tube measurements can only provide normal incidence absorption coefficients, whereas the reverberation room method can provide random incidence values. Both methods have their advantages and disadvantages. In metamaterial research, impedance tube tests are used predominantly as they are time-saving and cost-efficient. That said, in the discussion of acoustical enhancement below, relative values rather than absolute values are compared for the states of the studios with solid reflective surfaces and with the AMM surfaces.

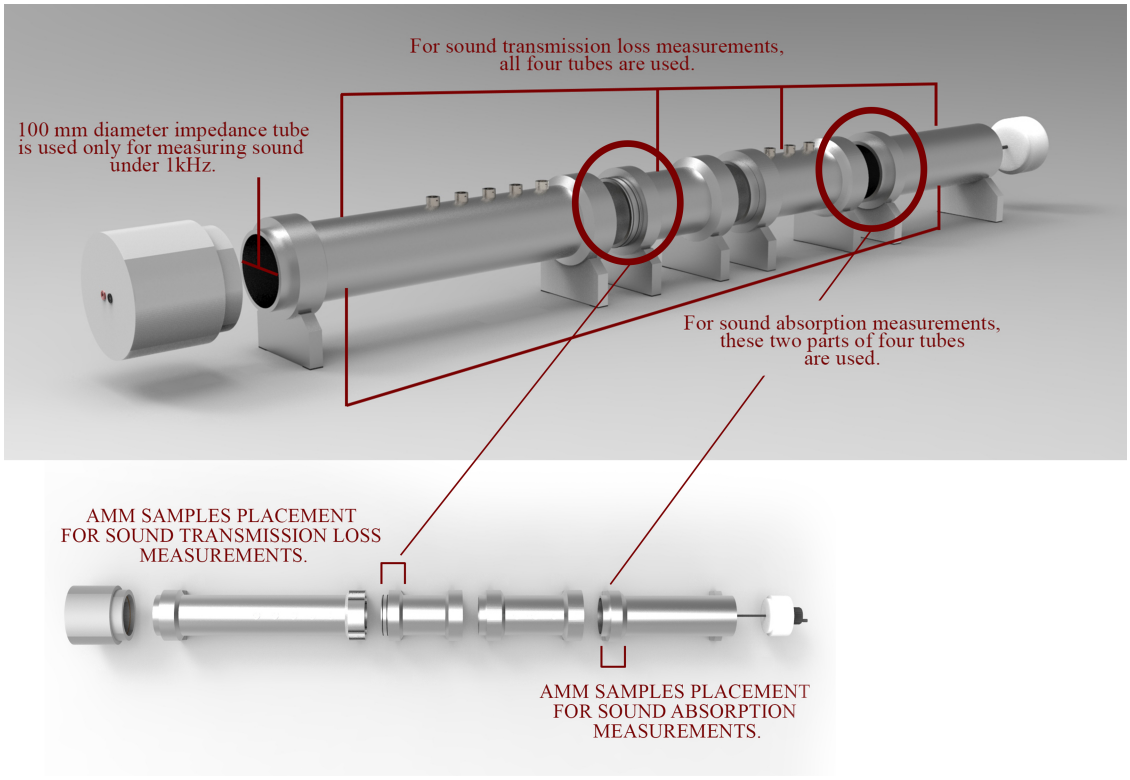

Figure 4.1: 3D model of impedance tube set up for sound absorption and transmission loss measurements (prepared by the author).

The drawing below (Fig.4.2) symbolizes how the sound absorption coefficient measurements are done with the impedance tube method. As can be seen inside of the tube (on the left side of the cavity), there is a cylindrical plate with a wall thickness of 5 mm. The depth of the cavity can be adjusted with the help of linear the apparatus behind the cylindrical plate. Therefore, the amount of air gap can be reduced or increased. Fig.4.2 represents the "5 cm gap between AMM and tube plate" configuration. There may be no gap between the cylindrical plate and AMM samples, which refers to "without gap" configurations. Also, special to DNA module, the composition with a 5 cm gap can be also modified by 2.5 cm, 5 cm, 7.5 cm, 10 cm, 12.5 cm gap compositions for testing the sound absorption performance of DNA module with varied cavities behind the material since this module shows the best potential in sound absorption overall. These tests are

conducted in order to understand how much space/air is required between the AMM panel and the existing wall in actual applications and more promising sound absorption.

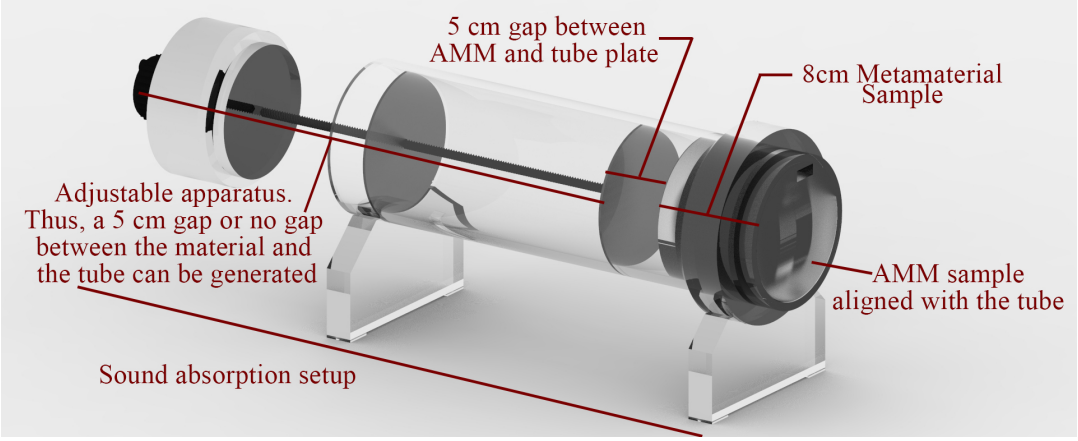

Figure 4.2: Sound absorption coefficient measurement set-up: abstracted 3D model of impedance tube indicating AMM sample locations under different configurations (prepared by the author).

Table 4.1 presents the descriptions of the GR, WL and DNA module configurations and the solid sample in the impedance tube for sound absorption (alpha) and transmission loss (TL in dB) measurements. Table 4.1 also includes descriptions of a number of wall section configurations that are only theoretically estimated (see below). Since the proposed AMMs are intended for architectural applications, the air space behind the modules is a critical variable. The openings on the rear sides of the modules are closed in some configurations to check whether there are any meaningful differences between their performance when both sides are open and when one side is closed. When the apertures on the rear sides of the samples are closed, the AMMs may act more like a Helmholtz resonator [57, 69].

Table 4.1: Configurations of the material samples tested by impedance tube and for those theoretical transmission (TL) estimates are obtained.

Code of Sample	Description
SS1	8 cm (resin) solid sample + 5 cm gap
SS2	8 cm (resin) solid sample without gap
SS3	8 cm (resin) solid sample (for TL measurementTL measurement)
GR1	8 cm GR, two side open+ 5 cm gap
GR2	8 cm GR, one side closed + 5 cm gap
GR3	8 cm GR without gap
WL1	8 cm WL, two side open+ 5 cm gap
WL2	8 cm WL, one side closed + 5 cm gap
WL3	8 cm WL without gap
DNA1	8 cm DNA, two sides open+ 5 cm gap
DNA2	8 cm DNA, one side closed + 5 cm gap
DNA3	8 cm DNA without gap
DNA4	8 cm DNA, two sides open+ 2.5 cm gap
DNA5	8 cm DNA, two sides open+ 7.5 cm gap
DNA6	8 cm DNA, two sides open+ 10 cm gap
DNA7	8 cm DNA, two side open+ 12.5 cm gap
Y1	2cm resin panel-4 cm gap-2 cm resin panel
Y2	1cm resin panel -6 cm gap-1 cm resin panel
Y3	1cm resin panel-6 cm mineral wool (48kg/m3)-1 cm resin panel
Y4	1cm resin panel-5 cm gap-2 cm resin panel

4.2 Analytical Assessment of Sound Absorption Coefficients of Proposed Metamaterials

In this section, the analytical approaches in the assessment of impedance tube measurement results of proposed AMMs are presented. The aim is to critically evaluate the possible diagnostic tools that can augment the design process and interpretation of output data in metamaterial design.

4.2.1 Neckless Helmholtz Resonator Calculations

Studies have pointed out that AMMs may act like Helmholtz Resonators in certain configurations. The internal structures of the three different AMM samples proposed in this study are also similar to Neckless Helmholtz Resonator. In order to check whether the sound wave behavior can be explained by a Neckless Helmholtz Resonator function for certain types of proposed modules, theoretical calculations are held.

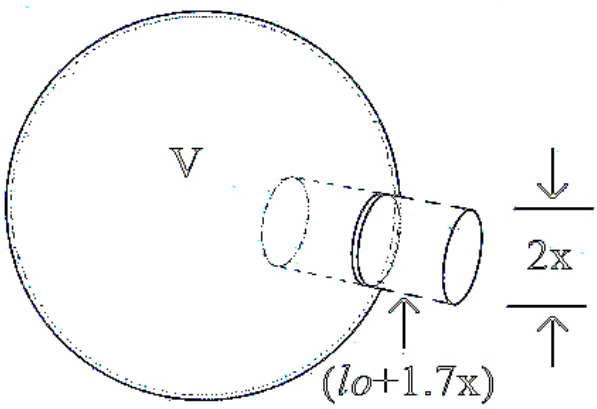

Figure 4.3: A conceptual drawing of a neckless Helmholtz resonator.

A special type of air-spring oscillator, so-called Helmholtz resonator, is a volume with an opening at the one end and a small neck that is activated in its specific resonant frequency. Using the relationship shown in Fig. 4.3, the resonant frequency of the system can be calculated by Eq. 4.1 below [89];

$$f_n = \frac{c_0}{2\pi}\sqrt{\frac{\pi x^2}{V(l_0 + 1.7x)}} \tag{4.1}$$

where fn is the natural frequency of the system, c_0 is the speed of the sound in

the air, V is enclosed volume, x is the radius of the opening, l_0 is the thickness of the plate. Equation 4.1 is utilized in the interpretation of the results as detailed in the following sections.

4.2.2 Passive Destructive Interference (PDI) Calculations

As a second analytical method, Passive Destructive Interference (PDI) is included in this study since AMMs can also dampen sound waves as they pass through the structure by creating destructive interference. Passive destructive interference can occur where the sound waves combine with a phase difference of 180 degrees, or half of the wavelength, and therefore neutralize each other. This method uses the sound itself to greatly reduce its amplitude. Passive means that active sound sources such as speakers are not used [73]. Fig. 4.4 illustrates the basic principle of Herschel-Quincke Tube [90] which has a similar form with PDI absorber along an airway of a certain length, where incoming sound waves enter from either one or both sides.

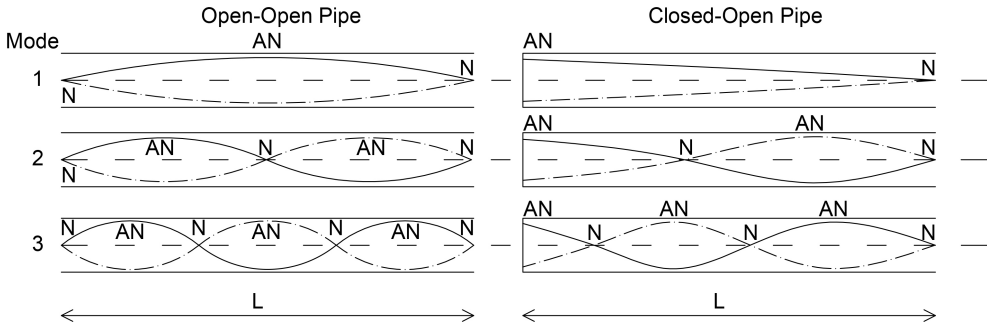

Figure 4.4: Acoustic pressure circulation of an open-open pipe and a closed-open pipe. Pressure anti-nodes shown as AN and pressure nodes shown as N.

There is a relation between the length of air-path and the frequency where the peak value of the sound absorption coefficient of PDI is detected [8]. As shown by Eq. 4.2, the value of n is a positive integer (1, 2, 3, 4. . .), f (Hz) is the frequency, c (m/s) is the speed of sound in air and ΔL (m) is the length difference of the transmission. The transmission length difference ΔL relates to the location of the interference point. According to this research done by Setaki et al. [73]. this

interference occurs above one-quarter of the air path and below the total length of it. In Eq. 4.3, ΔL is represented as a set of limits that anticipates the frequencies where destructive interference may occur as shown in Eq. 4.4.

$$f = \frac{(2n-1)c}{2\Delta L} \tag{4.2}$$

$$\frac{L_{tot}}{2} < \Delta L < L_{tot} \tag{4.3}$$

$$\frac{(2n-1)c}{2L_{tot}} < f < \frac{(2n-1)c}{L_{tot}} \tag{4.4}$$

4.3 Case Study Set-up

The final step in the study involves testing the performance of the proposed materials in a real design problem through the use of room acoustics simulations. For this purpose, two design studios are selected which currently have no acoustical interventions. In shared rooms like studios, open-plan offices or restaurants, noise control is an important comfort parameter, but interior design is also a significant concern. To attenuate the high noise levels in the studios at low frequencies resulting from the highly reflective painted brick and concrete surfaces, some of the proposed AMM units are developed into wall partitions (panel systems) with a modular layout and two different heights. These partitions are then placed between the drawing tables. Also taken into consideration here is the fact that these translucent, resin-based AMMs can be in different color combinations, some of which better highlight the inner structure of the AMM designs (Fig. 4.6c), and can give a rhythm to the studio space.

It has previously been demonstrated in practice that when metamaterials are placed in a repeating lattice structure [91, 92], such as in the form of origami

folding [93], the efficiency of the material structure increases and a better performance is obtained. In order to estimate the acoustic performance of the AMM modules, the studios are first field-tested to determine their current acoustic parameters. Then the acoustical models are generated and tuned according to the field-test data for further experimental study as described below.

4.3.1 Field Measurements

The field tests of the studios were held during the summer break in the academic year, on August 6th, 2019, between the hours of 12:30 and 14:00. The studios are in empty and with minimum background noise condition (Fig. 4.5). To estimate the basic parameters specifying the sound field, the room impulse responses are collected. The equipment used is in accordance with the ISO 3382-1.35 standard. A B&K (Type 4292-L) dodecahedron omnidirectional sound source is used for acoustic excitation, with a B&K (Type 2734-A) power amplifier. The room impulse responses at various measurement points are captured by a B&K (Type 4190ZC-0032) microphone. The sampling frequency of the recorded multi-spectrum impulse is 48 kHz. The height of the omnidirectional sound source is 1.5 m from the floor, and the microphone height is maintained at 1.2 m. The DIRAC Room Acoustics Software Type 7841 v.4.1 is used to generate e-sweep noise signals. Two source and six receiver locations are used for Studio#1, and two source and seven receiver locations for Studio#2 (Fig. 4.5a). These numbers are considered to be sufficient given the dimensions of the studios. The acoustical metrics, particularly the reverberation times (T20 and T30), obtained over the post-processed impulse responses are utilized for tuning the materials assigned in the acoustical models as described in the following paragraphs.

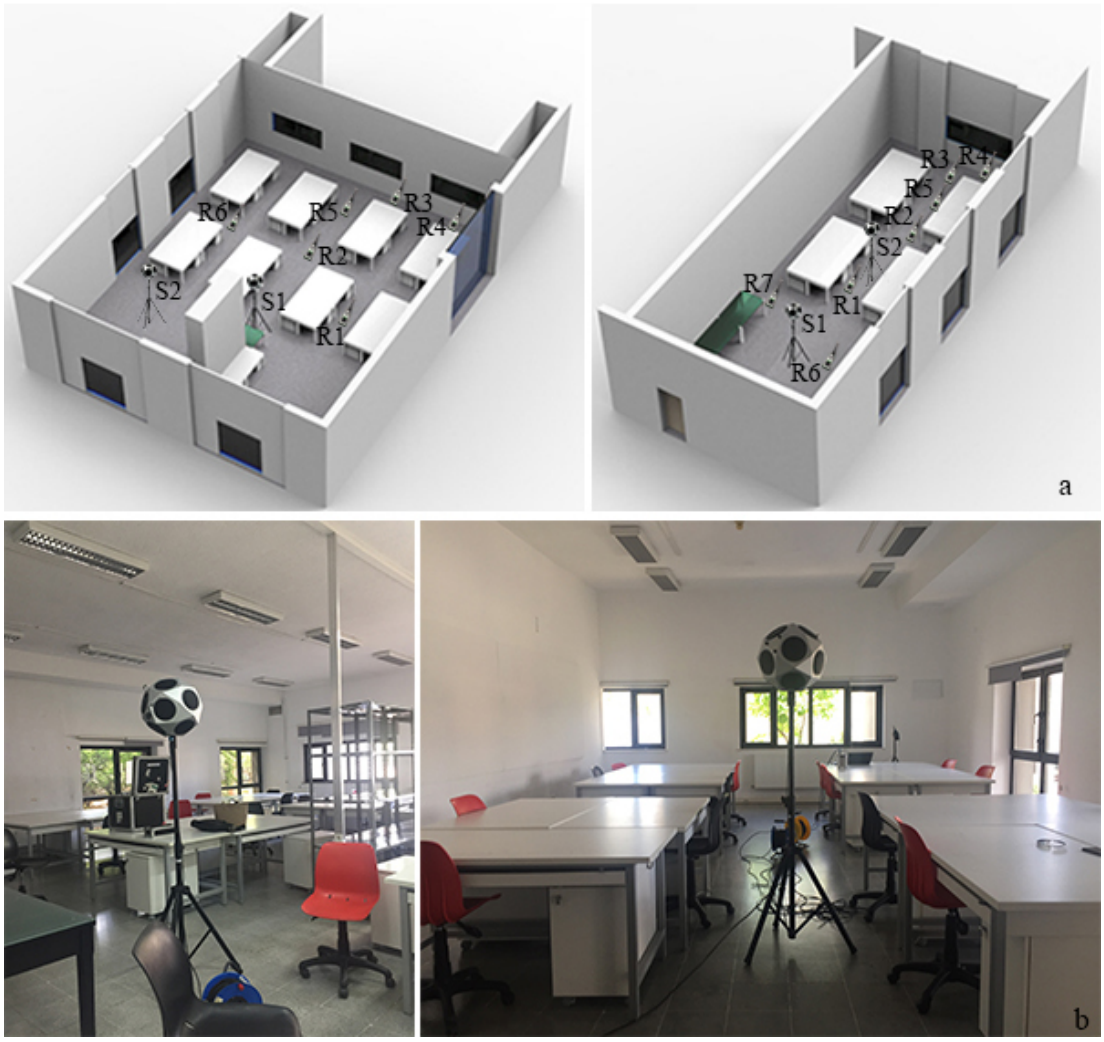

Figure 4.5: 3D models showing sound source and receiver positions in Studio#1 (on the left) and Studio#2 (on the right), b) photographs of the field tests in Studio#1 (on the left) and Studio#2 (on the right).

4.3.2 Room Acoustics Simulations

The aim of the room acoustics simulations is to assess the relative improvement that can be achieved in an architectural application of the proposed AMMs by comparing values before and after the intervention, rather than to obtain the

absolute acoustic parameter results of the room impulses. In this process, simplified 3D graphical models of the existing studios (Studio#1 and Studio#2) were initially developed for use with ODEON Room Acoustics Software version 14.04. These studios were selected from Bilkent University FF building and studio names respectively are FF-05 and FF-08. As shown in Fig.4.5, Studio#1 has a capacity of 32 students and has an estimated acoustic volume of $\sim 997\ m^3$. The student capacity for Studio#2 is 16 and it has an estimated acoustic volume of $\sim 526\ m^3$. The study focuses on T30 values at 63, 125, 250, 500 and 1000 Hz, SPL (A), and STI results. For the STI grid results, the sources are positioned 1.20 m off the floor and the distance between receivers is 0.4 m. In the analysis of speech intelligibility in the proposed scenario, the background noise level is assumed not to exceed the NC30 level.

Simulations are run for the current condition of the studios and for two different scenarios in which the proposed AMMs are applied for acoustical enhancement (Fig.4.6a and Fig.4.6b). The difference between the results of the simulations of the empty studios and the results of the field tests for T30 over-tested receiver positions is around 0.03 s, which is smaller than one Just Noticeable Difference (JND). This shows that the tuning of the acoustical model is sufficiently accurate.

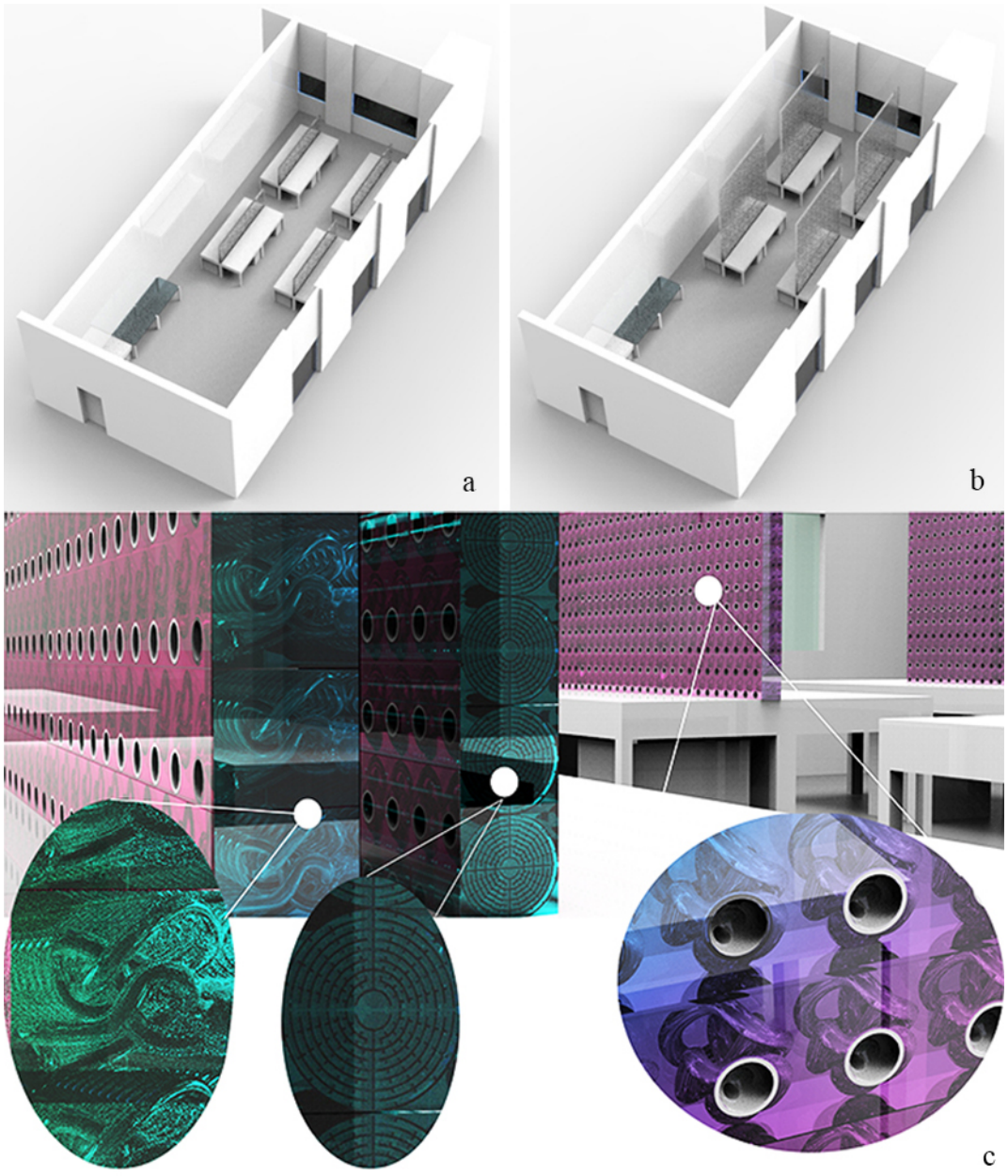

Figure 4.6: Studio#2 a) 3D Model with design proposal $\frac{1}{5}$ height of the room AMM panels, b) with design proposal using $\frac{3}{4}$ height of the room AMM panels, c) panels with DNA5 on one side and WL on the other, with a 7.5 cm gap in between, shown in Studio#1 and Studio#2.

Fig.4.6a and Fig.4.6b show the positions and heights of the proposed partitions, built up of AMM modules, in Studio#2. In Studio#1, the locations of the

partitions are the same – i,e., in between each pair of drawing tables. The heights of the partitions are also the same. The proposal in which the partitions are $\frac{1}{5}$ of the height of the studio (Fig.4.6a) is referred to as proposal A1 and the proposal in which the partitions are $\frac{3}{4}$ of the height of the studio (Fig.4.6b) is designated proposal A2. Fig.4.6c represents the 3D model drawing of actual application in practice. The panel includes DNA5 on the left side and WL on the right, with a 7.5 cm gap in between. The thickness of the AMM specimens is 9.5 cm for DNA5 module and 8 cm for WL, so in total, the thickness of the panel is 25 cm. DNA5 is the best composition for sound absorption performance overall and WL has the most efficient result in terms of sound transmission performance. That is why they are selected to be applied in simulations for getting the most effective results.

The interior finish materials and the corresponding absorption coefficients obtained in the simulations are listed by frequency in Table 4.2.

Table 4.2: List of materials and sound absorption coefficients over 1/1 octave bands from 63 Hz to 1000 Hz.

Material Location	Name	63	125	250	500	1000
Wall Surfaces	Paint and plaster on brick wall	0.06	0.06	0.06	0.10	0.10
Ceiling Surfaces	Painted concrete	0.10	0.10	0.05	0.06	0.07
Floor Surfaces	Concrete or terrazzo flooring	0.01	0.01	0.01	0.02	0.02
Drawing Table	Wood boards on a profile	0.15	0.15	0.20	0.10	0.10
Windows	Ordinary window glass	0.35	0.35	0.25	0.18	0.12
Door	Wood, 1 layer, 20mm	0.25	0.25	0.18	0.11	0.08
Stuff in the Studio1	Corrugated sheet, foam-like plastic material, etc.	0.30	0.30	0.45	0.65	0.56
*Proposed partitions	DNA 5 AMM, DNA with 7.5 cm air gap behind	0.77	0.31	0.12	0.07	0,18

**Proposed partitions sound absorption coefficient values are obtained from impedance tube measurement results.*

Chapter 5

Results and Discussion

5.1 Impedance Tube Measurement Results

All three prototypes and solid samples are tested in an impedance tube with the different configurations listed in Table 4.1. Each configuration is tested a minimum of ten times to ensure the replicability and reliability of the results. The sound absorption coefficients (α) and transmission loss values in dB over 1/3 octave bands below 1200 Hz are presented in the following paragraphs.

5.1.1 Sound Absorption Coefficient Measurement Results

The sound absorption measurement results of the sample GR, WL and DNA units are compared in Fig. 5.1 and 5.2. Among the various GR configurations tested, GR1 shows the least efficient sound absorption performance (Fig. 5.1a). All the GR configurations perform better than the solid samples SS1 and SS2. Peak absorption is detected in the range of 100-125 Hz, at 400 Hz and at 630 Hz.

The sample WL unit demonstrates the lowest performance (Fig. 5.1b). Its

performance tends to parallel the reflectivity of the base material. The configuration WL2 has a peak absorption coefficient of 0.07 at 500 Hz and WL3 has a peak absorption coefficient of 0.05 at 80 Hz with a value of 0.05. However, neither sample offers any notable advantage in comparison to the solid sample. Thus the design parameters of the WL module need to be improved and optimized for better performance in sound absorption.

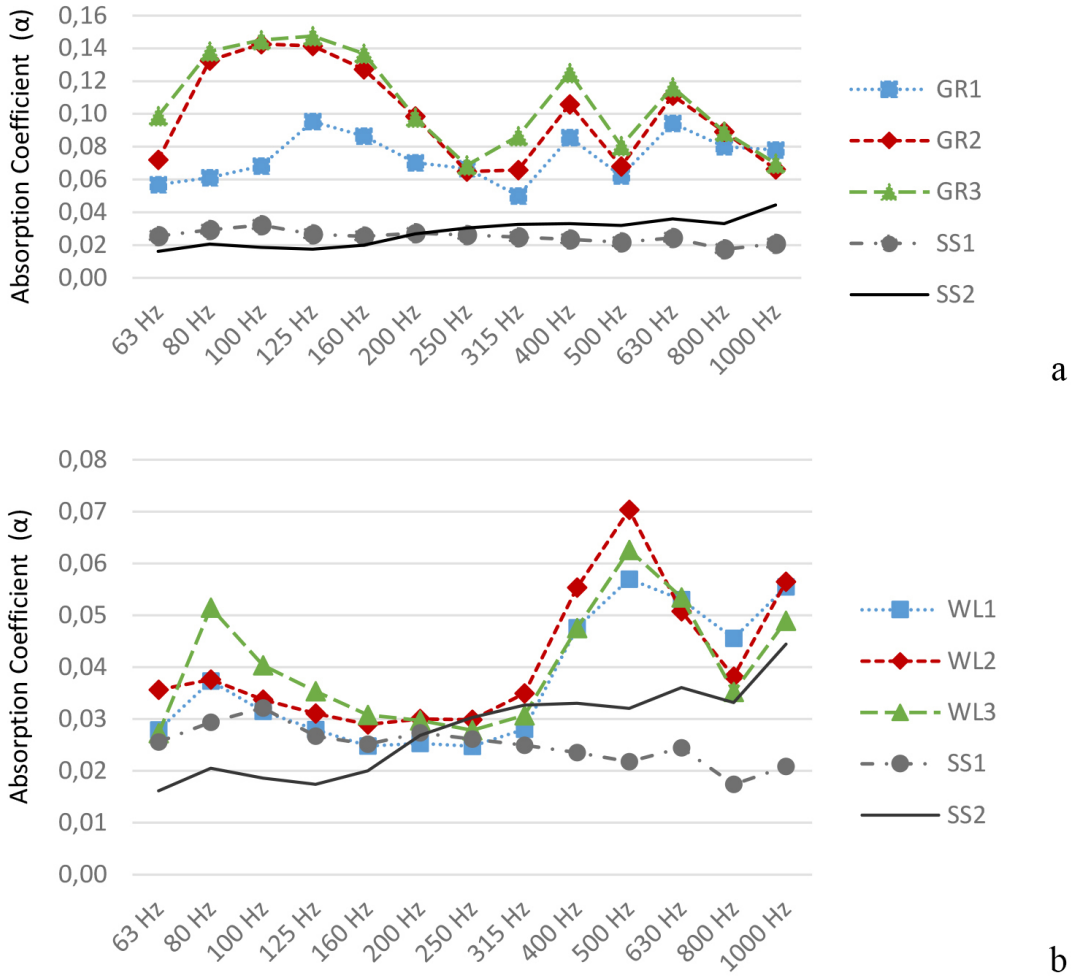

Figure 5.1: Measured sound absorption coefficients over 1/3 octave bands (Hz) for the following configurations of the AMM modules tested with the impedance tube: a) GR1, GR2, GR3, SS1, SS2, b) WL1, WL2, WL3, SS1, SS2.

The sample DNA unit shows more potential for sound absorption, as presented

in Fig. 5.2a. In particular, the DNA1 configuration (two sides open, 5 cm air gap behind) achieves sound absorption coefficient values of up to 0.70 at 80 Hz, which is remarkably above average. By contrast, the solid (unperforated) samples, SS1 and SS2, have absorption coefficients in the range of 0.02-0.03. The only difference between DNA2 and DNA1 is that the opening on the rear surface is closed. This difference causes DNA2 to achieve the least effective sound absorption result. In other words, the aperture on the rear surface is of great importance for increasing the sound absorption efficiency of the DNA module. The DNA3 configuration (no air gap behind), has higher sound absorption values at frequencies between 250 and 315 Hz.

Since DNA1, is the best sound absorber among the alternatives tested, additional configurations are developed by changing the size of the gap between the tube and the DNA AMM module. The measurements were performed again for the "two sides open" variation of the DNA module with air gaps of different dimensions behind the module (Fig. 5.2b).

As can be observed from Fig. 5.2b, configuration DNA5 (two sides open, 7.5 cm air gap) achieves its maximum sound absorption value at 63 Hz with an absorption coefficient of 0.77. However, DNA1 still performs better than the other configurations across the tested frequency spectrum as a whole. For all DNA types, sound absorption is greater in the 63-100 Hz frequency range than in the octave bands above 250 Hz, in which it shows a pattern little different from the solid sample. To conclude, the DNA module in its current state offers an effective sound absorption mechanism in a range of 63 to 200 Hz. The peak frequencies, or the effective region on the frequency spectrum, can be adjusted by optimizing the design parameters/dimensions of the internal tubes.

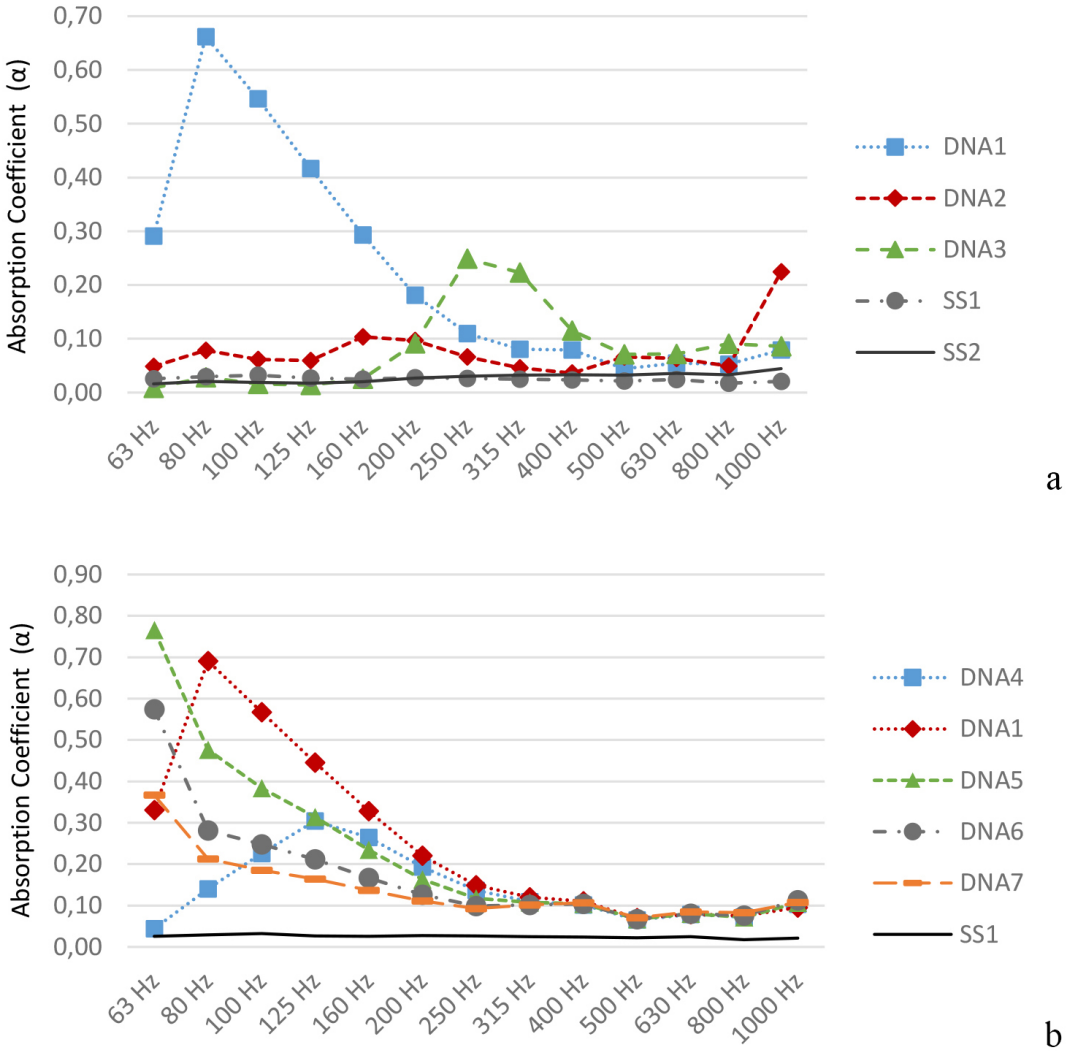

Figure 5.2: Measured sound absorption coefficients over 1/3 octave bands (Hz) for the following configurations of the AMM modules tested with the impedance tube: a) DNA1, DNA2, DNA3, SS1, SS2, b) DNA4, DNA1, DNA5, DNA6, DNA7 and SS1.

5.1.2 Transmission Loss (TL) Measurement Results

The transmission loss (TL) measurement results of the GR, WL, and DNA modules are compared in Fig. 5.3a. In contrast with their poor sound absorption performance, the sample WL unit is much more effective than the other proposed AMMs with respect to sound transmission loss. For the frequency range below 1200 Hz, the TL values for WL (approx. 48-55 dB) are significantly higher than the results for the DNA and GR modules. The TL values of the solid sample SS3 range from 35 to 43 dB in the frequency interval of 125-160 Hz, whereas the TL values of the WL configurations range from 48 to 55 dB. Thus, the TL values of the WL unit are on average 12 dB higher than the values found for SS3. Meanwhile, the GR module gives approximately the same TL values as the solid sample SS3 since the inner structure of GR module is not efficient for sound transmission performance. The sample DNA unit achieves the least sound transmission loss of all. Thus, it is important to note that the pipes of DNA sample are not suitable for sound transmission and even show less effective in terms of sound transmission loss in comparison to the solid sample. The DNA proposal has more potential for sound absorption as shown previously in Fig. 5.2.

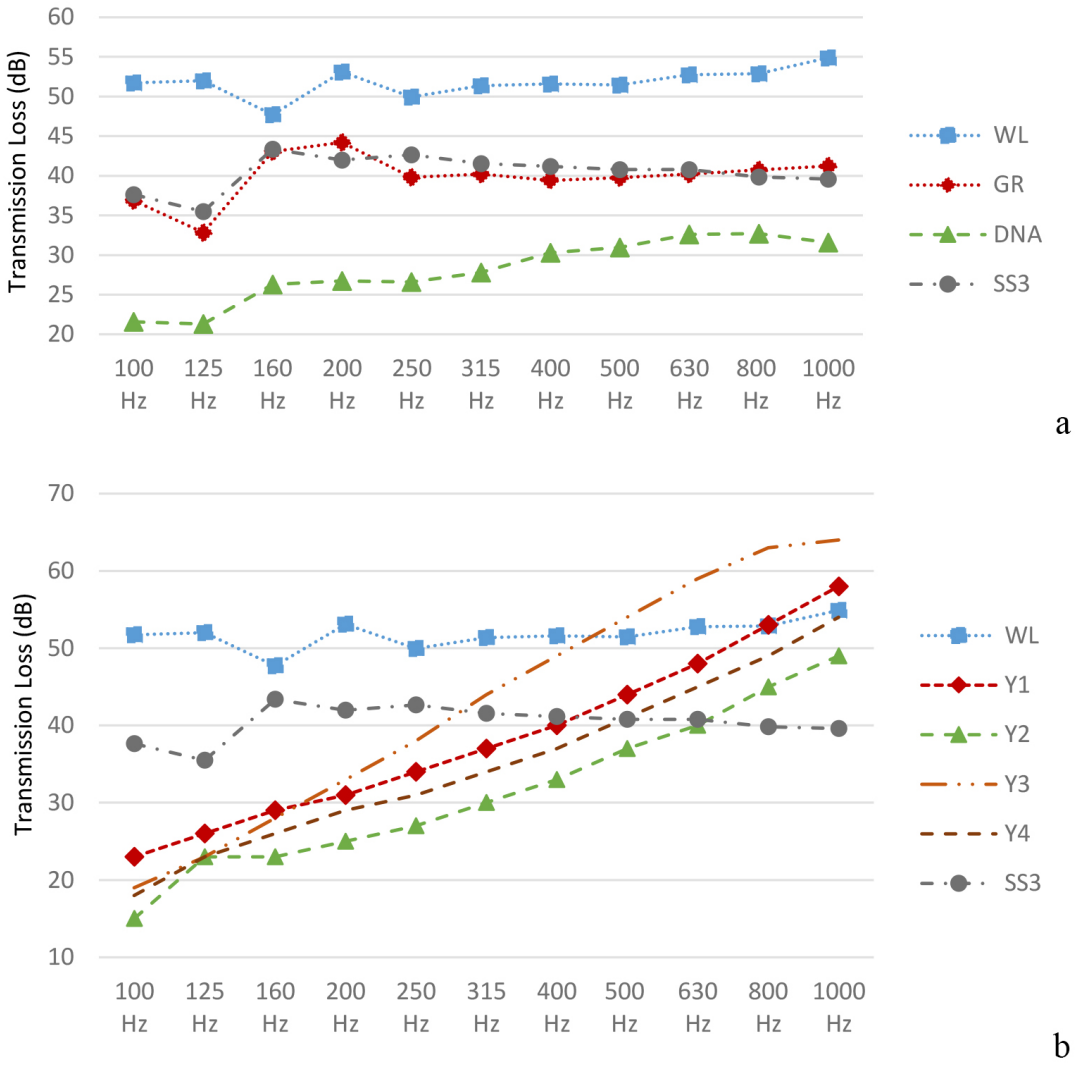

Figure 5.3: Transmission loss measurement results of a) WL, GR, DNA and SS3 samples over 1/3 octave bands (Hz) below 1200 Hz, b) WL in comparison to theoretically estimated Y1, Y2, Y3, Y4 and SS3.

Overall, these results suggest that the DNA and GR units are not suitable for use as a noise barrier, in their current form, but can be utilized in room acoustics for sound absorption. The WL proposal has more potential for use in noise control applications and can therefore be considered for use in practice as a separating wall/partition between two rooms/spaces (This was tested in the case

study). The structure of WL specimen has masses and cavity between them in much smaller scales overall, DNA sample has two pipes and GR includes void and masses in larger-scale comparing to WL sample, so all three samples have different working systems themselves. That is why all of them vary in terms of the sound absorption and transmission performance.

As part of the impedance tube tests, theoretical transmission loss estimates are also made for typical lightweight walls using the same base material (epoxy resin) as the proposed AMMs (Fig. 5.3b). The purpose of making these estimates is to discuss the effectiveness of the TL performances of the sample AMMs in comparison to those of drywall systems with an air gap. Estimates are made both for wall sections in which the air gap is left unfilled, and for wall sections in which a fibrous material is included within the air gap. This makes it possible to compare the performances of the proposed AMMs with the performances of conventionally used wall sections such as those with a mineral wool infill. The density of epoxy resin is taken to be 1098 kg/m^3.

To this end, the epoxy resin material is shaped into modules with standard configurations which are considered to exemplify the real wall applications (see Table 4.1 for cross-section definitions). The impedance tube results obtained from these modules are presented and compared with the results for WL and a solid sample in Fig. 5.3b. The total thickness of each wall section module is 8 cm – the same as for the AMM modules. The WL module has the best TL performance overall. Above 500 Hz, the Y3 configuration (1cm resin panel -6cm mineral wool of 48 kg/m^3 -1cm resin panel) generates higher TL values than the other wall section configurations and the WL module. The Y1 configuration (2cm resin panel-4cm air gap-2cm resin panel) performs better than the Y2 configuration (1cm resin panel -6cm air gap-1cm resin panel). The mineral wool filling used within the air cavity is the main reason for the higher performance of the Y3 configuration. However, this study pays specific attention to the use of non-fibrous and semi-translucent to transparent materials.

5.2 Results and Discussions of Analytical Estimations

In this section, the analytical estimation methods are compared to the impedance tube measurement results. The analytical analysis, including Helmholtz equation and Passive Destructive Interference (PDI) equation estimations, comparisons to measured data are important to search their applicability in the design stage of AMMs. In Fig. 5.4, the results obtained from the Helmholtz equation and the PDI estimations are compared with the tube measured results in the same graph.

In Helmholtz equation estimations of DNA sample initially, one inner pipe is taken into consideration, and the resonant frequency is estimated to be 2164 Hz. Later, both two inner pipes are included in the estimations, and the resonant frequency is calculated to be 848 Hz. The impedance test results of the DNA module indicate that the peak absorption occurs in between 63 and 80 Hz, which is comparatively much lower than the estimated resonance frequencies. The Helmholtz equation estimations for GR sample indicate a resonant frequency of 788 Hz and for WL sample shows a resonant frequency of 298 Hz. None of the AMM prototypes in this research can be explained with Helmholtz Resonator equations (Fig. 5.4).

The second set of comparisons is held for PDI estimations. For PDI equation estimations, the positive integer, n, which is defined in Eq (2), is 1 for DNA and GR sample, and 2 for WL sample. The reason for the value of the given numbers is for providing consistent results with impedance tube results for each sample. PDI estimations designate the possible interval for resonant frequency where the absorption peaks can be observed. As shown in Fig. 5.4, the peak absorption range for GR is between 112 to 224 Hz, for DNA the range is between 261 to 523 Hz and for WL the range is between 462 to 925 Hz. Comparatively the peak sound absorption coefficients in tube measurements are obtained at 125 Hz for GR, 63 Hz for DNA, and 500 Hz for WL. When the distribution of the sound absorption coefficients over 1/3 octave bands for the GR module is analyzed, the frequency range with the highest results coincides with the results of the

PDI calculations, which is between 63-200 Hz. The measurement and the PDI estimations are coherent for GR and WL samples, which provides an initial guess of the frequency range during design phases. Although DNA module cannot be explained either by Helmholtz or PDI method. This is due to the complexity of the inner voids that cannot be simplified to the input parameters of the two analytical methods. For this reason, numerical studies on the DNA module is necessary for the future optimization phase.

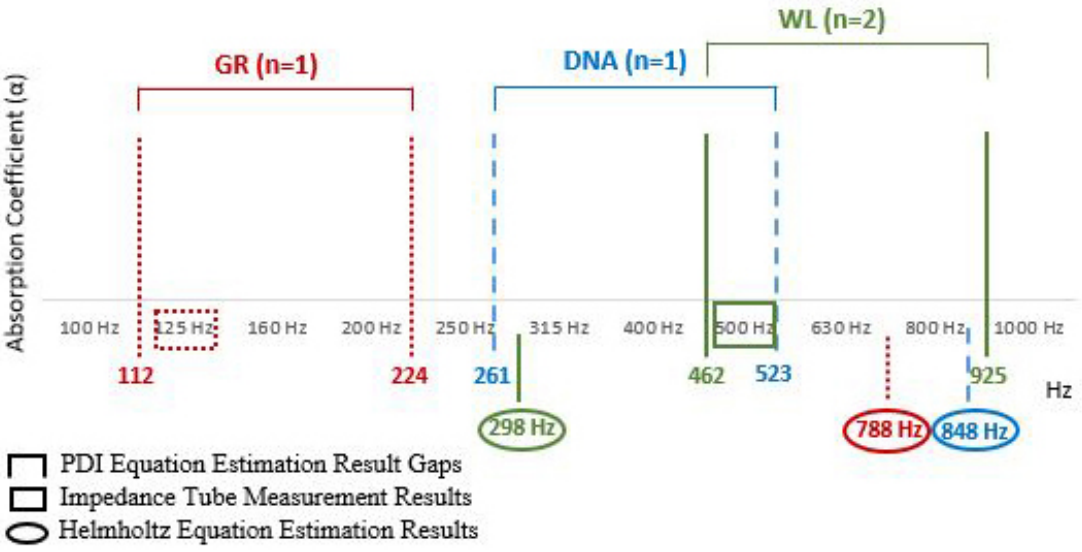

Figure 5.4: PDI and Helmholtz equation estimation results of GR, DNA, and WL in comparison to the results of impedance tube measurements for all three samples.

5.3 Assessment of proposed AMM application for the acoustical enhancement of design studios

As detailed in section 4.3, a case study was conducted in two studios, Studio#1 and Studio#2, using field tests and simulations, to assess the likely efficiency of

the proposed AMMs in a real-life situation. The T30 values obtained from field measurements and the acoustical simulation results for the current condition of the studios and under the proposed acoustical intervention are given in Fig. 5.9. The T30 results for the studios in their current condition indicate a high level of reverberance of up to 2 s in both studios (Fig. 5.5 and 5.6) – far above the recommended limits for learning and studying environments, which should be 1 s at most for the given sizes of the studios. As previously noted, the control of low-frequency sound build-up within enclosed spaces, especially in a case like this with highly reflective massive wall and floor surfaces, is always challenging.

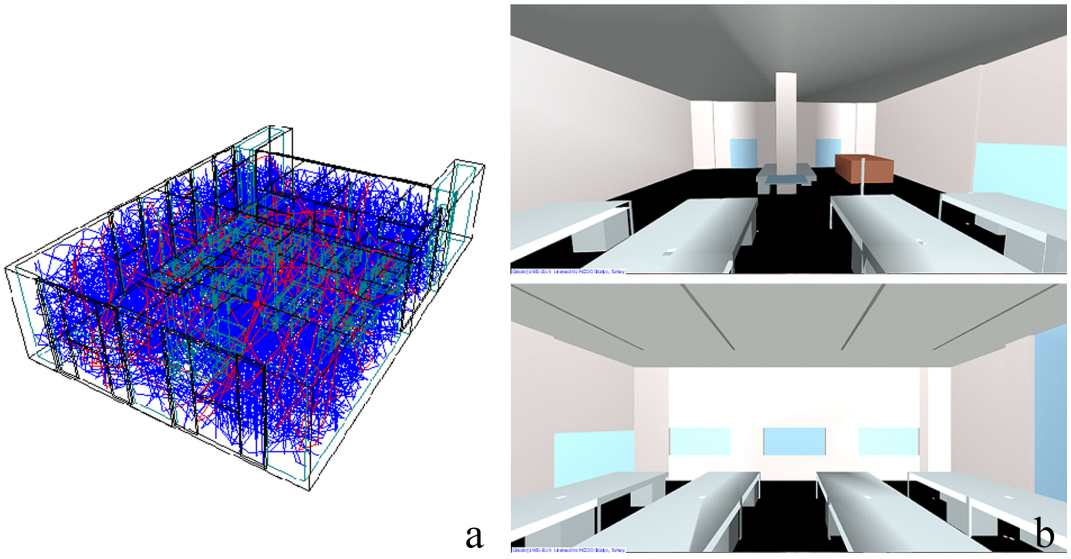

Figure 5.5: Studio#1 simulated-current situation: a) ray tracing acoustic simulation, b)3D OpenGL views.

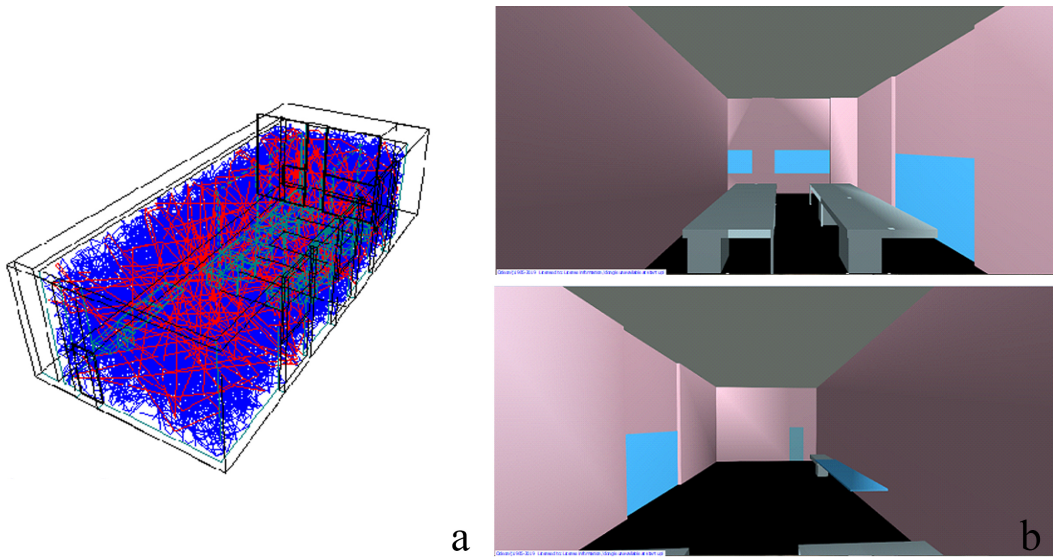

Figure 5.6: Studio#2 simulated-current situation: a) ray tracing acoustic simulation, b)3D OpenGL views.

The proposed partitions are composed of DNA5 units, which achieved the highest sound absorption, on one face, and WL units, which achieved the highest TL values, on the reverse face. The acoustical simulations make use of the absorption coefficients and TL values obtained from the impedance tube measurements for the units in question.

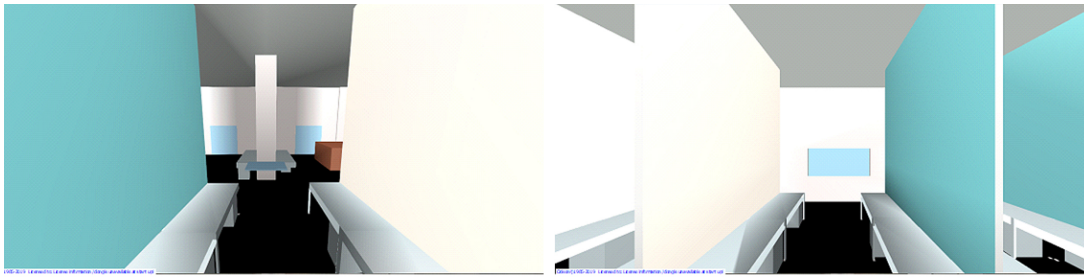

Figure 5.7: Studio#1 with proposal A2 3D OpenGL views.

In proposal A1 ($\frac{1}{5}$ height partition), the T30 values improve by about 0.14-0.30 s in the range of 63-125 Hz. In frequency ranges above 125 Hz, the T30 values gradually approach the readings for the current condition of the studios.

In proposal A2 ($\frac{3}{4}$ height partition) the improvement is much more significant, with T30 values varying between 1.1 s and 1.69 s across the tested range of 63 Hz to 1000 Hz (Fig. 5.7). At 125 Hz, for example, T30 shows a decrease of 0.43 s in Studio#1 by comparison with the current condition of the studio. This is a significant improvement for this frequency range, particularly given the volume of the studio (Fig. 5.9a).

Figure 5.8: Studio#2 with proposal A2 3D OpenGL views.

Studio#2 shows a similar pattern to Studio#1 in terms of the improvements achieved under the proposed interventions A1 (Fig. 5.9a) and A2 (Fig. 5.9b). In its current condition, Studio#2 produces T30 results ranging from 1.34 s to 2.11 s across the tested frequency range (Fig. 5.8). In proposal A2, the lowest T30 value is 1.1 s, while in proposal A1 the lowest value is 1.28 s. At 125 Hz a reduction of 0.58 s is obtained in proposal A2. The reason for this is that the sound absorption of the DNA5 configuration used in the proposed partition is high in this octave band.

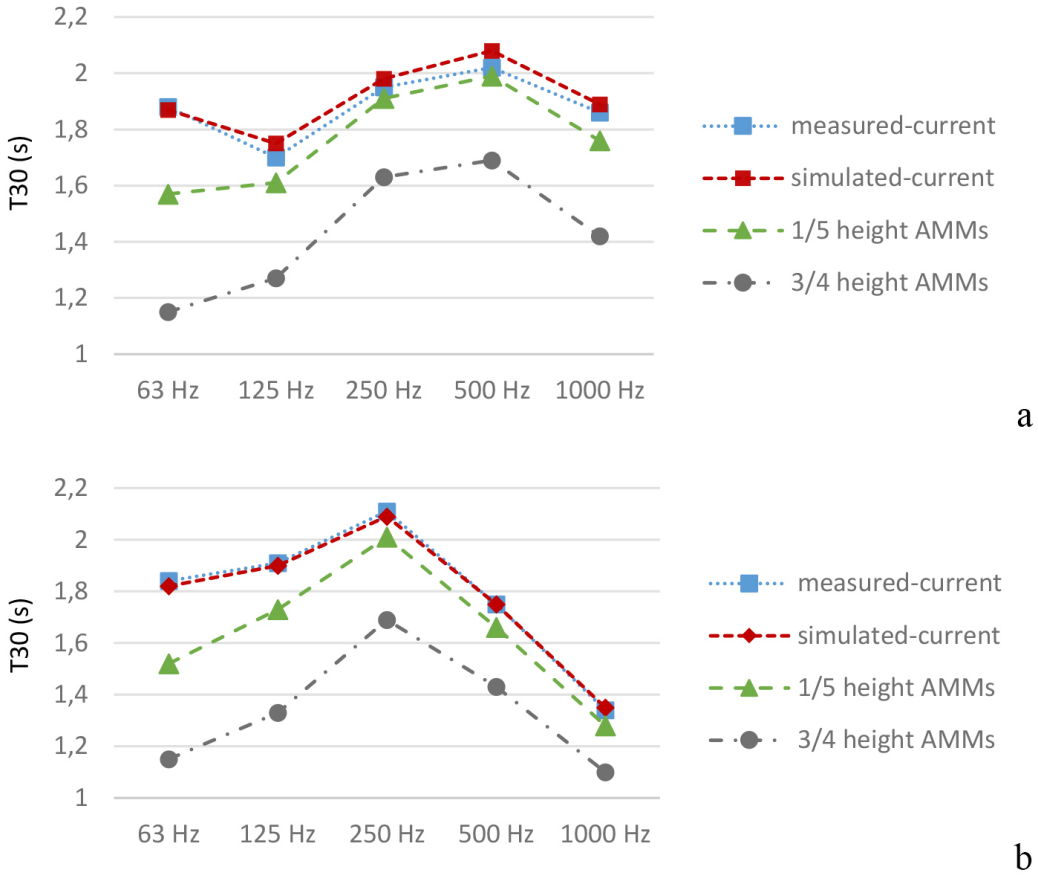

Figure 5.9: T30 values of a) Studio#1 and b) Studio#2 over octave bands from 63 Hz to 1000 Hz, comparing measured current results, simulated current results without AMM panels, simulated results after installing $\frac{1}{5}$ height of the room partitions (A1), and simulated results after installing $\frac{3}{4}$ height of the room partitions (A2).

The distribution maps in Fig. 5.10 show the speech transmission index (STI) results for the studios in their current condition and after the proposed AMM intervention (A2). In the scenario represented for Studio#1, an instructor is talking to the whole class from a central position. While intelligibility in Studio#1 is generally 'poor' in the current condition of the studio (Fig. 5.10a), this improves to 'fair' and 'good' with the proposed installation of the AMM partitions (Fig. 5.10b). For Studio#2, the instructor is positioned to one side of the

studio, which is a common situation when the studio is shared by two sections (classes) and two instructors. In the current condition of the studio, the STI values indicate 'fair' intelligibility in most of the receiver positions on the same side of the partition where the instructor is standing (Fig. 5.10c). However, after the proposed AMM intervention, the STI values show that 'good' intelligibility is achieved at the drawing tables on the same side of the partition as the instructor (Fig. 5.10d). These results highlight the improvements inside the studios and the potential benefits of the composite use of barrier-plus-absorptive AMMs in a real architectural acoustics problem. Moreover, the proposed AMM applications do not use porous materials, and it is always an option to improve the aesthetic features of the space in question through the use of integrated lighting over these semi-translucent prototypes.

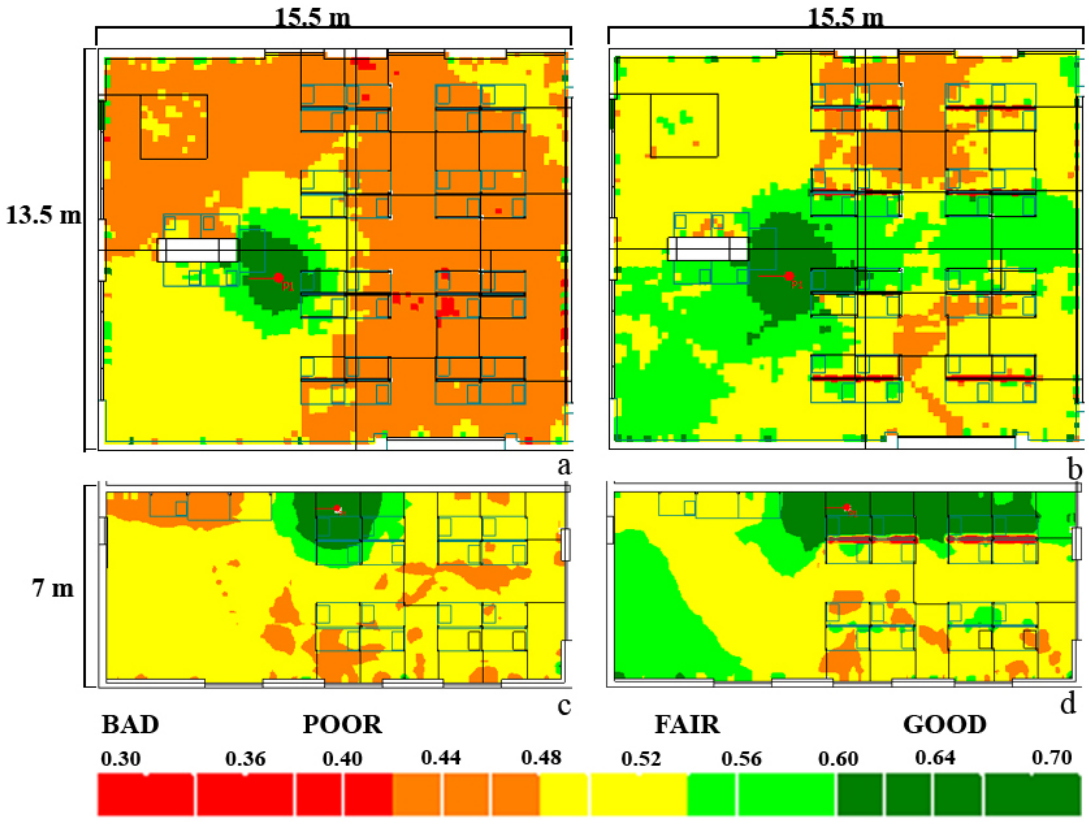

Figure 5.10: Studio#1 STI distribution maps a) for the current condition of the studio, b) under the A2 AMM proposal and Studio#2 STI distribution maps c) for the current condition of the studio, d) under the A2 AMM proposal.

Chapter 6

Conclusion and Future Works

6.1 Conclusion

In this study, different types of acoustical metamaterials have been developed to investigate their potential applications in architecture. The space-coiled modules developed utilize some forms and ratios taken from nature in line with a biomimicry approach, albeit on a sub-wavelength scale. Basically, three types of units named after the golden ratio (GR), the web-labyrinth (WL) form and DNA are designed and produced. The samples are then tested in an impedance tube to obtain their sound absorption coefficients and transmission loss values.

The impedance tube test results are initially compared to two analytical methods including the Helmholtz equation and Passive Destructive Interference (PDI) method. The analytical comparisons indicate that DNA module cannot be explained by either Helmholtz or PDI methods, due to its complex inner structure. For this reason, the optimization studies of DNA module for sound absorption should be followed by numerical simulations, which is one of the future research recommendation. On the other hand, GR and WL modules can partially be explained by PDI method for specifying their possible peak absorption frequencies during the design stage.

The study focuses on acoustical enhancement in the mid- to low-frequency spectrum. This is because higher frequencies can be controlled easily with traditional materials without taking up much space inside the rooms. Besides, the presence of audiences or students augments the attenuation of sound in the mid- to high-frequency range. The analysis and the impedance tube tests are therefore conducted for frequencies of between 63 Hz and 1000 Hz for sound absorption and for frequencies of between 100 Hz and 1000 Hz for sound transmission loss. Different configurations of the proposed units are tested including configurations with one side closed, with both sides open, with different thicknesses and with different air gaps behind them. The results indicate that all the proposed AMM modules achieve higher sound absorption than a solid sample of the same thickness. The sample DNA module achieves the best overall sound absorption performance in the tested frequency ranges. Among the different configurations of this module, the DNA5 configuration (8 cm thick, two sides open, 7.5 cm air gap behind) reaches the maximum sound absorption value of 0.77 at 63 Hz. The basic drawback of the AMMs in sound absorption is their relatively narrow band behavior. Modules of two or three kinds, with alternating interior void dimensions, could be used jointly in order to increase the effective frequency interval.

The sample WL module achieved the highest performance in terms of sound transmission loss, with values ranging from 48 dB to 55 dB across the entire tested frequency spectrum. The results achieved by the WL module are approximately 12 dB better than those obtained for a solid sample of the same thickness (8 cm). This is a significant contribution considering the relatively low thickness of the sample modules.

The sound transmission loss achieved by the WL module is also compared to the sound transmission loss achieved by panel walls made of the same base material (resin) in different configurations similar to those used in standard lightweight construction systems. For this purpose, TL results are obtained for theoretical panel wall sections consisting of two layers of solid resin panels of different thicknesses and with different air gaps in between, and with the same total thickness as the WL module. When the results are compared, the WL unit is found to display a greater TL performance than all of these estimated resin wall sections.

Up to a frequency of 500 Hz, it also performed better than a similar panel wall section with a mineral infill.

Finally, to observe the potential benefits in an architectural environment, partitions made up of AMMs are designed using the DNA5 module on one side and WL blocks on the other. This design solution is tested in two architectural studios by means of simulations over field test-tuned acoustical models. A comparison is made of the reverberation time (T30) and STI metrics for the studios in their current condition and under acoustical design scenarios using AMM partitions of different heights. The use of the partitions lowers the T30 values for Studio#1 by 0.73 s and for Studio#2 by 0.69 s at 63 Hz. The use of the partitions is also found to raise the STI values from 'poor' to 'fair' and 'good' rating in Studio#1 and from 'fair' to 'good' rating in Studio#2 in overall receiver positions/student desks.

To sum up, the results highlight the potential use of AMMs in reverberation and noise control in architectural applications. AMMs can be utilized as part of a partition, as furniture or as a design element without occupying large spaces and without using allergenic porous materials. Also, AMMs are highly preferable materials in terms of indoor air quality and can be used as a diffuser in HVAC systems. So they can be utilized for attenuating noise without interrupting airflow. They do not emit any hazardous particles to the air and provide natural ventilation, which of two are important factors in sound insulation. On the other hand, as different manufacturing techniques make it possible to use a variety of base materials, including semi-transparent to translucent materials, light can always be integrated into AMM modules as a design element. In acoustical terms, the inner geometrical structures of the modules proposed in this study can still be improved further in order to obtain higher values, either in absorption or transmission loss, in a broader range of frequencies. For improving the acoustic properties of designed modules and proposing more alternatives the future work recommendations are presented in the following section.

6.2 Future Work

In this section, recommendations on design, production, application and also numerical techniques to be used in design development are presented. Based on the literature review and the results of the experimental and theoretical studies conducted the thesis, three alternatives for future studies are proposed. These novel alternatives are for the sake of extending the effective frequency range of materials by increasing the path length and complexity of inner structures. These three alternatives are detailed in the following sections.

Although the materials proposed in this study are not lightweight, there are other application systems that can be lighter for future studies. To illustrate, a hybrid material application is recommended. For example, the part currently molded with resin after 3D printing phase can be combined with a suitable and lightweight conventional material. In addition, it may not be necessary to mold the material in actual applications. As shown in Fig. 6.1, surface plates can be placed only on the front and back of the AMM sample by protecting the openings on the material, and the middle of the panel remains empty without any filling. The materials of surface plates are important for this application. With the help of the application structure, the sound oscillates more in comparison to the filled form of the AMM module and causes the energy of the sound to lessen. This allows the AMM sample to show a better result in terms of sound transmission performance.

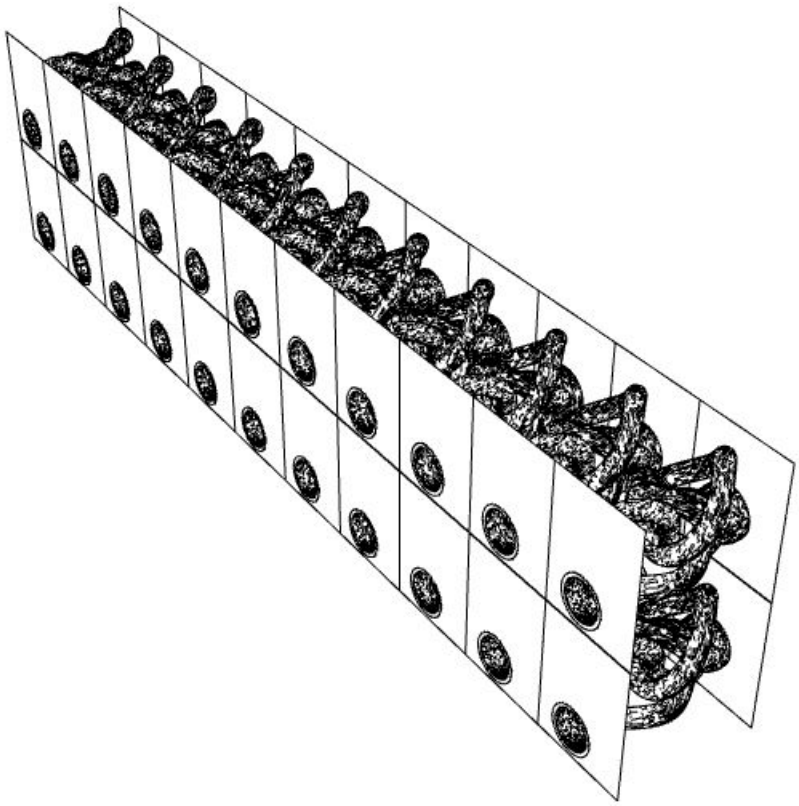

Figure 6.1: An example of alternative application systems for providing a lighter solution: two surface plates integrated with DNA AMM sample.

For the future, in terms of production, there is a different method that can be a suggestion. It is CNC machining technique used in furniture production, which has advantages both in time and budget. For example, the production time is short for final results (one layer can be produced in approximately 1-2 seconds). Therefore, this method can be an alternative for the manufacturing technique used in this study because it is appropriate for mass production of the modules with today's technology.

The phases of CNC machine are as follows. First, a mold is created. The inner structure of this mold should be in the form of the designed metamaterial. But it should be the reverse in terms of mass and void. The parts which are empty/air in the material should be filled with material in the mold, and the parts with the material should be empty in the mold. This is because the material is filled

into the mold with a liquid that is initially fluid and becomes solid when it dries. Therefore, the empty spaces in the mold are filled with liquid material and filled spaces are converted into empty/air when the mold is removed. Thus, the resulting product, the inner structure of the mold, becomes the same as 3D modelling of the product designed in architectural software. Additionally, the mold can include layers to make the process easier and practical when removing the mold. Then, layers can be merged to give the module its final shape for reuse.

6.2.1 Alternative 1

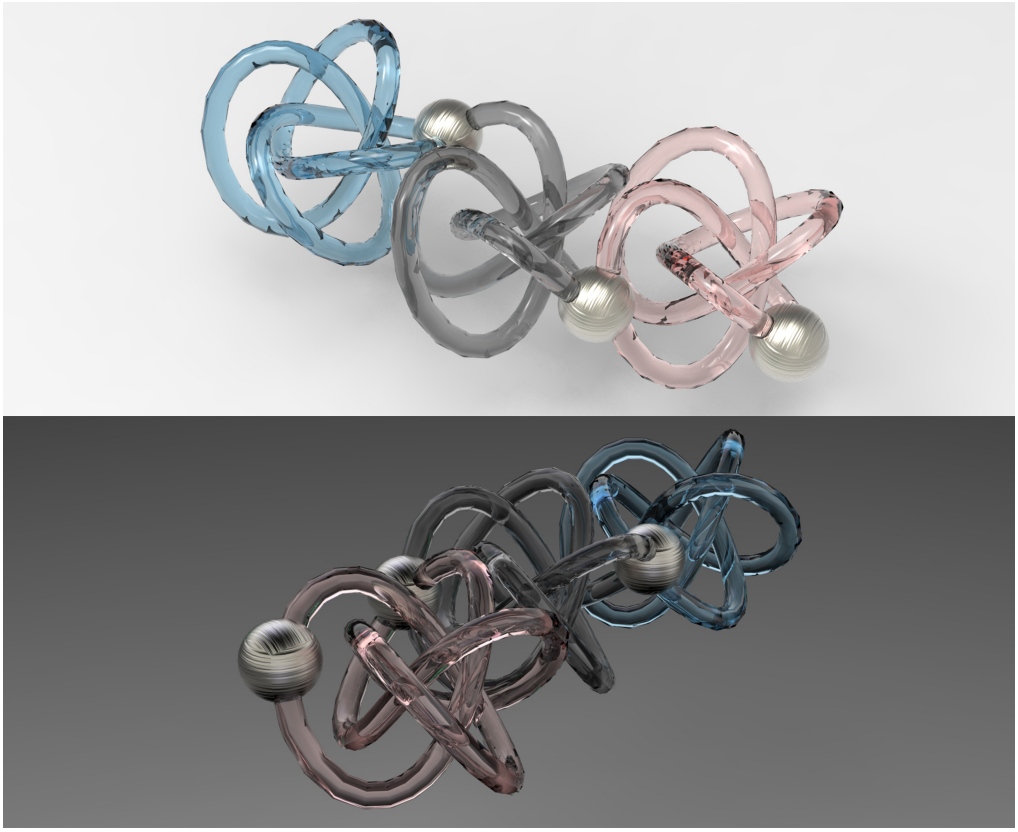

Figure 6.2: Alternative 1 as a variation of DNA specimen.

The DNA structure of Alternative 1 (Fig. 6.2) has narrower gap (4-5 mm) in the sound channels in comparison to the current DNA sample's tube width which is 9 mm. If the channels are narrowed by 4-5 mm, they can be clustered and connected

to each other with spherical nodes (Fig. 6.2) and can give more effective results. This is due to the composition, volumetric connections that make impedance difference are diversified. Fig. 6.2 shows three interconnected units.

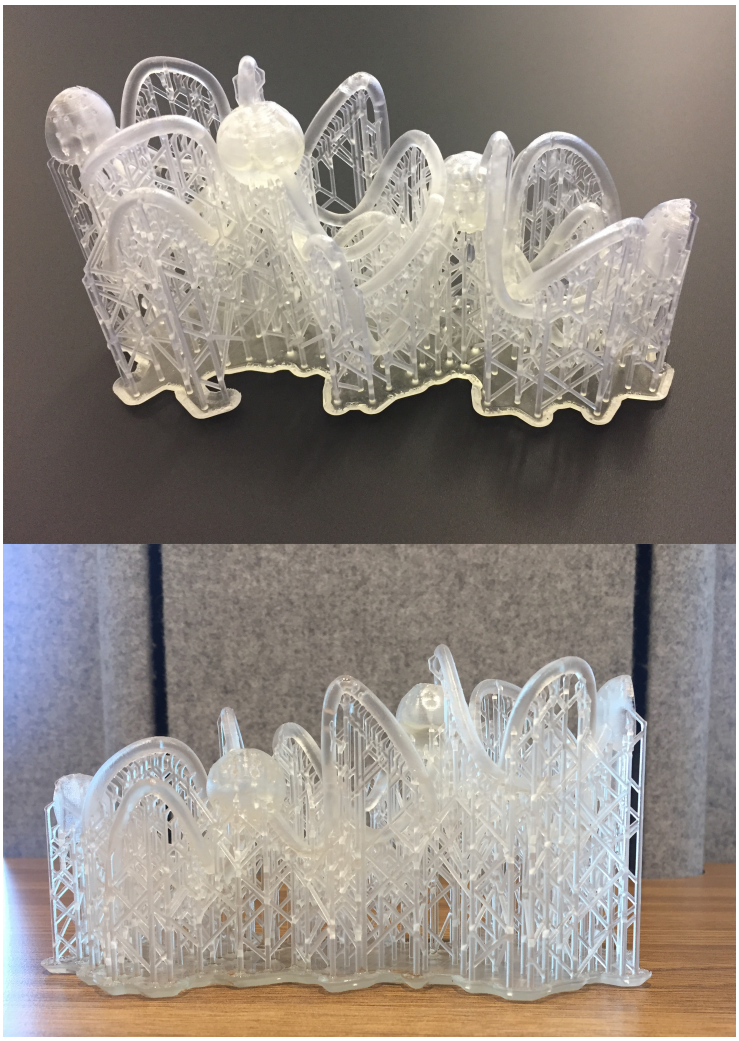

Figure 6.3: Unsatisfactory results of Alternative 1.

As shortly discussed in Section 3.1.3, when this variation was printed in 3D CNC printer with available technology, no accurate result could be obtained because the printing is not sensitive enough to print such small tubes. In this production, inner channels/tubes were filled with resin due to the printing tolerance of the available printer. Fig. 6.3 presents the unsatisfactory printouts. It is anticipated that with more advanced printers it can be possible to reduce the

channel/tube widths. So, Alternative 1 can be manufactured with these printers in the future.

6.2.2 Alternative 2

Altenative 2 is developed for enhancing DNA module. By keeping the void volume in the tube stable, the three-dimensional coordinates of the tube can be changed and even the number of tubes can be increased (Fig. 6.4). As the length and number of tubes with different lengths increase, it is predicted that the sound path will increase resulting in a higher sound absorption performance in a broader frequency range.

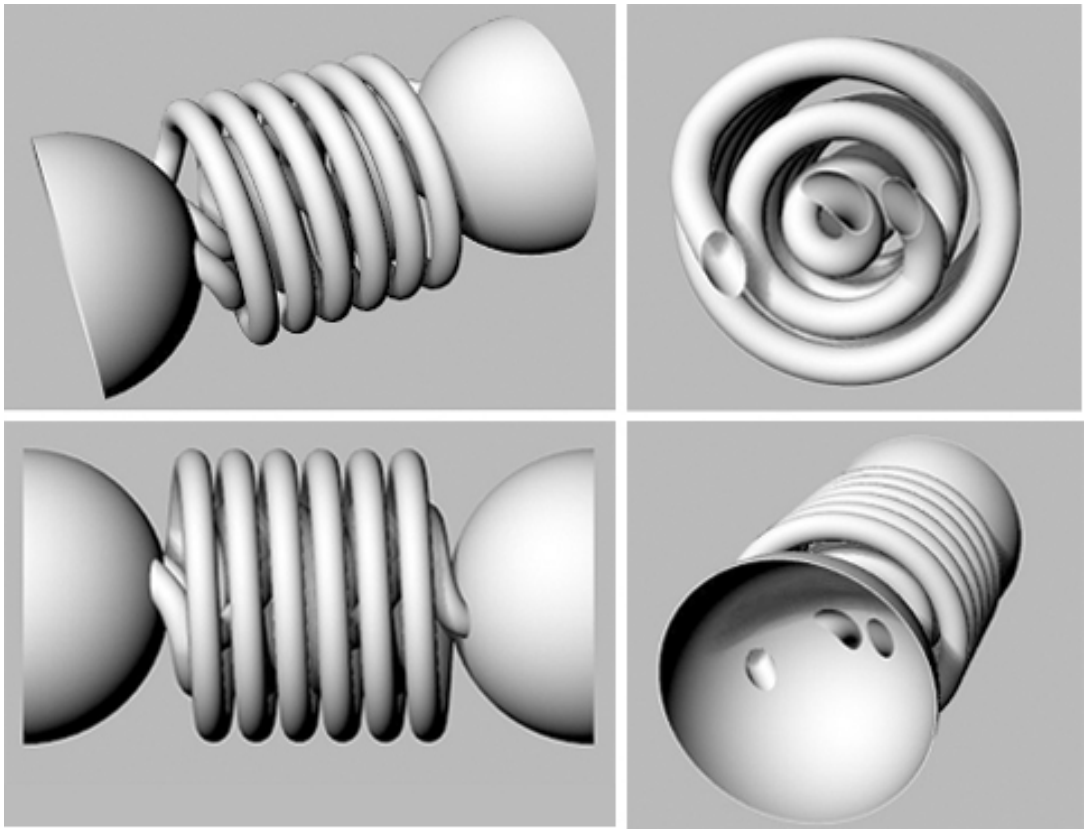

Figure 6.4: Alternative 2 as a variation of DNA specimen.

Since the diversity and rotation/movement/orientation of folds in the 3D

Cartesian system of DNA will be greater than the 2D system (and also many labyrinth types), sound energy damping mechanisms will increase. In Alternative 2, rotations are axial and it has more regular shape than DNA module proposed in this research. Increasing the number of folds/tubes will expand the frequency spectrum.

6.2.3 Alternative 3

Altenative 3 is developed as a variation for WL specimen. Traditional (architectural) patterns can be applied or utilized for form generation of maze structures within metamaterials.

In Turkish culture, there are many patterns that can be used and Seljukid is one of them. The pattern has symbolic meanings of traditional elements. Figure and ground relationship has a lot of potentials to generate alternative maze structures and is highly suitable for getting effective results both technically and aesthetically [10]. Within the structure in 2D, there are narrow gaps between lines with symmetrical order. When the two-dimension lines are extrapolated to three dimensions, the lines transform into layers of the small partitions and the background of the pattern becomes the gap between these layers, which is desirable for creating labyrinthine type 3D acoustic metamaterial (Fig.6.5 and Fig. 6.6). WL specimen that is proposed in this study is also the most similar to this alternative in terms of its structure.

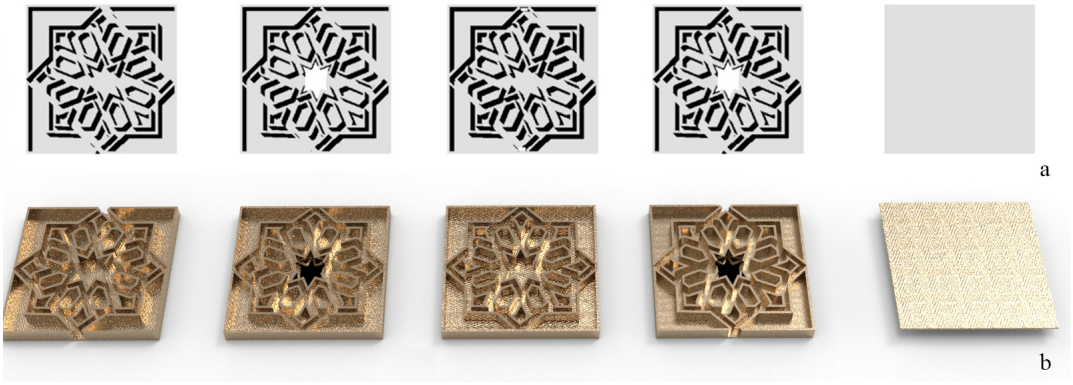

Figure 6.5: a) Top view of Alternative 3 layers inspired by Seljuk-id pattern, b) a perspective view.

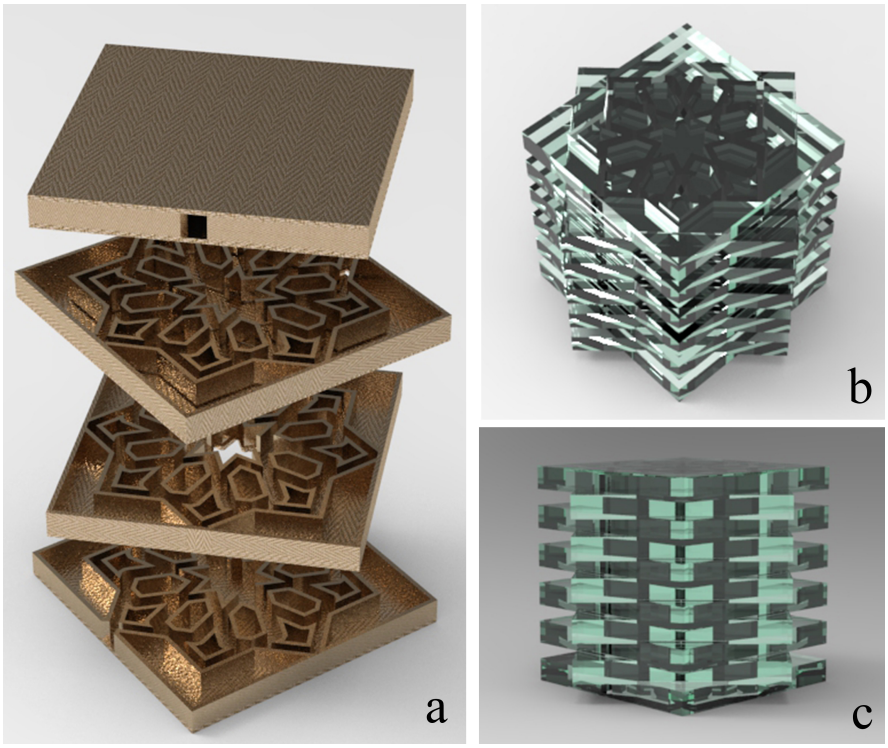

Figure 6.6: Alternative 3 a) exploded scheme, b) an axonometric view from top, c) front elevation.

For future work, the experimental results presented in this study will be utilized to simulate material properties for the optimization of the modules by a

numerical implementation. For the new alternatives, it is suggested that the acoustic performance of all three samples should be estimated in software numerically before production for achieving optimum values. While making these estimations, the process should be based on the measurement results obtained by the modules proposed in this thesis. When effective values are obtained, all the steps followed by the materials presented in the thesis should be applied for these alternatives too. Finally the results from the numerical implementation will be cross-checked with the tube measurements for validation.

Bibliography

[1] V. G. Magorien, "What is bulk modulus and when is it important?," *Hydraulics and Pneumatics*, vol. 22, pp. 98–101, 1969.

[2] P. Belov, "Backward waves and negative refraction in uniaxial dielectrics with negative dielectric permittivity along the anisotropy axis," *Microwave and Optical Technology Letters*, vol. 37, no. 4, pp. 259–263, 2003.

[3] M. Barron, *Auditorium acoustics and architectural design*. Routledge, 2009.

[4] M. McGrory, D. C. Cirac, O. Gaussen, D. Cabrera, and G. Engineers, "Sound absorption coefficient measurement: Re-examining the relationship between impedance tube and reverberant room methods," in *Proceedings of the Acoustics*, pp. 21–23, 2012.

[5] Z. Liu, X. Zhang, Y. Mao, Y. Zhu, Z. Yang, C. T. Chan, and P. Sheng, "Locally resonant sonic materials," *science*, vol. 289, no. 5485, pp. 1734–1736, 2000.

[6] T.-Y. Huang, C. Shen, and Y. Jing, "Membrane-and plate-type acoustic metamaterials," *The Journal of the Acoustical Society of America*, vol. 139, no. 6, pp. 3240–3250, 2016.

[7] Z. Liang and J. Li, "Extreme acoustic metamaterial by coiling up space," *Physical review letters*, vol. 108, no. 11, p. 114301, 2012.

[8] Y. Xie, B.-I. Popa, L. Zigoneanu, and S. A. Cummer, "Measurement of a broadband negative index with space-coiling acoustic metamaterials," *Physical review letters*, vol. 110, no. 17, p. 175501, 2013.

[9] T. Frenzel, J. David Brehm, T. Bückmann, R. Schittny, M. Kadic, and M. Wegener, "Three-dimensional labyrinthine acoustic metamaterials," *Applied Physics Letters*, vol. 103, no. 6, p. 061907, 2013.

[10] A. O. Krushynska, "Between science and art: thin sound absorbers inspired by slavic ornaments," *Frontiers in Materials*, vol. 6, p. 182, 2019.

[11] C. Liu, B. Xia, and D. Yu, "The spiral-labyrinthine acoustic metamaterial by coiling up space," *Physics Letters A*, vol. 381, no. 36, pp. 3112–3118, 2017.

[12] M. Akhtaruzzaman and A. A. Shafie, "Geometrical substantiation of phi, the golden ratio and the baroque of nature, architecture, design and engineering," *International Journal of Arts*, vol. 1, no. 1, pp. 1–22, 2011.

[13] Y. Bar-Cohen, *Biomimetics: biologically inspired technologies*. CRC Press, 2005.

[14] C. J. Alden and S.-H. Kim, "Solvent-accessible surfaces of nucleic acids," *Journal of molecular biology*, vol. 132, no. 3, pp. 411–434, 1979.

[15] A. D. Smith and J. P. Bolam, "The neural network of the basal ganglia as revealed by the study of synaptic connections of identified neurones," *Trends in neurosciences*, vol. 13, no. 7, pp. 259–265, 1990.

[16] D. C. Phillips, "The three-dimensional structure of an enzyme molecule," *Scientific American*, vol. 215, no. 5, pp. 78–93, 1966.

[17] S. A. Cummer, J. Christensen, and A. Alù, "Controlling sound with acoustic metamaterials," *Nature Reviews Materials*, vol. 1, no. 3, p. 16001, 2016.

[18] Y.-L. Tsai and T. Chen, "Band gap structure of acoustic wave in hexagonal phononic crystals with polyethylene matrix," *Procedia Engineering*, vol. 79, pp. 612–616, 2014.

[19] M. Stewart and K. Arnold, "Surface production operations," *Pump and Compressor Systems: Mechanical Design and*, 2016.

[20] S. A. Ramakrishna and T. M. Grzegorczyk, *Physics and applications of negative refractive index materials*. CRC press, 2008.

[21] A. C. Gade, "Acoustics in halls for speech and music," in *Springer handbook of acoustics*, pp. 317–366, Springer, 2014.

[22] Z. Maekawa, "Lord," *P.,"Environmental and Architectural Acoustics 1st ed.", E&FN Spon, Londra*, pp. 1–33, 1994.

[23] M. D. Egan, *Architectural acoustics*. 1988.

[24] L. Cremer, H. A. Müller, and T. D. Northwood, "Principles and applications of room acoustics," *PhT*, vol. 37, no. 1, p. 86, 1984.

[25] " Ergonomics Assessment of speech communication," standard, International Organization for Standardization, August 2003.

[26] " Acoustics Measurement of sound absorption in a reverberation room," standard, International Organization for Standardization, October 2003.

[27] "Acoustics -determination of sound absorption coefficient and impedance in impedance tubes- part 2: Transfer-function method," standard, International Organization for Standardization, November 1998.

[28] J. B. Pendry, A. Holden, W. Stewart, and I. Youngs, "Extremely low frequency plasmons in metallic mesostructures," *Physical review letters*, vol. 76, no. 25, p. 4773, 1996.

[29] J. B. Pendry, A. J. Holden, D. J. Robbins, and W. Stewart, "Magnetism from conductors and enhanced nonlinear phenomena," *IEEE transactions on microwave theory and techniques*, vol. 47, no. 11, pp. 2075–2084, 1999.

[30] R. A. Shelby, D. R. Smith, and S. Schultz, "Experimental verification of a negative index of refraction," *science*, vol. 292, no. 5514, pp. 77–79, 2001.

[31] R. Fleury, D. Sounas, and A. Alu, "An invisible acoustic sensor based on parity-time symmetry," *Nature communications*, vol. 6, no. 1, pp. 1–7, 2015.

[32] G. Ma and P. Sheng, "Acoustic metamaterials: From local resonances to broad horizons," *Science advances*, vol. 2, no. 2, p. e1501595, 2016.

[33] Y. Chen, G. Hu, and G. Huang, "A hybrid elastic metamaterial with negative mass density and tunable bending stiffness," *Journal of the Mechanics and Physics of Solids*, vol. 105, pp. 179–198, 2017.

[34] M. I. Hussein, M. J. Leamy, and M. Ruzzene, "Dynamics of phononic materials and structures: Historical origins, recent progress, and future outlook," *Applied Mechanics Reviews*, vol. 66, no. 4, 2014.

[35] E. Yablonovitch, "Inhibited spontaneous emission in solid-state physics and electronics," *Physical review letters*, vol. 58, no. 20, p. 2059, 1987.

[36] M. Lapine, "The age of metamaterials," *Metamaterials*, vol. 1, no. 1, p. 1, 2007.

[37] E. Shamonina and L. Solymar, "Metamaterials: How the subject started," *Metamaterials*, vol. 1, no. 1, pp. 12–18, 2007.

[38] M. Gil, J. Bonache, and F. Martin, "Metamaterial filters: A review," *Metamaterials*, vol. 2, no. 4, pp. 186–197, 2008.

[39] J. Franklin, *Classical electromagnetism*. Courier Dover Publications, 2017.

[40] V. G. Veselago, "The electrodynamics of substances with simultaneously negative values of ϵ and μ," *Physics-Uspekhi*, vol. 10, no. 4, pp. 509–514, 1968.

[41] D. R. Smith, W. J. Padilla, D. Vier, S. C. Nemat-Nasser, and S. Schultz, "Composite medium with simultaneously negative permeability and permittivity," *Physical review letters*, vol. 84, no. 18, p. 4184, 2000.

[42] D. Sivukhin, "The energy of electromagnetic waves in dispersive media," *Opt. Spektrosk*, vol. 3, no. 4, pp. 308–312, 1957.

[43] J. B. Pendry, "Negative refraction makes a perfect lens," *Physical review letters*, vol. 85, no. 18, p. 3966, 2000.

[44] J. Hao, J. Wang, X. Liu, W. J. Padilla, L. Zhou, and M. Qiu, "High performance optical absorber based on a plasmonic metamaterial," *Applied Physics Letters*, vol. 96, no. 25, p. 251104, 2010.

[45] J. Hao, L. Zhou, and M. Qiu, "Nearly total absorption of light and heat generation by plasmonic metamaterials," *Physical Review B*, vol. 83, no. 16, p. 165107, 2011.

[46] Y. Fan, F. Zhang, Q. Zhao, Z. Wei, and H. Li, "Tunable terahertz coherent perfect absorption in a monolayer graphene," *Optics letters*, vol. 39, no. 21, pp. 6269–6272, 2014.

[47] J. Allard and N. Atalla, *Propagation of sound in porous media: modelling sound absorbing materials 2e*. John Wiley & Sons, 2009.

[48] L. Zigoneanu, B.-I. Popa, and S. A. Cummer, "Three-dimensional broadband omnidirectional acoustic ground cloak," *Nature materials*, vol. 13, no. 4, pp. 352–355, 2014.

[49] L.-W. Cai and J. Sánchez-Dehesa, "Analysis of cummer–schurig acoustic cloaking," *New journal of physics*, vol. 9, no. 12, p. 450, 2007.

[50] H. Ma, S. Qu, Z. Xu, and J. Wang, "Numerical method for designing approximate cloaks with arbitrary shapes," *Physical Review E*, vol. 78, no. 3, p. 036608, 2008.

[51] S. Zhang, C. Xia, and N. Fang, "Broadband acoustic cloak for ultrasound waves," *Physical review letters*, vol. 106, no. 2, p. 024301, 2011.

[52] N. Kaina, F. Lemoult, M. Fink, and G. Lerosey, "Negative refractive index and acoustic superlens from multiple scattering in single negative metamaterials," *Nature*, vol. 525, no. 7567, pp. 77–81, 2015.

[53] R. Fleury, D. L. Sounas, C. F. Sieck, M. R. Haberman, and A. Alù, "Sound isolation and giant linear nonreciprocity in a compact acoustic circulator," *Science*, vol. 343, no. 6170, pp. 516–519, 2014.

[54] B. Liang, X. Guo, J. Tu, D. Zhang, and J. Cheng, "An acoustic rectifier," *Nature materials*, vol. 9, no. 12, pp. 989–992, 2010.

[55] Y. Li, B. Liang, X. Tao, X.-f. Zhu, X.-y. Zou, and J.-c. Cheng, "Acoustic focusing by coiling up space," *Applied Physics Letters*, vol. 101, no. 23, p. 233508, 2012.

[56] Y. Xie, W. Wang, H. Chen, A. Konneker, B.-I. Popa, and S. A. Cummer, "Wavefront modulation and subwavelength diffractive acoustics with an acoustic metasurface," *Nature communications*, vol. 5, no. 1, pp. 1–5, 2014.

[57] V. M. García-Chocano, J. Christensen, and J. Sánchez-Dehesa, "Negative refraction and energy funneling by hyperbolic materials: An experimental demonstration in acoustics," *Physical review letters*, vol. 112, no. 14, p. 144301, 2014.

[58] A. Krushynska, F. Bosia, M. Miniaci, and N. Pugno, "Fractal and spider web-inspired labyrinthine acoustic metamaterials," in *2017 11th International Congress on Engineered Materials Platforms for Novel Wave Phenomena (Metamaterials)*, pp. 187–189, IEEE.

[59] S. H. Lee, C. M. Park, Y. M. Seo, Z. G. Wang, and C. K. Kim, "Acoustic metamaterial with negative modulus," *Journal of Physics: Condensed Matter*, vol. 21, no. 17, p. 175704, 2009.

[60] S. H. Lee, C. M. Park, Y. M. Seo, Z. G. Wang, and C. K. Kim, "Composite acoustic medium with simultaneously negative density and modulus," *Physical review letters*, vol. 104, no. 5, p. 054301, 2010.

[61] J. Fey and W. M. Robertson, "Compact acoustic bandgap material based on a subwavelength collection of detuned helmholtz resonators," *Journal of Applied Physics*, vol. 109, no. 11, p. 114903, 2011.

[62] S. H. Lee, C. M. Park, Y. M. Seo, Z. G. Wang, and C. K. Kim, "Composite acoustic medium with simultaneously negative density and modulus," *Physical review letters*, vol. 104, no. 5, p. 054301, 2010.

[63] R. Fleury and A. Alù, "Extraordinary sound transmission through density-near-zero ultranarrow channels," *Physical review letters*, vol. 111, no. 5, p. 055501, 2013.

[64] C. Shen, J. Xu, N. X. Fang, and Y. Jing, "Anisotropic complementary acoustic metamaterial for canceling out aberrating layers," *Physical Review X*, vol. 4, no. 4, p. 041033, 2014.

[65] N. Fang, D. Xi, J. Xu, M. Ambati, W. Srituravanich, C. Sun, and X. Zhang, "Ultrasonic metamaterials with negative modulus," *Nature materials*, vol. 5, no. 6, pp. 452–456, 2006.

[66] B.-I. Popa, L. Zigoneanu, and S. A. Cummer, "Experimental acoustic ground cloak in air," *Physical review letters*, vol. 106, no. 25, p. 253901, 2011.

[67] Z. Liang, T. Feng, S. Lok, F. Liu, K. B. Ng, C. H. Chan, J. Wang, S. Han, S. Lee, and J. Li, "Space-coiling metamaterials with double negativity and conical dispersion," *Scientific reports*, vol. 3, p. 1614, 2013.

[68] Y. Li, B. Liang, Z.-m. Gu, X.-y. Zou, and J.-c. Cheng, "Reflected wavefront manipulation based on ultrathin planar acoustic metasurfaces," *Scientific reports*, vol. 3, p. 2546, 2013.

[69] Y. Cheng, C. Zhou, B. Yuan, D. Wu, Q. Wei, and X. Liu, "Ultra-sparse metasurface for high reflection of low-frequency sound based on artificial mie resonances," *Nature materials*, vol. 14, no. 10, pp. 1013–1019, 2015.

[70] Z. Yang, H. Dai, N. Chan, G. Ma, and P. Sheng, "Acoustic metamaterial panels for sound attenuation in the 50–1000 hz regime," *Applied Physics Letters*, vol. 96, no. 4, p. 041906, 2010.

[71] A. Krushynska, F. Bosia, M. Miniaci, and N. Pugno, "Spider web-structured labyrinthine acoustic metamaterials for low-frequency sound control," *New Journal of Physics*, vol. 19, no. 10, p. 105001, 2017.

[72] O. Godbold, R. Soar, and R. Buswell, "Implications of solid freeform fabrication on acoustic absorbers," *Rapid Prototyping Journal*, 2007.

[73] F. Setaki, M. Tenpierik, M. Turrin, and A. van Timmeren, "Acoustic absorbers by additive manufacturing," *Building and Environment*, vol. 72, pp. 188–200, 2014.

[74] Z. Guo and F. Yang, *Surfaces and Interfaces of Biomimetic Superhydrophobic Materials*. John Wiley & Sons, 2017.

[75] N. J. Shirtcliffe, G. McHale, and M. I. Newton, "The superhydrophobicity of polymer surfaces: recent developments," *Journal of Polymer Science Part B: Polymer Physics*, vol. 49, no. 17, pp. 1203–1217, 2011.

[76] P. Roach, N. J. Shirtcliffe, and M. I. Newton, "Progess in superhydrophobic surface development," *Soft matter*, vol. 4, no. 2, pp. 224–240, 2008.

[77] T. Sun, L. Feng, X. Gao, and L. Jiang, "Bioinspired surfaces with special wettability," *Accounts of chemical research*, vol. 38, no. 8, pp. 644–652, 2005.

[78] X. Liu, Y. Liang, F. Zhou, and W. Liu, "Extreme wettability and tunable adhesion: biomimicking beyond nature?," *Soft matter*, vol. 8, no. 7, pp. 2070–2086, 2012.

[79] N. Sui, X. Yan, T.-Y. Huang, J. Xu, F.-G. Yuan, and Y. Jing, "A lightweight yet sound-proof honeycomb acoustic metamaterial," *Applied Physics Letters*, vol. 106, no. 17, p. 171905, 2015.

[80] R. J. Lang, "Origami: Complexity increasing," *Engineering & Science*, vol. 52, no. 2, pp. 16–23, 1989.

[81] F. Goldman, "Using the snapology technique to teach convex polyhedra," in *Fifth International Meeting of Origami Science, Mathematics, and Education*, pp. 99–110, 2011.

[82] H. Strobl, "Special snapology: A simple and cheap method to make convex polyhedra models," in *Didaktik-Kolloquium am*, vol. 26, 2010.

[83] J. T. Overvelde, T. A. De Jong, Y. Shevchenko, S. A. Becerra, G. M. Whitesides, J. C. Weaver, C. Hoberman, and K. Bertoldi, "A three-dimensional actuated origami-inspired transformable metamaterial with multiple degrees of freedom," *Nature communications*, vol. 7, no. 1, pp. 1–8, 2016.

[84] C. Shao, H. Long, Y. Cheng, and X. Liu, "Low-frequency perfect sound absorption achieved by a modulus-near-zero metamaterial," *Scientific reports*, vol. 9, no. 1, pp. 1–8, 2019.

[85] M. Vomhof, L. Vasey, S. Brauer, K. Eggenschwiler, J. Strauss, F. Gramazio, and M. Kohler, "Robotic fabrication of acoustic brick walls," 2014.

[86] K.-M. M. Tam and C. T. Mueller, "Additive manufacturing along principal stress lines," *3D Printing and Additive Manufacturing*, vol. 4, no. 2, pp. 63–81, 2017.

[87] S. Lim, R. A. Buswell, T. T. Le, S. A. Austin, A. G. Gibb, and T. Thorpe, "Developments in construction-scale additive manufacturing processes," *Automation in construction*, vol. 21, pp. 262–268, 2012.

[88] Z. Quan, A. Wu, M. Keefe, X. Qin, J. Yu, J. Suhr, J.-H. Byun, B.-S. Kim, and T.-W. Chou, "Additive manufacturing of multi-directional preforms for composites: opportunities and challenges," *Materials Today*, vol. 18, no. 9, pp. 503–512, 2015.

[89] M. Long, *Architectural acoustics*. Elsevier, 2005.

[90] T. Lato and A. Mohany, "Passive damping of pressure pulsations in pipelines using herschel-quincke tubes," *Journal of Sound and Vibration*, vol. 448, pp. 160–177, 2019.

[91] M. R. Haberman and M. D. Guild, "Acoustic metamaterials," *Phys. Today*, vol. 69, no. 6, pp. 42–48, 2016.

[92] S. Varanasi, J. S. Bolton, and T. Siegmund, "Experiments on the low frequency barrier characteristics of cellular metamaterial panels in a diffuse sound field," *The Journal of the Acoustical Society of America*, vol. 141, no. 1, pp. 602–610, 2017.

[93] S. Babaee, J. T. Overvelde, E. R. Chen, V. Tournat, and K. Bertoldi, "Reconfigurable origami-inspired acoustic waveguides," *Science Advances*, vol. 2, no. 11, p. e1601019, 2016.

Appendix A

Distribution Maps

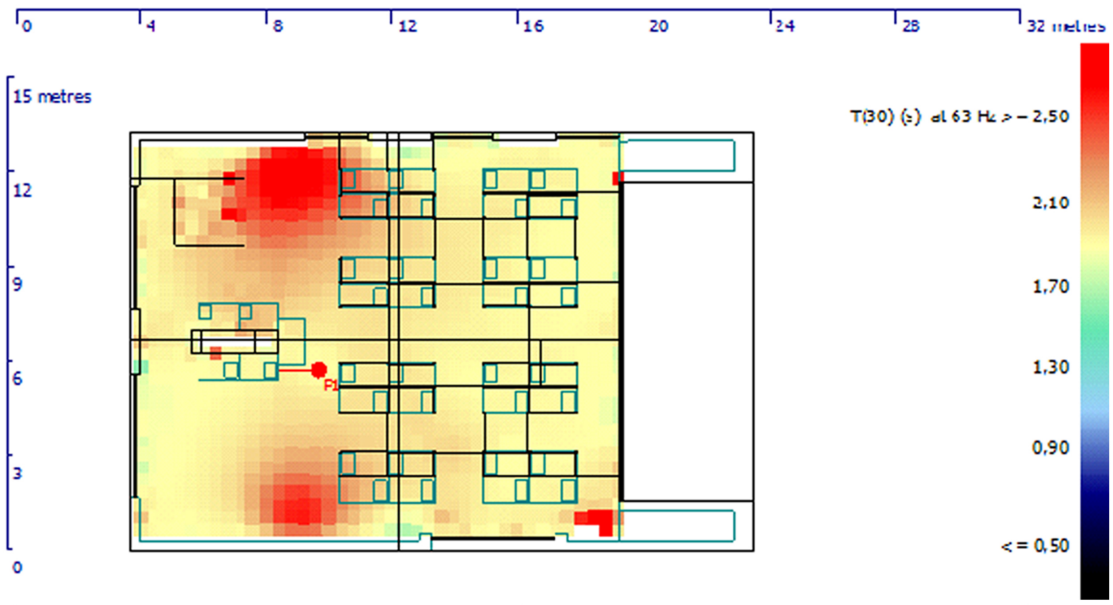

Figure A.1: Studio#1 T30 distribution map at 63 Hz for the current condition of the studio.

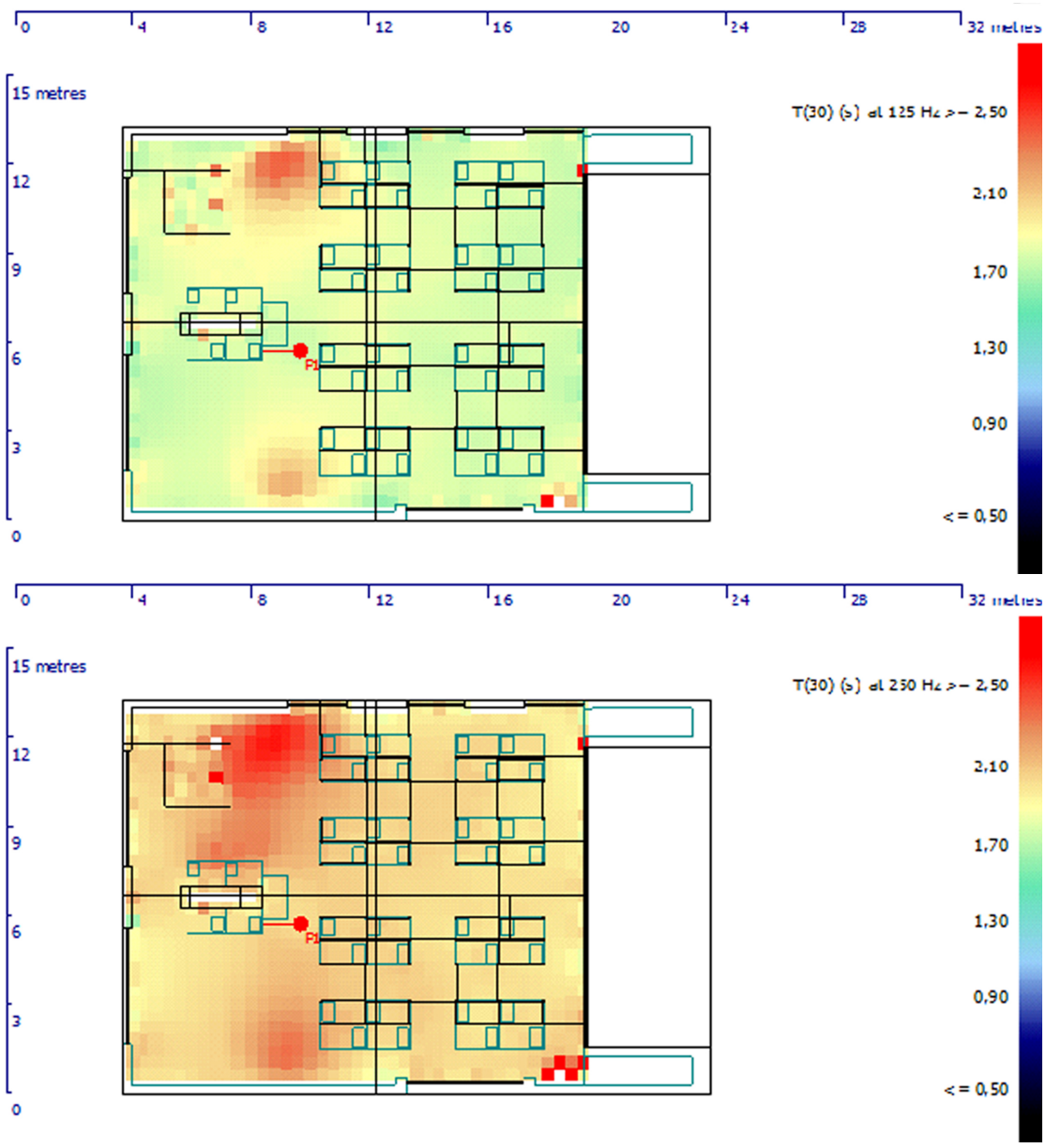

Figure A.2: Studio#1 T30 distribution maps at 125 Hz (on the top) and 250 Hz (at the bottom) for the current condition of the studio.

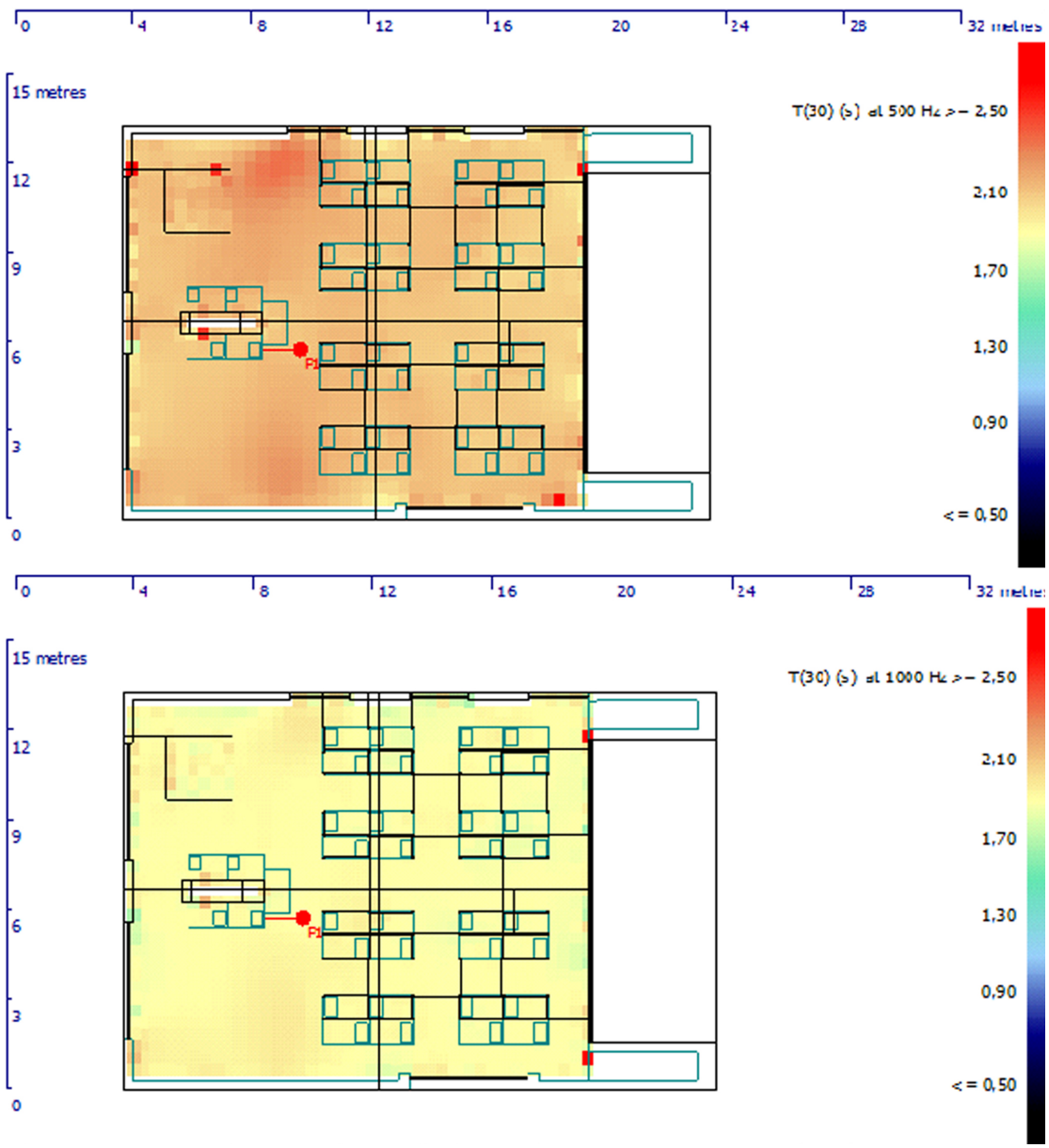

Figure A.3: Studio#1 T30 distribution maps at 500 Hz (on the top) and 1000 Hz (at the bottom) for the current condition of the studio.

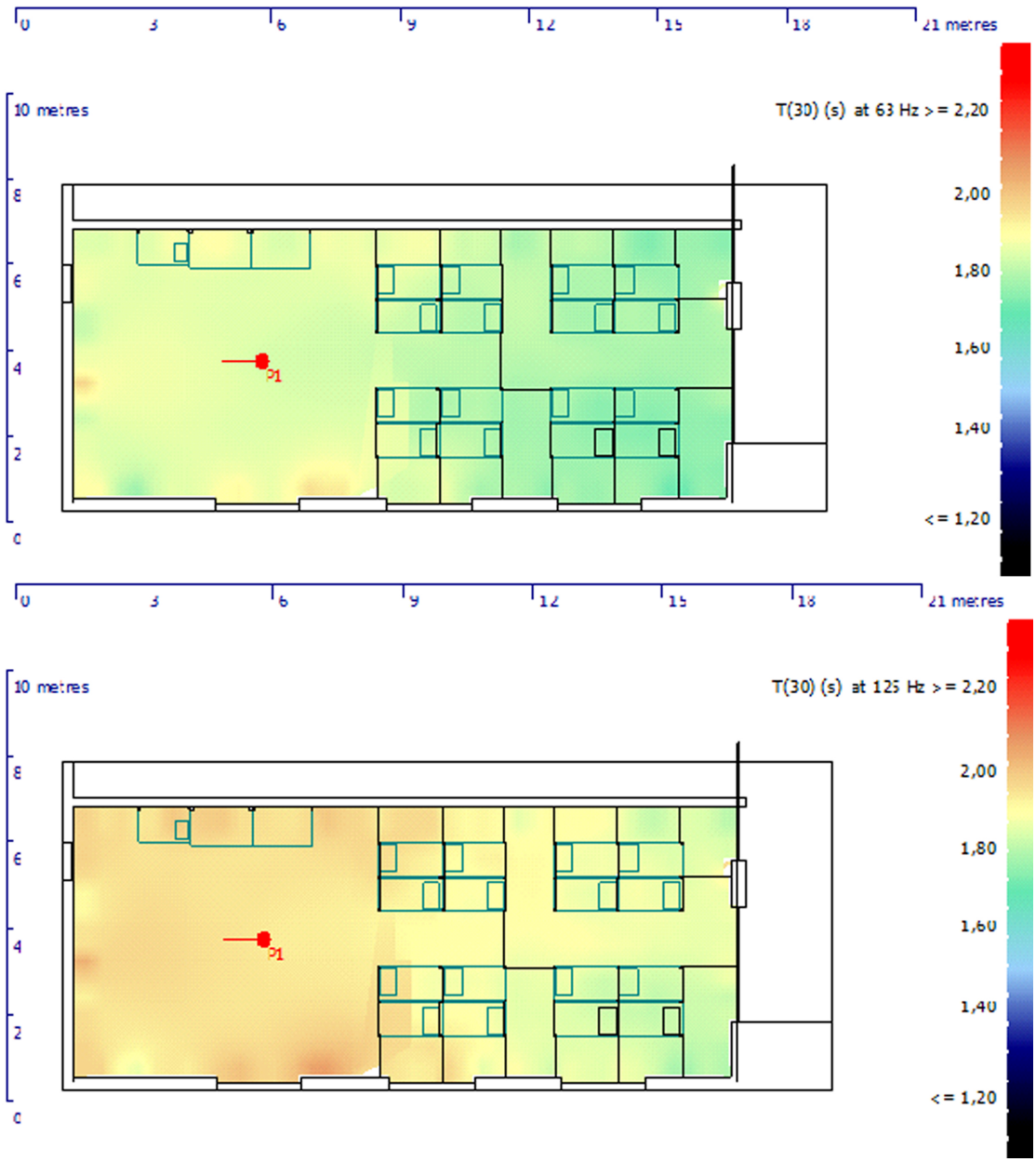

Figure A.4: Studio#2 T30 distribution maps at 63 Hz (on the top) and 125 Hz (at the bottom) for the current condition of the studio.

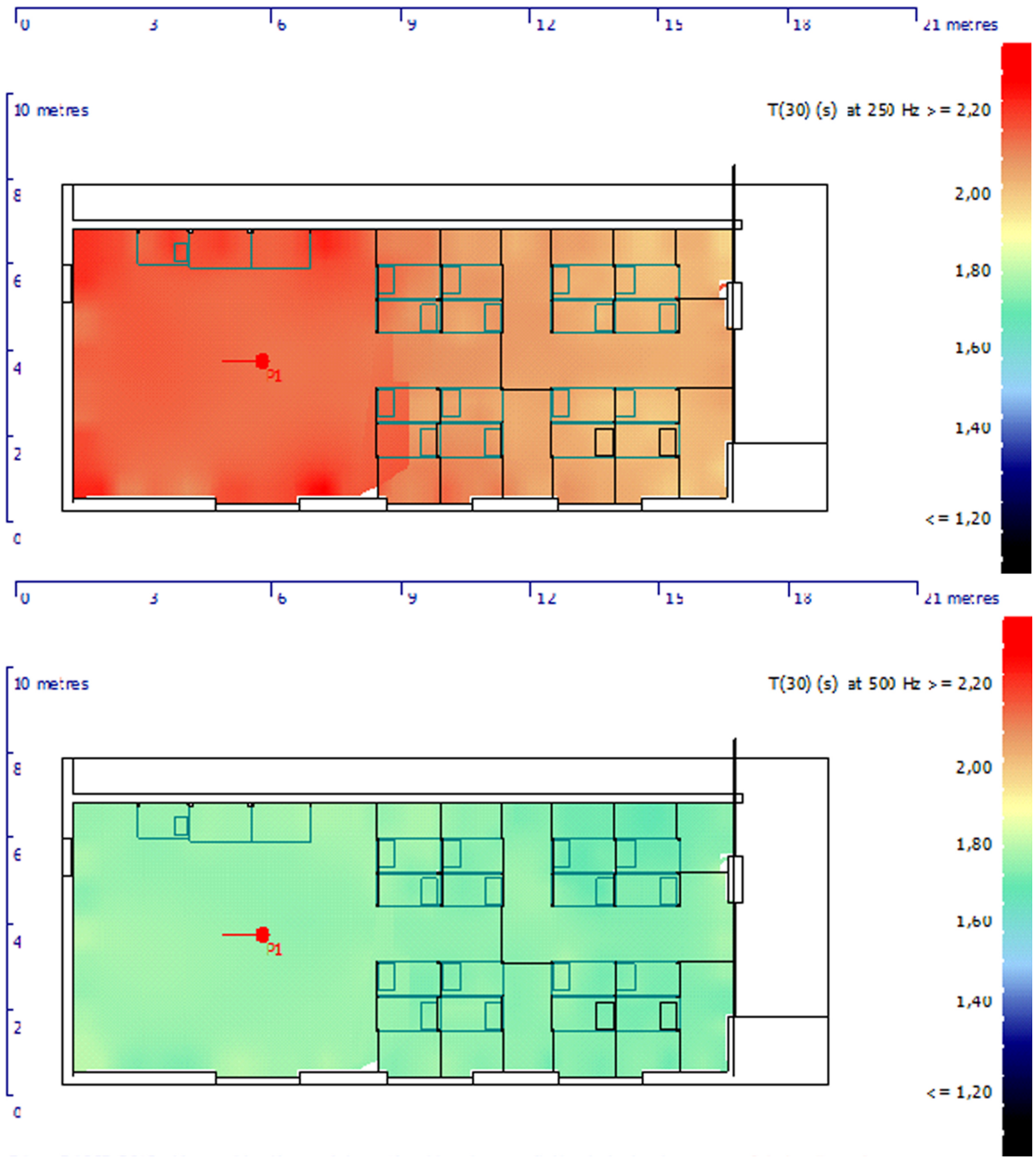

Figure A.5: Studio#2 T30 distribution maps at 250 Hz (on the top) and 500 Hz (at the bottom) for the current condition of the studio.

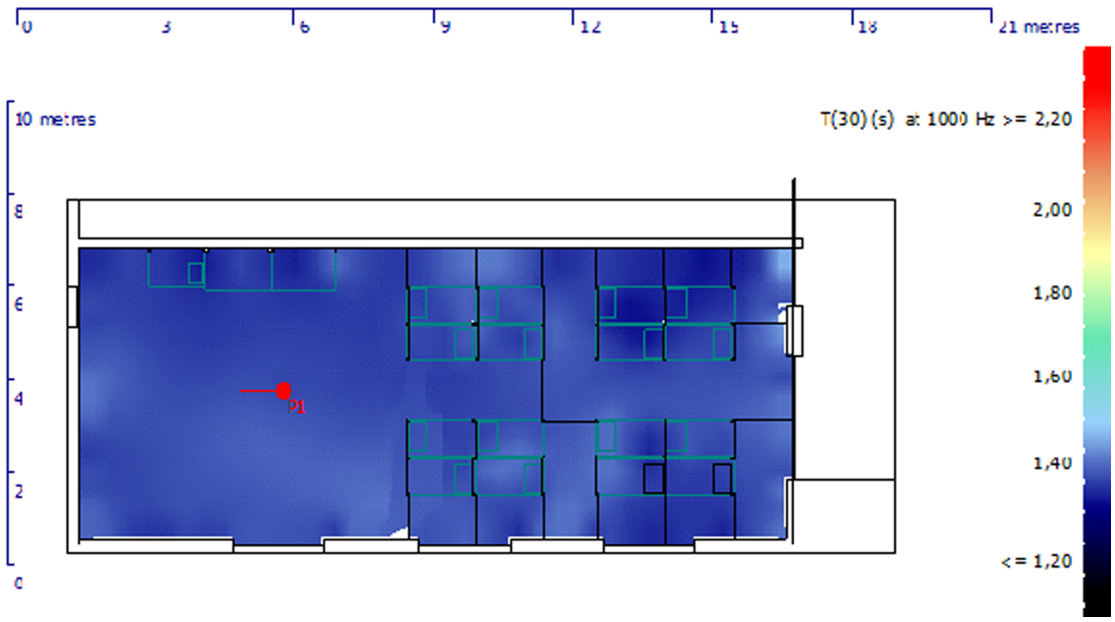

Figure A.6: Studio#2 T30 distribution map at 1000 Hz for the current condition of the studio.

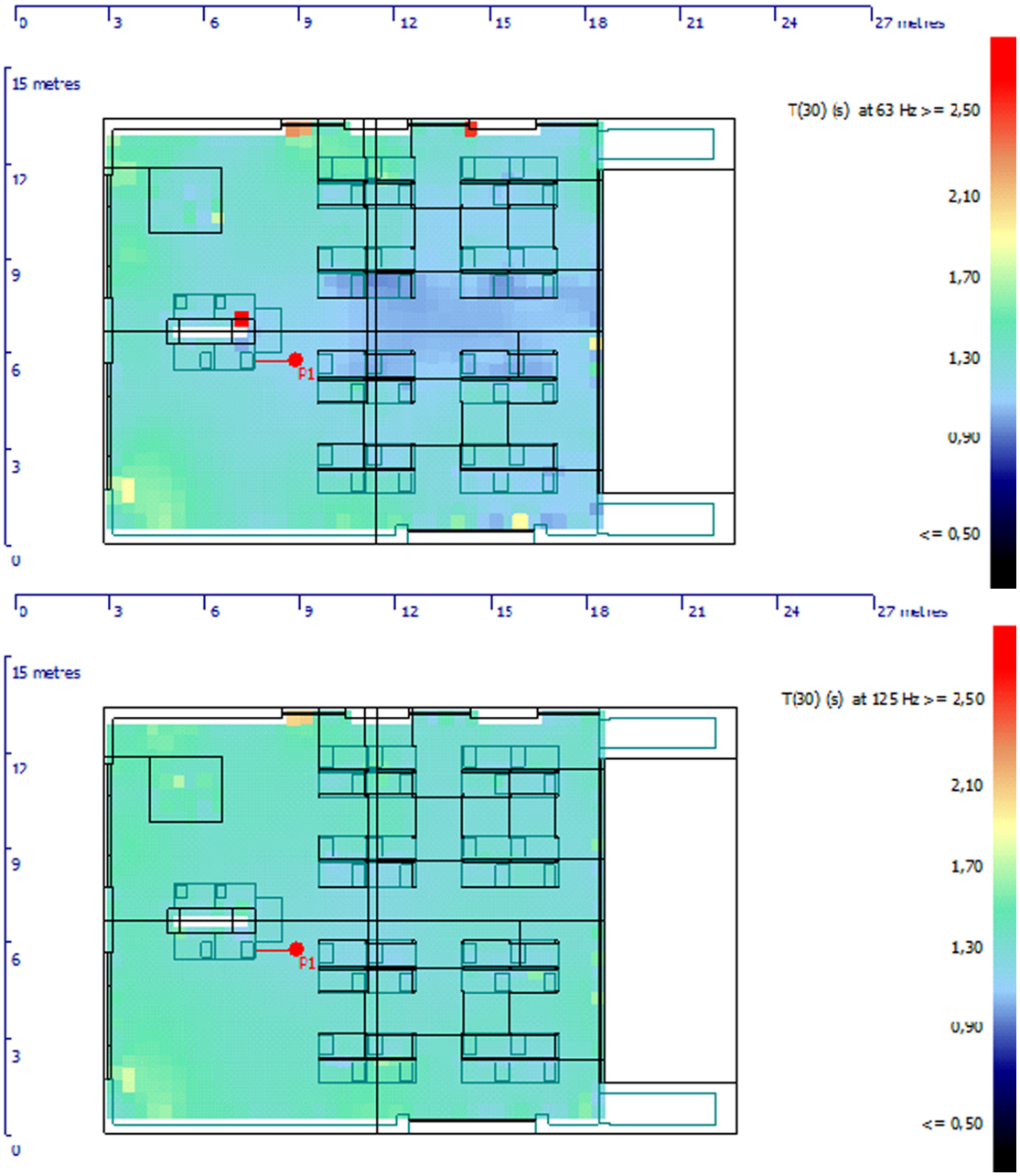

Figure A.7: Studio#1 T30 distribution maps at 63 Hz (on the top) and 125 Hz (at the bottom) under the A2 AMM proposal.

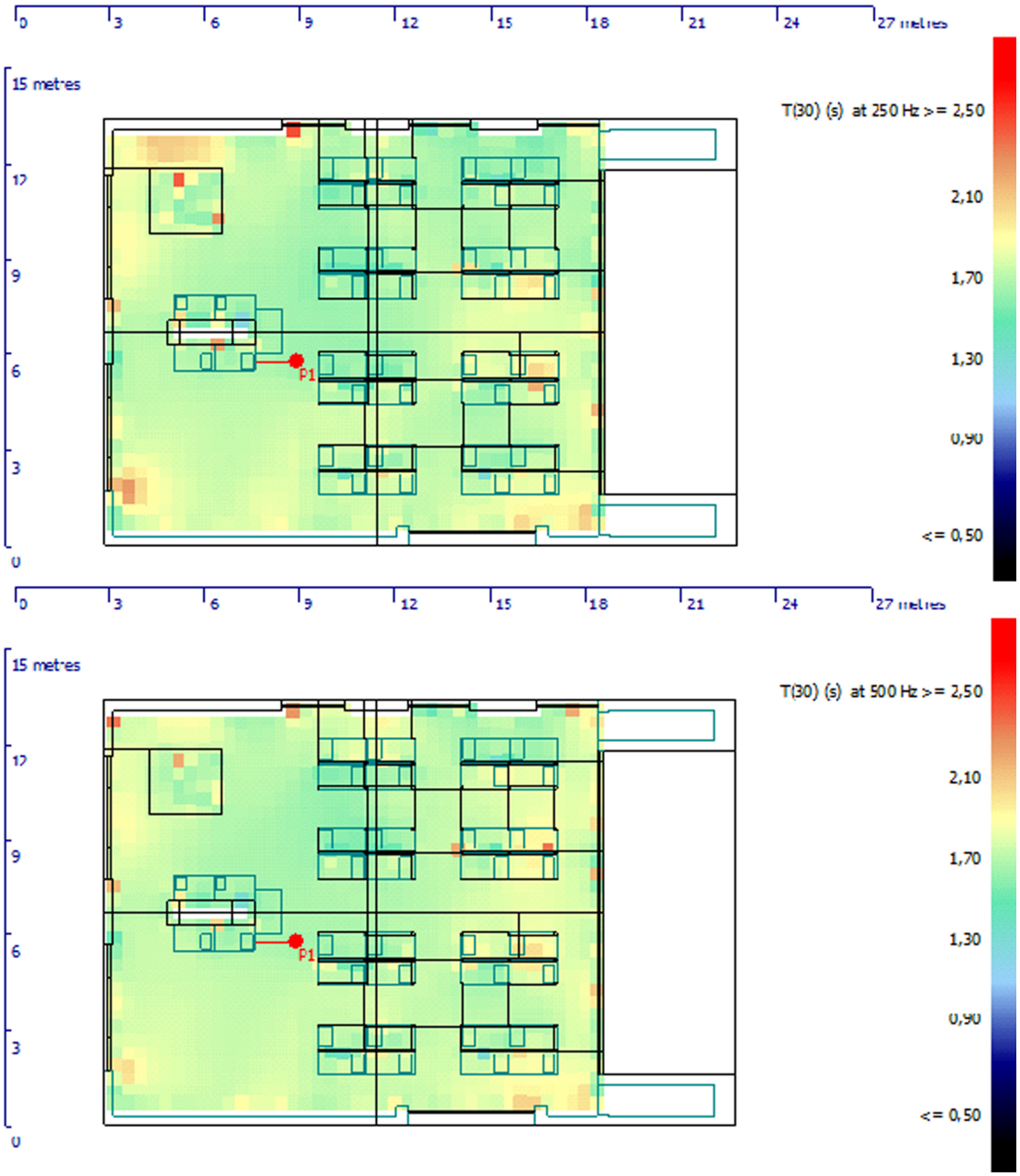

Figure A.8: Studio#1 T30 distribution maps at 250 Hz (on the top) and 500 Hz (at the bottom) under the A2 AMM proposal.

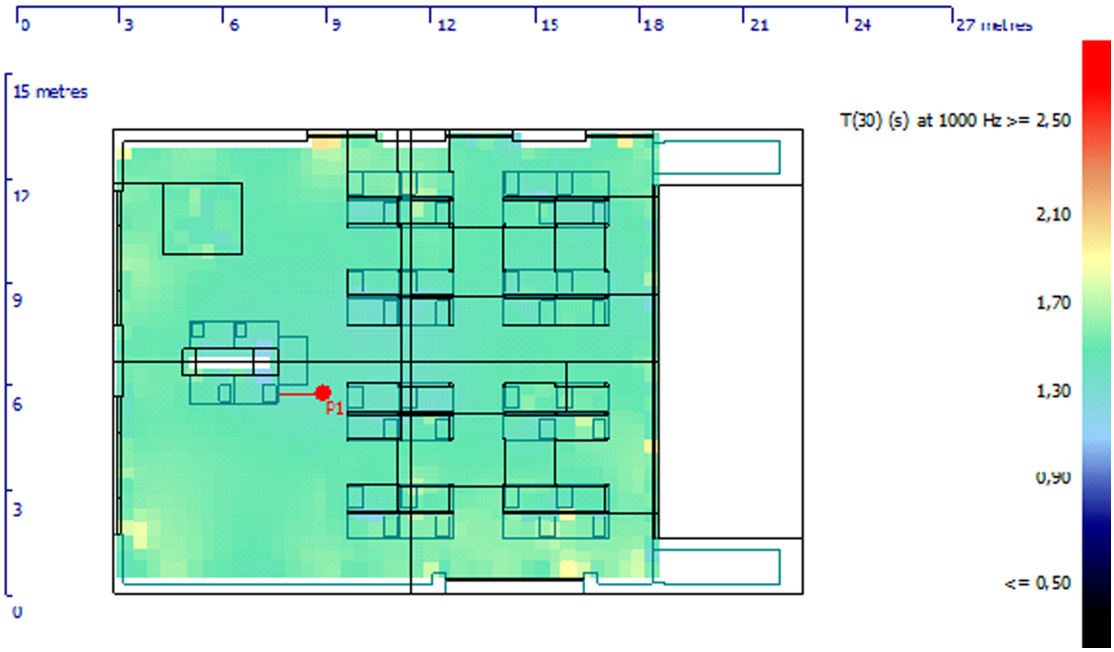

Figure A.9: Studio#1 T30 distribution map at 1000 Hz under the A2 AMM proposal.

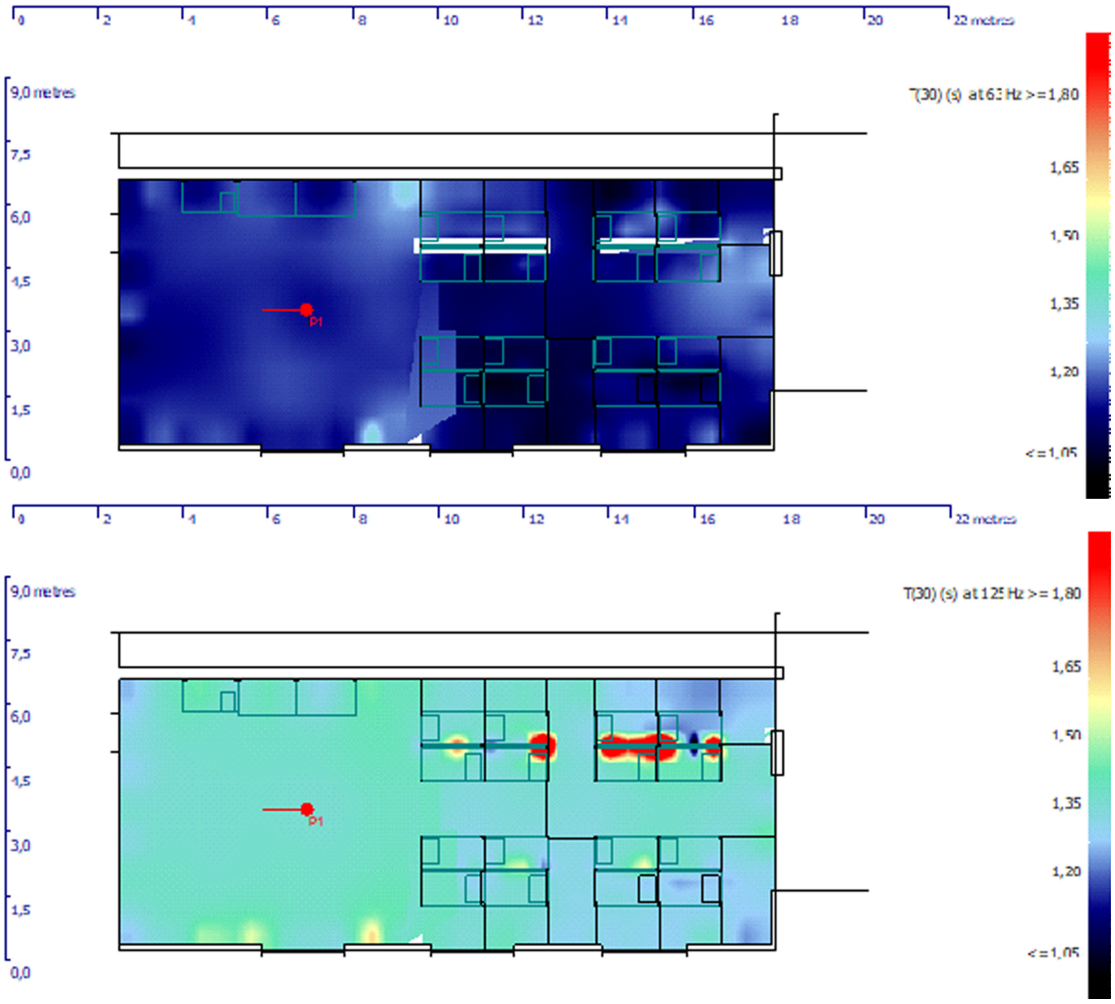

Figure A.10: Studio#2 T30 distribution maps at 63 Hz (on the top) and 125 Hz (at the bottom) under the A2 AMM proposal.

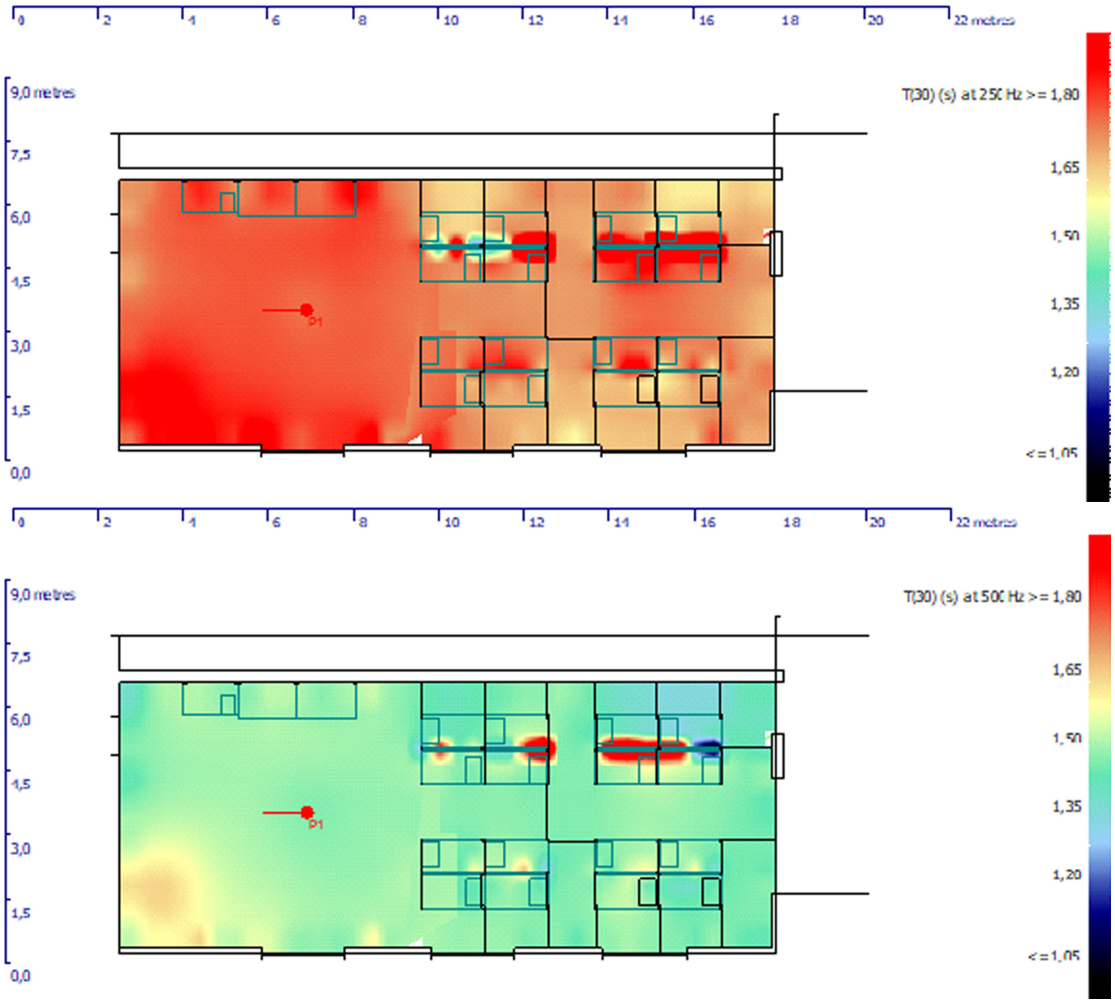

Figure A.11: Studio#2 T30 distribution maps at 250 Hz (on the top) and 500 Hz (at the bottom) under the A2 AMM proposal.